DISSERTATION FOR THE DEGREE OF DOCTOR OF PHILOSOPHY (PHD)

The role of retinol saturase enzyme and adenosine A3 receptor in skeletal muscle development and regeneration

by Nastaran Tarban

UNIVERSITY OF DEBRECEN
DOCTORAL SCHOOL OF MOLECULAR CELLULAR AND IMMUNE BIOLOGY

DEBRECEN, 2024

DISSERTATION FOR THE DEGREE OF DOCTOR OF PHILOSOPHY (PHD)

The role of retinol saturase enzyme and adenosine A3 receptor in skeletal muscle development and regeneration

by Nastaran Tarban

Supervisor: Dr. Zsolt Sarang

UNIVERSITY OF DEBRECEN
DOCTORAL SCHOOL OF MOLECULAR CELLULAR AND IMMUNE BIOLOGY

DEBRECEN, 2024

Table of contents:

1. Abbreviations

AR	Adenosine receptor
Arg 1	Arginase 1
ATP	Adenosine triphosphate
BAI-1	Brain angiogenesis inhibitor-1
BMDMs	Bone marrow-derived macrophages
CCR2	C-C chemokine receptor type 2
CD206	Mannose receptor C type 1
ChREBP	Carbohydrate response element-binding protein
COPD	Chronic obstructive pulmonary disease
CREB	Cyclic AMP response element-binding protein
CRT	Calreticulin
CSA	Cross-sectional area
CSF	Colony-stimulating factor
CTX	Cardiotoxin
CX3CL1	Cx3c motif chemokine ligand 1
CX3CR1	CX3C motif chemokine receptor 1
DAMP	Damage-associated molecular patterns
DAPI	4',6-diamidino-2-phenylindole
ECM	Extracellular matrix
EDL	Extensor digitorum longus
FAPs	Fibro-adipogenic progenitors
GDF3	Growth differentiation factor-3
GPCR	G protein-coupled receptor
H&E	Hematoxylin and eosin
HMGB1	High-mobility group box 1 protein

HSPs	Heat shock proteins
IGF-1	Insulin-like growth factor 1
IL	Interleukin
IRF	Interferon regulatory factor
LPC	Lysophosphatidylcholine
LRP1	Low density lipoprotein receptor-related protein 1
Ly6C	Lymphocyte antigen 6 complex locus C
Ly6G	Lymphocyte antigen 6 complex locus g6d
MAPKs	Mitogen-activated protein kinases
MCP-1	Monocyte chemoattractant protein-1
MFG-E8	Milk fat globule-EGF factor 8 protein
MRF4	Myogenic factor 4
MRFs	Myogenic regulatory factors
Myf5	Myogenic factor 5
MYHC	Myosin heavy chain
MyoD	Myoblast determination protein 1
Myogenin	Myogenic factor 4
Mϕs	Macrophages
NFIX	Nuclear factor I X
NF-κB	Nuclear factor kappa B
NO	Nitric oxide
NPY	Neuropeptide Y
Nur77/NR4A1	Nuclear receptor subfamily 4 group A member 1
PAMP	Pathogen-associated molecular patterns
PAX	Paired box transcription factor
PBS	phosphate-buffered saline
PDGFRα	Platelet-derived growth factor receptor alpha

PLC	Phospholipase C
PPARγ/δ	Peroxisome proliferator-activated receptor-gamma/delta
RetSat	Retinol saturase
ROS	Reactive oxygen species
S1P	Sphingosine-1-phosphate
Sca1	Stem cell antigen 1
SLE	Systemic lupus erythematosus
SOL	Soleus
SPMs	Specialized pro-resolving mediators
STAT	Signal transducer and activator of transcription
TA	Tibialis anterior
TGF-β	Transforming growth factor β
TIM	T-cell immunoglobulin and mucin domain
TLR	Toll-like receptor
TNF-α	Tumor necrosis factor-α
UTP	Uridine triphosphate
ZFX	Zinc Finger Protein X-Linked

2. Abstract

Following skeletal muscle injury, the regeneration begins with local inflammation, which is accompanied by the removal of dead cells. Phagocytosis of dead cells regulates the inflammatory program in macrophages (Mϕ) by promoting the transformation of inflammatory macrophages into "healing" macrophages. The pro-inflammatory cytokines initiate the activation and proliferation of muscle stem cells, called satellite cells, while growth factors, produced by healing macrophages drive myoblast differentiation, fusion, and myotube growth. Therefore, impaired phagocytosis or inflammation can lead to decreased muscle regeneration. The oxidoreductase enzyme retinol saturase (RetSat) is required for proper Mϕ phagocytosis while A3 adenosine receptor (A3R) was shown to modulate inflammatory responses. Therefore, our aim was to investigate the impact of RetSat enzyme and A3R deficiency on skeletal muscle development and regeneration in mice.

Tibialis anterior (TA) muscle damage was induced by intramuscular cardiotoxin (CTX) injection. Muscle fiber cross-sectional area (CSA), collagen deposition, and the extent of tissue necrosis were measured to evaluate the regeneration process. Flow cytometric analysis was used to quantify intramuscular leukocyte infiltration and detect SCs. Gene expression was measured in total muscles and muscle-infiltrating $CD45^+$ cells. In vivo muscle force measurements were used to determine the impact of A3R ablation on physical performance.

We found that RetSat ablation did not affect the body and TA muscle weights. In addition, the structure and the fiber size of the regenerating muscles ultimately were similar in both strains. In accordance with the previous findings, the in vitro phagocytosis assay showed lower phagocytic capacity of the Mϕs in $RetSat^{-/-}$ mice. Parallel with this, we detected decreased milk fat globule-EGF factor 8 protein (MFG-E8), arginase 1, and neuropeptide Y expression and increased IL1-β and nitric oxide synthase expression in muscle-derived $CD45^+$ in $RetSat^{-/-}$ mice. There was a decreased $CD45^+$ cell infiltration in the regenerating muscles of $RetSat^{-/-}$ mice. However, the size of the necrotic areas in the regenerating TA muscles was similar between the two mouse strains. In line with this, we detected a robust MFG-E8 expression in the regenerating TA muscles of both strains. A3R ablation did not affect body and muscle weights, but a higher percentage of bigger muscle fibers was detected in fast twitch muscles of $A3R^{-/-}$ mice, as well as decreased muscle strength in mice. There was an increased $CD45^+$ cell infiltration in the regenerating muscles of $A3R^{-/-}$ mice and these mice exhibited a more rapid clearance of necrotic tissue and a reduced

collagen 1 deposition during TA muscle regeneration. Moreover, we detected a significantly increased myofiber CSA in the regenerating muscles of A3R$^{-/-}$ mice at day 22 post-injury. We have found that in the RetSat$^{-/-}$ mice, there are multiple compensatory mechanisms between the cells that participate in the skeletal muscle regeneration which ultimately results in normal muscle repair in the absence of RetSat enzyme despite the observed decreased Mϕ function. In the case of adenosine A3R, our data support the role of this receptor as a negative regulator of both injury-related regenerative inflammation and muscle fiber growth in the TA muscle. Consequently, the inhibition of A3R may hold therapeutic promise for enhancing skeletal muscle regeneration after injury.

3. Introduction

3.1. Phagocytosis of dead cells

Phagocytosis refers to the cellular process in which particles larger than 0.5 μm including microorganisms and cells in the process of dying are engulfed within a plasma-membrane envelope (Uribe-Querol & Rosales, 2020; Fu & E. Harrison, 2021). Phagocytosis plays a multifaceted role in multicellular organisms, encompassing tasks such as eliminating apoptotic cells (AC), contributing to tissue restructuring, and serving as a vital component of the immune defense mechanism (Yutin, et al., 2009). The primary participants in this process, referred to as professional phagocytes, include macrophages (Mϕs), neutrophils, monocytes, and dendritic cells, which execute phagocytosis efficiently, effectively eliminating microorganisms. Conversely, fibroblasts, epithelial cells, and endothelial cells can also perform phagocytosis but with lower efficiency, classifying them as non-professional phagocytes. Although these non-professional phagocytes cannot ingest microorganisms, they play a crucial role in removing dead cells and preserving the body's internal balance (Uribe-Querol & Rosales, 2020; Rosales & Uribe-Querol, 2017) as every minute, approximately three hundred million cells in the adult human body are thought to undergo the process of cell death (Riegman, et al., 2019). The predominant forms of cell death include apoptosis and necrosis (Krüger & Richter, 2022). The term "apoptosis" signifies programmed cell death, while "necrosis" is regarded as non-programmed or accidental cell death (Yan, et al., 2020). Recent categorizations of necrosis have expanded to include pyroptosis, necroptosis, parthanatos, ferroptosis, oxytosis, NETosis, and secondary necrosis (Westman, et al., 2020). Apoptotic cells exhibit distinct morphological features, including cell shrinkage, fragmentation into membrane-bound apoptotic bodies, and swift phagocytosis by nearby cells (Saraste & Pulkki, 2000). Unlike, necrosis is identified by the swelling of cellular organelles, rupture of the plasma membrane, and subsequent inflammation due to the release of intracellular contents (Chen, et al., 2018)(Figure 1). Without proper phagocytic capability, apoptotic cells are not efficiently removed. Consequently, they progress to late apoptosis, featuring a compromised membrane and structural breakdown. Subsequently, apoptosis transits transition into secondary necrosis, displaying similar characteristics to necrotic cell death (Sachet, et al., 2017; Berghe, et al., 2010). Multiple studies demonstrate that impaired clearance of dead cells, leading to the buildup of secondary necrotic cells, triggers chronic inflammation instead of acute inflammation. This impaired clearance occurs in various chronic conditions, including chronic

granulomatous disease, Sjögren's syndrome, and chronic obstructive pulmonary disease (COPD) (Sachet, et al., 2017).

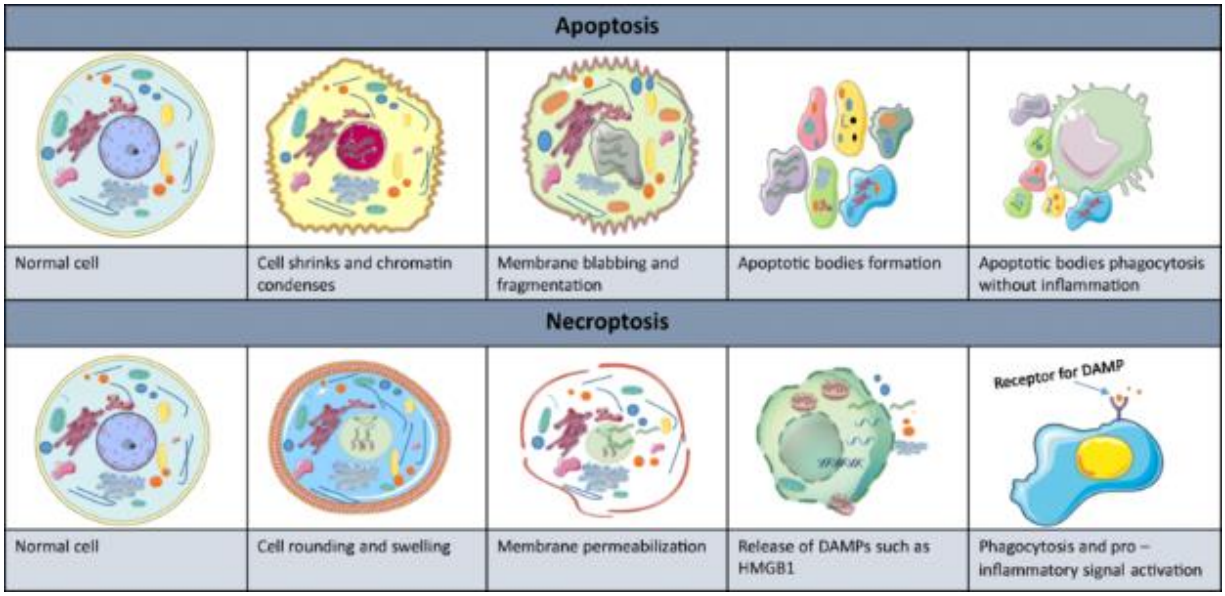

Figure 1: Morphological differences between necrosis and apoptosis cell death. *Apoptosis involves nuclear and cytoplasmic changes, and membrane blebbing, leading to cell fragmentation into apoptotic bodies. Necrosis occurs due to chemical or physical insult, causing cell swelling and immediate membrane damage.* (Sepand, et al., 2020).

Phagocytosis is controlled primarily by three signal types: "find-me", "eat-me", and "don't eat-me" signals (Figure 2). Apoptotic cells secrete "find me" signals such as lysophosphatidylcholine (LPC), sphingosine-1-phosphate (S1P), CX3C motif chemokine ligand 1 (CX3CL1, also referred to as fractalkine), and nucleotides (Adenosine triphosphate (ATP) and Uridine triphosphate (UTP)) to attract the phagocytes to themselves via activating the G protein-coupled receptor (GPCR) G2A, the family of the S1P receptors (S1PR1-5), CX3C motif chemokine receptor 1 (CX3CR1), and purinergic P2Y2 receptor on the phagocyte's surface, respectively (Park & Kim, 2017; Cockram, et al., 2021). Once phagocytes are attracted, they can interact by recognizing "eat-me" signals on the surface of dead cells. The most well-studied "eat-me" signal is the phosphatidylserine displayed on the cell surface. Phosphatidylserine, a phospholipid normally located on the inner membrane of healthy cells, is externalized to the cell surface in response to apoptotic signals (Park & Kim, 2017). Phosphatidylserine can be directly identified by Mϕ receptors, like T-cell immunoglobulin and mucin domain (TIM) family receptors TIM-1/3/4, brain angiogenesis inhibitor-1 (BAI-1), and

stabilin-2 and indirectly such as TAM receptors (Tyro, Axl, and MerTK), formyl peptide receptor 2 (FPR2) or the phosphatidylserine receptor, integrin αvβ3/5 and CD36, via growth arrest-specific 6 (Gas6) and protein S, Annexin A1, milk fat globule-EGF factor 8 protein (MFG-E8) and cellular communication network factor 1 (CCN1) and thrombospondin 1 (TSP1) bridging molecules (Cockram, et al., 2021). The exposure of phosphatidylserine on the cell surface is a common trait shared by both apoptotic cells and necrotic cells, which plays a crucial role in enabling the phagocytosis of these cells (Zargarian, et al., 2017; Cockram, et al., 2021). Interestingly, various bridging molecules, like complement proteins, collectins, and pentraxins, which assist in phosphatidylserine binding for efferocytosis (a term describing the engulfment of apoptotic cells, and their debris by phagocytes which is involved in tissue repair and homeostasis), have also been recognized in the binding of necrotic cells. It has been demonstrated that the presence of complement C1q deposition is a distinctive feature of necrotic debris, absent in apoptotic debris (Westman, et al., 2020). Indeed, annexin A1 serves as another distinct "eat-me" signal, enhancing the phagocytic uptake of necrotic cells (Blume, et al., 2009). Another “eat-me” signal is the Calreticulin (CRT), an endoplasmic reticulum protein. During apoptosis, CRT moves to the cell surface, serving as an eat-me signal to phagocytes through the low-density lipoprotein receptor-related protein 1 (LRP1) receptor. CRT can bind directly to LRP1 or through C1q to trigger phagocytosis (Cockram, et al., 2021). Upon identifying the target particle, phagocytic receptors, trigger signaling pathways that lead to membrane remodeling and regulation of the actin cytoskeleton. This allows the extension of the cell membrane around the particle (Rosales & Uribe-Querol, 2017).

Upon phagocytic uptake of apoptotic cells, phagosomes form and subsequently fuse with primary lysosomes, leading to the formation of phagolysosomes (Levin, et al., 2016). This maturation process enables the phagolysosomes to efficiently degrade apoptotic cells, facilitating the clearance of cellular debris and preventing inflammation. Impaired apoptotic cell phagocytosis and the appearance of secondary necrotic debris can lead to prolonged inflammation and potential autoimmune diseases, including systemic lupus erythematosus (SLE) (Westman, et al., 2020). Efficient engulfment of deceased cells involves not just the presence of "eat-me" signals but also the reduction of surface "don't eat-me" signals (Hochreiter-Hufford & Ravichandran, 2013). Cells employ this type of signal to prevent their uptake by phagocytes. These signals, including CD47, CD31, CD24, Plasminogen activator inhibitor (PAI)-1, MHC class I, and sialic acid residues on the cell surface, inhibit the process (Brown, 2023; Westman, et al., 2020). The importance of CD47 was highlighted by Oldenborg

and colleagues, who noted that when mice were injected with erythrocytes lacking CD47, these cells were eliminated more rapidly by splenic Mϕs than CD47-expressing erythrocytes (Oldenborg, et al., 2000). Kojima and his team signified CD47's role as a "don't eat-me" signal. They showed that when dying cells upregulate CD47 instead of downregulating it, they resist phagocytic clearance, leading to atherosclerotic plaque formation (Kojima, et al., 2016). Apoptotic cells emit signals known as 'keep out' or 'stay away' signals, actively hindering the recruitment of inflammatory cells (Park & Kim, 2017). In a recent study, lactoferrin, a 75 to 80 kDa iron-binding protein, was discovered to function as a repellent signal for apoptotic cells. It hampers neutrophil migration without affecting Mϕs (Bournazou, et al., 2009).

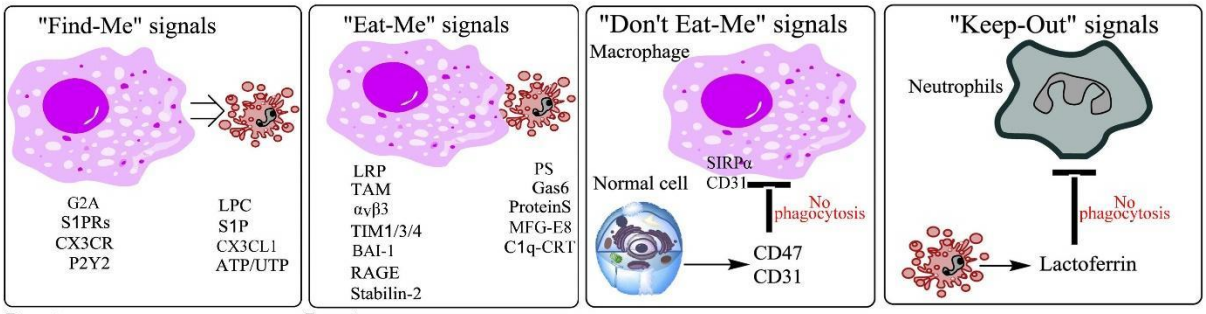

Receptors:
G2A: G protein coupled receptor 132
S1PR: S1P receptor
CX3CR: CX3C motif chemokine receptor
P2Y2: purinergic receptor P2Y2
Ligands:
LPC: lysophosphatidylcholine
S1P: sphingosine-1-phosphate
CX3CL1: CX3C motif chemokine ligand 1
ATP/UTP nucleotides

Receptors:
LRP: Low density lipoprotein receptor-related protein
TAM: Tyro, Axl, MerTK
αvβ3: integrin αvβ3
TIM: T-cell immunoglobulin and mucin domain
BAI-1: brain angiogenesis inhibitor 1
RAGE: receptor for advanced glycation endproducts
SIRPα: signal regulatory protein α
Ligands:
PS: phosphatidylserine
Gas6: growth arrest-specific 6
MFG-E8: milk fat globule-EGF factor 8 protein
CRT: calreticulin

Figure 2: Signals emitted by apoptotic cells and their corresponding receptors in phagocytosis. *"Find-me" signals, including S1P, LPC, nucleotides (ATP or UTP), and CX3CL1, are emitted by apoptotic cells to attract phagocytic cells. These signals interact with receptors (S1PR, G2A, P2Y2, and CX3CR) located on phagocytic cells, guiding them towards the apoptotic cells. Simultaneously, in reaction to apoptotic stimuli, apoptotic cells exhibit surface "eat-me" signals like phosphatidylserine and CRT. Professional phagocytes recognize these signals either directly through receptors or indirectly via bridging molecules. On the contrary, healthy cells display "do not eat-me" signals like CD47 and CD31 on their surfaces to prevent inadvertent phagocytosis. CD47 binds with SIRPa on phagocytes, halting their actin rearrangement, while CD31 generates a repulsive signal between live cells and phagocytes.*

Additionally, apoptotic cells *release lactoferrin as a "keep out" signal, inhibiting the recruitment of granulocytes. (modified from* (Tajbakhsh, et al., 2020)*).*

Phagocytes also possess the ability to detect molecular patterns common to diverse groups of pathogenic microbes. These structures are termed pathogen-associated molecular patterns (PAMPs) and encompass various structures, including unmethylated CpG motifs in DNA, double-stranded RNA (dsRNA), single-stranded RNA (ssRNA), and 5′-triphosphate RNA, lipoproteins, surface glycoproteins, and membrane components like peptidoglycans, lipoteichoic acid, lipopolysaccharide (LPS), and glycosylphosphatidylinositol. These structures can be recognized by pattern recognition receptors (PRRs) on phagocytic cells, and this recognition leads to the activation of Mϕs and subsequently triggers the immune system response aiding the pathogen elimination and restraining pathogen proliferation (Chen, et al., 2018; Tang, et al., 2012; Rai, et al., 2022). Apart from PAMPs, damage-associated molecular patterns (DAMPs) refer to signals released from necrotic cells and are considered internal warning signals to the immune system and cause sterile inflammation. DAMPs are diverse cellular molecules, released due to membrane rupture and influenced by the external environment. These molecules derive from different cellular compartments, including cytosol (e.g., uric acid, heat shock proteins (HSPs), ATP), mitochondria (such as mtDNA, formyl peptides, ATP), nucleus (including high-mobility group box 1 protein (HMGB1), histones, DNA), plasma membrane (e.g., syndecans, glypicans), and endoplasmic reticulum. When released, these DAMPs activate innate immune cells and initiate a robust pro-inflammatory response (Sachet, et al., 2017). For instance, by releasing the nuclear protein HMGB1 into the extracellular space, inflammation is induced as HMGB1 activates the nuclear factor kappa B (NF-κB) pathway through binding with toll-like receptor (TLR)2/4/9, and the receptor for advanced glycation end products (RAGE) (Roh & Sohn, 2018). A recent study found that HMGB1-induced muscle fatigue occurs through the TLR-4 pathway within muscle tissues. This HMGB1-TLR4 pathway is also implicated in the pathogenesis of myositis in patients (Rayavarapu, et al., 2013). In damaged tissues, proteins like HMGB1, HSPs, and histones are recognized by leukocyte receptors TLR2 and TLR4. This recognition activates signaling pathways involving mitogen-activated protein kinases (MAPKs) and inhibitor of nuclear factor kappa B kinase (IKK), leading to increased production of inflammatory cytokines by activated leukocytes through activator protein 1 (AP-1) and NF-κB transcription factors (Tu & Li, 2023).

Inflammation serves as a crucial defense mechanism essential for overall health (Chen, et al., 2018). The inflammatory response comprises two primary stages: the pro-inflammatory phase involving the infiltration of leukocytes to promote inflammation, followed by the anti-inflammatory or resolution phase (Cicchese, et al., 2018). To avoid the shift from acute inflammation to enduring chronic inflammation such as cardiovascular diseases, atherosclerosis, type 2 diabetes, rheumatoid arthritis, and cancers, it is essential to regulate the inflammatory response carefully (Chen, et al., 2018). The anti-inflammatory step requires precisely regulated interactions between diverse non-immune cells and immune cells, including granulocytes, tissue-resident Mϕs, innate lymphoid cells, lymphocytes (Neurath, 2019), myeloid-derived suppressor cells and T_{reg} (Ortega-Gómez, et al., 2013). Soluble mediators, including specialized pro-resolving mediators (SPMs) and anti-inflammatory cytokines like IL-10 and transforming growth factor β (TGF-β), are crucial for orchestrating inflammation resolution. These molecules are produced by various immune cells, including Mϕs and lymphocytes, to regulate the process effectively (Neurath, 2019). One of the initiators of the anti-inflammatory program is the neutrophils undergoing apoptosis after their function at the inflamed site. These cells release SPMs that hinder additional neutrophil recruitment and induce apoptosis, facilitating their clearance by Mϕs (Sugimoto, et al., 2016). This clearance of apoptotic neutrophils initiates a shift from a pro-inflammatory M1 to an anti-inflammatory M2 Mϕ phenotype and it is significant for tissue repair and hemostasis (Ortega-Gómez, et al., 2013). The anti-inflammatory transcriptional program is characterized by the secretion of IL-10 and TGF-β and the downregulation of pro-inflammatory cytokines such as IL-6, (Sugimoto, et al., 2016) IL-1β, and tumor necrosis factor-alpha (TNF-α) (Yu, et al., 2022).

Additionally, the production of SPMs, including lipoxins (e.g., LXA4), resolvins (e.g., RvD1), protectins, maresins, proteins, and peptides (e.g., annexin A1), plays a vital role in facilitating the resolution process (Sugimoto, et al., 2016). Phosphatidylserine binding to its receptors induces the expression of TGF-β which shifts the balance toward an actively anti-inflammatory state, potentially promoting the resolution of inflammation (Huynh, et al., 2002). Effective resolution of inflammation involves not just removing apoptotic cells but also actively suppressing the production of inflammatory mediators. Dysregulation in either process is associated with chronic inflammatory conditions and autoimmune disorders. Phagocytes that clear apoptotic cells release anti-inflammatory cytokines like IL-10, TGF-β, platelet-activating factor, and prostaglandin E2, while concurrently inhibiting pro-inflammatory cytokines, including TNF-α, granulocyte-macrophage colony-stimulating factor (CSF), IL-12, IL-1β, and

IL-18 (Chung, et al., 2006). The switch from the pro-inflammatory M1 phenotype to the anti-inflammatory M2 phenotype is also accompanied by changes in cell surface markers, chemokines, and enzymes. M1 Mϕs exhibit increased levels of cell surface CD80, CD86, and CD16/32 and produce pro-inflammatory cytokines. Later, upon engulfing dying neutrophils, they convert to anti-inflammatory M2 Mϕs, aiding in tissue repair and healing. M2 Mϕs show elevated expression of arginase 1 (Arg1), mannose receptor C type 1 (CD206), and chemokines such as CC chemokine ligand 17 (CCL17) and C-C motif chemokine 22 (CCL22) (Yunna, et al., 2020). Crucial transcription factors like Signal transducer and activator of transcription (STAT)6, interferon regulatory factor (IRF)4, and peroxisome proliferator-activated receptor (PPAR) δ, and γ have been demonstrated to control the activation of M2 genes (Yao, et al., 2019).

3.2. Retinol Saturase enzyme (RetSat)

RetSat is an oxidoreductase enzyme dependent on NADH/NADPH, exhibiting substantial expression in metabolically active tissues including the liver, adipose tissue, intestine, kidneys (Heidenreich, et al., 2017; Weber, et al., 2020; Schupp, et al., 2009; Jiang, et al., 2021) and at a decreased level in skeletal muscle and heart (Weber, et al., 2020; Heidenreich, et al., 2017). Structurally, the protein is composed of 609 amino acids, with a size of around 67 kDa (Figure 3). Its functional domains include an N-terminal signal peptide (amino acids 1–18) for endoplasmic reticulum membrane targeting and a dinucleotide-binding domain (amino acids 73–118), that can bind either FAD or NAD/NADP cofactors (Weber, et al., 2020). This preserved protein sequence remains uniform across homologs in both humans and rodents (Tu, et al., 2022).

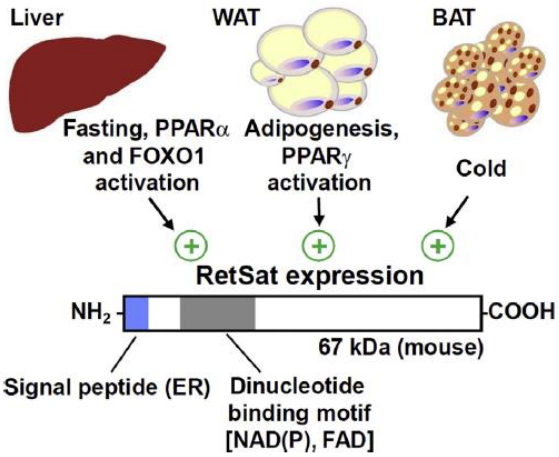

Figure 3: Control of the expression and structural configuration of RetSat. *In rodents RetSat exhibits robust expression in metabolically active organs such as the liver, white adipose tissue, and brown adipose tissue. Its induction occurs in a tissue-specific manner in response to specified conditions and transcriptional regulators. Besides featuring an N-terminal signal peptide guiding the protein to the ER, RetSat contains a dinucleotide binding motif essential for interaction with NAD(P) or FAD.* (Weber, et al., 2020)

Within the endoplasmic reticulum membrane, RetSat catalyzes a specific saturation of the C13–C14 double bond in all-trans-retinol, leading to the synthesis of (13R)-all-trans-13,14-dihydroretinol (Moise, et al., 2004). RetSat expression in human tissues follows a comparable distribution, with the highest levels observed in adipose tissue and the intestine based on databases such as BioGPS and Human Protein Atlas. Detection of RetSat mRNA is observable across various tissues, primary cells, and cultured cell lines. Mice exhibit elevated levels of both mRNA and protein expression primarily in the liver and kidney, followed by brown adipose tissue and white adipose tissue, intestine, and to a lesser degree in skeletal muscle and heart (Weber, et al., 2020). RetSat predominantly localizes to the endoplasmic reticulum through interaction with the endoplasmic reticulum marker disulfide isomerase. Removal of the N-terminal signal peptide disrupts endoplasmic reticulum localization, decreasing protein stability (Weber, et al., 2020). *In vivo* oxidation of all-trans-13,14-dihydroretinol yields all-trans-13,14-dihydroretinoic acid, a potent agonist for the retinoic acid receptor (RAR), and 9-cis-13,14-dihydroretinoic acid, a selective agonist for the retinoid X receptor (RXR) (Moise, et al., 2009). The regulation of RetSat expression is overseen by transcriptional regulators such as PPARα in the liver, PPARγ in adipose tissue, and forkhead box protein O1 (FOXO1) in

primary hepatocytes. This control is exerted through a peroxisome proliferator-activated receptor response element (PPRE) situated in intron 1 of both the murine and human genes (Tu, et al., 2022; Weber, et al., 2020; Schupp, et al., 2009). As it is mentioned, in adipocytes, PPARγ serves as the primary transcriptional regulator for RetSat and the main regulator of adipocyte differentiation. Schupp and colleagues showed that stimulation with the synthetic thiazolidinedione, (PPARγ agonist), increased the expression of RetSat in mature adipocytes (Schupp, et al., 2009).

In type 2 diabetes-related models and human tissues, bioinformatics identified RetSat as the gene with the highest differential mRNA expression, indicating its broad involvement in regulating glucose and fatty acid metabolism (Park, et al., 2009). Several studies, such as those conducted by Schupp et al. (2009) and Heidenreich et al. (2017), have underscored the crucial involvement of RetSat in liver metabolism. Depletion of RetSat in the adipocytes and hepatocytes, has been demonstrated to reduce the activity of carbohydrate response element-binding protein (ChREBP), a sensor for hexose-phosphate and a promoter of lipogenesis, as evidenced by the findings of Heidenreich et al. (2017) (Jiang, et al., 2021). RetSat expression also correlates with liver steatosis in humans and depleting RetSat in the liver reduces triglycerides and improves metabolic parameters in obese mice by interfering with ChREBP activity. These findings suggest a link between RetSat and sugar sensing in hepatocytes (Heidenreich, et al., 2017). Additionally, it is mentioned, that there is a positive correlation between RetSat expression in the liver and body weights in both mice and humans. This aligns with heightened hepatic *de novo* lipogenesis in individuals who are obese and insulin-resistant (Heidenreich, et al., 2017). Even though RetSat-deficient mice demonstrated elevated body weight, their overall and liver-specific insulin sensitivity remained unaffected (Pang, et al., 2017). Furthermore, there is a strong correlation between the expression of RetSat and canonical ChREBP target genes in the human liver. Indeed, RetSat depletion disrupts glucose sensing and ChREBP target gene expression in adipocytes (Weber, et al., 2020). Consistent with Witt and colleagues finding that activating ChREBP enhances adipocyte differentiation through high glucose concentrations or constitutive activation in precursor cells (Witte, et al., 2015), the need for *in vitro* adipocyte differentiation in RetSat might be attributed to its capability to activate ChREBP (Heidenreich, et al., 2017). Collectively, this suggests that RetSat plays a role in hepatic glucose and lipid metabolism, and specific loss-of-function effects have been identified depending on the context (Weber, et al., 2020).. In addition to the aforementioned functions, several studies showed the effect of this enzyme on the function of

Mϕs. Sarang et al. studied RetSat mRNA expression in the mouse thymus and found that inducing thymic apopto-phagocytosis with dexamethasone increased RetSat expression (Sarang, et al., 2014). They also showed deleting RetSat impaired long-term phagocytosis of apoptotic cells by Mϕs, which was rescued by providing the recombinant bridging molecule MFG-E8. Female RetSat knockout mice showed a tendency to develop mild SLE-like autoimmunity with increased spleen weights, delayed clearance of apoptotic cells, and immune complex deposition in organs such as the kidney (Sarang, et al., 2019). Autoimmunity can result from inadequate clearance mechanisms, stemming from the accumulation of apoptotic cells undergoing secondary necrosis and the impaired induction of anti-inflammatory processes during apoptotic cell uptake. Significantly, both MFG-E8 and neuropeptide Y (NPY), the latter not produced by RetSat$^{-/-}$ Mϕs, exhibit anti-inflammatory properties (Dimitrijević, et al., 2008). It is noteworthy that RetSat$^{-/-}$ Mϕs exhibit diminished levels of endogenous CSF-1 and proton-sensing ovarian cancer G-protein-coupled receptor 1 (OGR1, also known as GPR68) (Sarang, et al., 2019), potentially limiting their capacity for M2 polarization. CSF-1 is known to facilitate Mϕ differentiation towards the M2 direction (Martinez, et al., 2006), and Gpr68-deficient Mϕs display reduced expression of M2 markers (Yan, et al., 2014). Notably, the RetSat protein is found in both the endoplasmic reticulum and the nucleus. RetSat plays a role in enhancing heart function and facilitating the adaptation of mammals to hypoxic environments. Tu and colleagues' research has pinpointed RetSat as a shared gene among mammals adapted to high-altitude environments, highlighting its significance in the adaptation to hypoxic environments in mammals. In pancreatic ductal adenocarcinoma cells, they elucidate its supplementary function within the nucleus, where RetSat operates as a protein linked to replication forks. Its expression is enhanced by hypoxia-inducible factor (HIF)-1 α (HIF-1α) signaling. RetSat prevents conflicts between DNA replication and transcription processes, ensuring the integrity of fork restarting, minimizing damage, and inhibiting checkpoint kinase 1 (CHK1) activation, ultimately preventing apoptosis (Tu, et al., 2022). RetSat has been verified to be expressed in stem cells (Weber, et al., 2020), and its expression is regulated by Zinc finger protein X-linked protein (Zfx). Studies by Galan-Caridad and colleagues revealed that RetSat is consistently downregulated in Zfx-null pluripotent embryonic stem cells and hematopoietic stem cells in mice, establishing it as a direct target of Zfx (Galan-Caridad, et al., 2007) and affecting retinoid balance with potential implications for cell proliferation and tumorigenesis. Reduced RetSat levels are observed in certain cancers, suggesting a link to tumor development. However, it is unclear if RetSat loss of function can trigger oncogenic transformation. Additionally, a mutation in RetSat is linked to the

development of undifferentiated tongue sarcoma, and its expression shows a positive correlation with immune cell infiltration in tumors (Weber, et al., 2020). Jiang et al. findings suggest that RetSat may function as a tumor suppressor in various types of human cancers (Jiang, et al., 2021). RetSat is commonly underexpressed in different human cancers, and its diminished levels are correlated with unfavorable clinical outcomes. Elevated RetSat expression is positively correlated with increased immune infiltration in various human cancers. The promoter region of RetSat is extensively methylated in tumor tissues, resulting in diminished expression compared to normal tissues. Moreover, RetSat knockdown increases cell proliferation, while its overexpression inhibits proliferation *in vitro* in both mouse embryonic fibroblasts and B16 cells. Additionally, mice with the homozygous Q247R mutation in the RetSat gene demonstrate enhanced resistance to xenograft tumors and cutaneous keratinocyte carcinoma formation compared to their littermate wild-type counterparts (Jiang, et al., 2021). Apart from its other roles, RetSat protects fibroblasts against oxidative stress induced by ultraviolet (UV) or paraquat exposure, indicating that the absence of RetSat specifically enhances resistance to damage caused by peroxides (Tu, et al., 2022; Nagaoka-Yasuda, et al., 2007). Independent of retinol saturation, RetSat governs the cellular response to oxidative stress. RetSat has consistently been proven to regulate sensitivity to peroxides and the generation of reactive oxygen species (ROS) in both cells and the liver of mice (Weber, et al., 2020). RetSat was identified as a key regulator of oxidative stress sensitivity through an RNA interference screen in NIH3T3 cells. Depletion of RetSat significantly boosted cell viability when exposed to tert-butyl hydroperoxide or H_2O_2 (Nagaoka-Yasuda, et al., 2007). In brief, this enzyme has diverse biological functions such as influence on adipocyte differentiation, hepatic glucose and lipid metabolism, Mϕ function, vision, and ROS generation.

3.3. Neuropeptide Y (NPY)

NPY, a highly prevalent neuropeptide in the body, is extensively distributed throughout both the central and peripheral nervous systems (Zhang, et al., 2021). NPY plays a regulatory role in various physiological processes, including brain activity, stress resilience, digestion, blood pressure, heart rate, metabolism, and immune functions (Thorsell & Mathé, 2017). NPY exhibits prominent anti-inflammatory properties (Chen, et al., 2020). It acts on the Y1R receptor to suppress the release of interleukin-6 (IL-6) (Straub, et al., 2000). Blocking the Y1R signal reduces IL-12 production, and Y1R-knockout macrophages exhibit an increased response to inflammatory stimuli (M1 phenotype) while maintaining their alternative activation

phenotype (M2 phenotype) (Chen, et al., 2020). NPY induces a shift in macrophages towards the M2-like phenotype, with NPY (10^{-6} M) predominantly stimulating the secretion of anti-inflammatory cytokines such as IL-10 and IL-1RA, while inhibiting the release of pro-inflammatory cytokines such as TNF-α, IL-12, and IL-6 (Buttari, et al., 2017).

3.4. Adenosine receptors

Adenosine, derived predominantly from the metabolic breakdown of ATP, exerts diverse functions throughout the body (Sheth, et al., 2014). Adenosine elicits a range of physiological effects by engaging and activating specific adenosine receptors (ARs) located on the cell surface (Sheth, et al., 2014; Zhao, et al., 2002). ARs are extensively distributed throughout the body, and their ubiquitous presence in virtually all cells renders them a compelling target for pharmacological intervention in various pathophysiological conditions associated with elevated adenosine levels (Borea, et al., 2015) like ischemia, hypoxia, inflammation, and trauma (Nishat, et al., 2016). These receptors belong to the GPCR superfamily. They are categorized into four subtypes: adenosine A1 receptor (A1R), adenosine A2a receptor (A2aR), adenosine A2b receptor (A2bR), and adenosine A3 receptor (A3R) (Sheth, et al., 2014; Zhao, et al., 2002; Borea, et al., 2015) (Figure 4).

Structurally, they possess a seven-transmembrane alpha-helical structure with an extracellular amino-terminus and an intracellular carboxy-terminus. The N-terminal domain, with N-glycosylation sites, influences receptor trafficking to the plasma membrane. The carboxy terminus contains phosphorylation sites for protein kinases, enabling receptor desensitization. Additionally, both the carboxy-terminus and the third intracellular loop facilitate the coupling of ARs to G proteins (Sheth, et al., 2014). Among humans, there is a 49% sequence similarity between A1 and A3 ARs, and a 59% sequence similarity between A2a and A2b ARs (Nishat, et al., 2016). ARs exhibit distinctions in three aspects: 1) their adenosine affinity, 2) the types of G proteins they recruit, and 3) the downstream signaling pathways they activate in target cells (Sheth, et al., 2014; Borea, et al., 2015). The affinity of A1 and A2a ARs for adenosine is notably high, around 70 and 150 nM, respectively. In contrast, A2b and A3 receptors have considerably lower affinities for adenosine, approximately 5100 and 6500 nM, respectively (Bynoe, et al., 2015). This distinction in affinity levels contributes to the varying sensitivity and responsiveness of these receptors to adenosine concentrations in physiological processes. A1 and A3 ARs are associated with Gi protein,

whereas A2a and A2b ARs are linked to Gs protein (Zhong, et al., 2022). The activation of A2a and A2b ARs promotes cyclic AMP production, subsequent activation of protein kinase A (PKA), and phosphorylation of the cyclic AMP response element-binding protein (CREB). In contrast, the activation of A1 and A3 ARs hinders cyclic AMP production, leading to reduced PKA activity and CREB phosphorylation (Sheth, et al., 2014)..

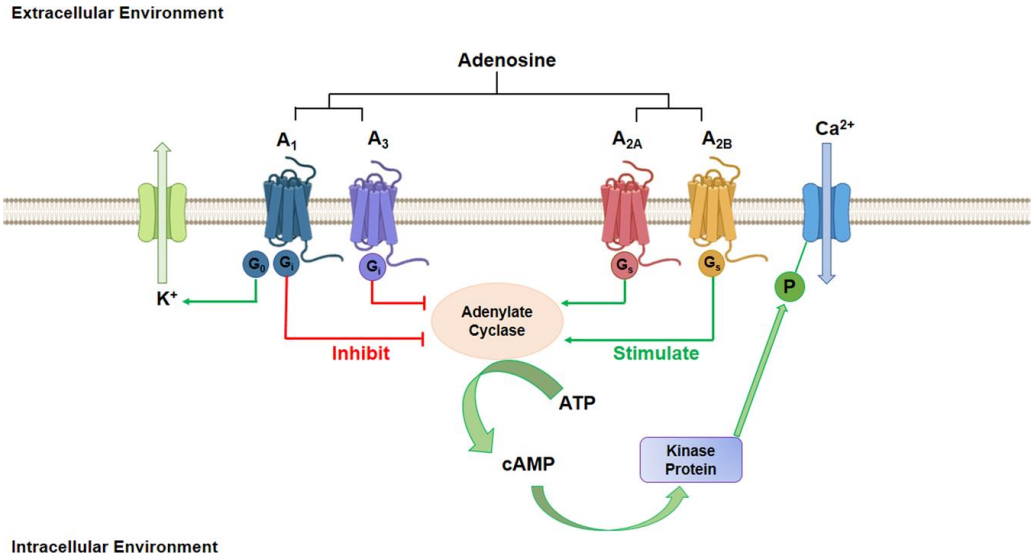

Figure 4: Schematic representation of ARs. *Under normal physiological conditions, adenosine activates four G-protein coupled receptors—A1, A2a, A2b, and A3—mainly associated with adenylate cyclase activation and inhibition. The buildup of cAMP is connected to the regulation of ion-channel activity* (Mazziotta, et al., 2022).

Adenosine serves as an endogenous regulator of monocyte-macrophage functions, initially promoting the release of significant amounts of inflammatory mediators during the early stages of inflammation and subsequently contributing to the resolution of this process (Borea, et al., 2015).

Several studies have highlighted the therapeutic potential of ARs as targets. Over the past two decades, progress in medicinal chemistry has led to the creation of agonists and antagonists distinguished by high affinity and outstanding selectivity for the human variants of all four receptors (Chen, et al., 2013). Countless studies have been conducted on the function of these receptors to date. For instance, the compelling evidence linking A2b receptor activation to inflammation in humans and rodents, along with the effective use of A2b receptor antagonism in stopping disease progression in rodents, indicates that A2b antagonists may be

a promising treatment for asthma and COPD in humans. Enprofylline, an anti-asthmatic agent, acts as a known, though not highly potent, A2b receptor antagonist (Haskó, et al., 2008).

Reportedly, BAY 60–6583, a selective human A2bR agonist, has shown promise in addressing ischemia, inflammation, diabetes, and asthma (Saini, et al., 2022). Additionally, it has been found to enhance the antitumor function of Chimeric Antigen Receptor (Tang, et al., 2021). Additionally, in the mouse model, inflammation and hyperplasia were alleviated by the selective and potent A3R antagonist PSB-10. IB-MECA, Cl-IB-MECA, and LJ-529, which are selective agonists of the human A3R receptor currently undergoing clinical development for the treatment of autoimmune diseases, liver conditions, and cardioprotection (Saini, et al., 2022). In a murine model of heart attack, the A3-specific agonist CP-532,903 demonstrated a safeguarding effect against damage caused by myocardial ischemia and reperfusion (Wan, et al., 2008).

3.4.1. Adenosine A3 receptor (A3R)

The gene for A3R is situated on human chromosome 1 p21–p13 and the produced protein encompasses a total of 318 amino acid residues (Borea, et al., 2015; Jacobson, et al., 2018). A3Rs are distributed in various cell types, including enteric neurons, epithelial cells, colon mucosa, lung parenchyma cells, chondrocytes, and osteoblasts. Moreover, they are found in cells associated with inflammatory processes, such as mast cells, eosinophils, neutrophils, monocytes, Mϕs, dendritic cells, lymphocytes, and bone marrow cells (Mazziotta, et al., 2022). In the neutrophils, the A3R assumes a pivotal role in modulating cell behavior. This modulation involves the inhibition of the oxidative burst and chemotaxis, thereby imparting anti-inflammatory effects (Borea, et al., 2015). Additionally, it has been demonstrated that rapid hydrolysis of released ATP by neutrophils leads to the generation of adenosine. This adenosine, in turn, acts through A3Rs, which are recruited to the leading edge, facilitating the promotion of cell migration (Chen, et al., 2006).

Adenosine plays a regulatory role in the functions of monocytes and Mϕs as well, contributing to both the production of inflammatory mediators and the induction of resolution. For instance, the activation of A3R inhibits the expression of various genes, including those involved in the respiratory burst, IL-1β, TNF-α, chemokine macrophage inflammatory protein (MIP) 1α, IRF 1, inducible nitric oxide (NO) synthase (iNOS), and CD36 (Jacobson, et al.,

2018). Moreover, Joós and his co-workers found that the lack of A3R signaling hinders the chemotactic navigation of Mϕs. While the phagocytic capacity remains unaltered, $A3R^{-/-}$ Mϕs displayed delayed clearance of intraperitoneally-injected apoptotic thymocytes *in vivo*. This underscores the significance of macrophage A3Rs in ensuring proper chemotactic navigation and subsequent *in vivo* clearance of apoptotic cells (Joós, et al., 2017). In another study, Duró and her colleagues investigated whether A3R regulates the AC-induced anti-inflammatory response in Mϕs. Their findings highlight the essential role of A3Rs in proper Mϕ chemotaxis. In Mϕs engulfing apoptotic cells, the initial activation of both A2aRs and A3Rs by adenosine establishes a balance, influencing the strength of adenylate cyclase signaling and subsequently affecting the degree of suppression of chemoattractant formation induced by apoptotic cells (Duró, et al., 2014).

Highly selective agonists targeting A3R effectively suppress the production of inflammatory cytokines by downregulating NF-κB. The NF-κB pathway, a classic pro-inflammatory signaling pathway, involves a transcription factor that induces the production of key pro-inflammatory cytokines such as TNF-α, IL-1, and IL-6. These cytokines play crucial roles in the pathogenesis of conditions like rheumatoid arthritis, inflammatory bowel disease, asthma, and COPD, impacting leukocyte recruitment and cell survival (Cohen & Fishman, 2019). It has been reported, that the activation of A3R influences various mast cell functions in both rodents and humans. These effects encompass degranulation, apoptosis, and the regulation of vasopermeability (Borea, et al., 2015). Animal models have definitively confirmed that the A3R is primarily responsible for mediating hypersensitivity to adenosine in mast cells, although the contribution of the A2bR has also been validated (Rudich, et al., 2012). In this regard, Ramkuma and his team identified A3R in RBL-2H3 mast cell, cell line as the main target for adenosine. Activation of these receptors enhances antigen-induced secretory responses, suggesting a potential role in mediating asthmatic attacks and allergic responses triggered by IgE receptor cross-linking on mast cells (Ramkumar, et al., 1993).

In recent findings, A3Rs have been identified as overexpressed in various autoimmune disorders like Crohn's disease and psoriasis. The observed upregulation in these pathologies is linked to the accumulation of adenosine in the extracellular environment, particularly under conditions of stress. Notably, many transcription factors, including NF-κB and CREB, known for promoting inflammation, exhibit an inverse association with the upregulation of A3R (Borea, et al., 2015). Activation of A3R also leads to the suppression of phosphatidylinositol

3' -kinase (PI3K)/Akt, causing a subsequent disruption of NF-κB and MAPK signaling pathways, resulting in both anti-inflammatory and anticancer effects (Cohen & Fishman, 2019).

Several investigations have indicated an upregulation of A3R in cancer (Mazziotta, et al., 2022). Moreover, considerable elevation in A3R protein expression was noted across various cancer cell lines (Borea, et al., 2015). However, the role of A3R in controlling cell proliferation and death is a debated issue, varying based on the tissue type in which it is expressed. Laboratory models suggest that low concentrations of selective synthetic A3R agonists in the nanomolar range protect against cell death in normal cells However, at higher concentrations in the micromolar range, these A3R agonists exhibit pro-apoptotic effects in both normal and tumor cells (Mazziotta, et al., 2022).

3.4.2. ARs in skeletal muscle

ARs are suggested to play a crucial role in regulating key physiological processes in skeletal muscle, including glucose uptake, contraction, and blood flow. Lynge and Hellsten found that A1Rs, A2aRs, and A2bRs were localized to vascular smooth muscle and endothelial cells. Notably, only the A2aR and A2bR were identified in the plasma membrane and cytosol of skeletal muscle (Lynge & Hellsten, 2000). Bryan and Marshalls' research marks the initial evidence of the presence of both A1R and A2aR receptors in rat hindlimb skeletal muscle, facilitating muscle vasodilation. However, their findings suggest that the vasodilation occurring in muscle during systemic hypoxia is primarily mediated by the adenosine A1 receptor (Bryan & Marshall, 1999).

Adenosine receptor signaling pathways were shown to regulate skeletal muscle homeostasis. The data presented by Gnad and colleagues reveal the pivotal role of the adenosine/A2b signaling pathway in upholding skeletal muscle mass and functionality. Activating A2bR not only alleviated age-related and obesity-induced sarcopenia but also restored the function and mass of skeletal muscle to levels similar to those observed in juveniles (Gnad, et al., 2020).

Multiple pieces of evidence distinctly outline the cytoprotective function of A1Rs, A2aRs, and A3Rs. The A3R can provide robust cytoprotection for skeletal muscle during ischemia and reperfusion injury. Specifically, the A3R, distinct from the A1R or A2aR, utilizes phospholipase C (PLC)-β2/β3 signaling pathways to confer its protective effects on skeletal

muscle (Zheng, et al., 2007). Urso and colleagues suggest that activation of the adenosine A3 receptor shields skeletal muscle from physical injury by modulating MMP/TIMP signaling, which reduces damage to muscle fibers observed 24 hours after injury. These protective effects are attributed to the actions of Cl-IBMECA during the early stages of inflammation (Urso, et al., 2012). In addition, the utilization of PLC-β2/β3 knockout mice revealed that the adenosine A3 receptor-mediated protection against ischemia in skeletal muscle operates through this specific phospholipase isoform. Conversely, the protective effects of adenosine A1 and A2A receptors do not require the involvement of this PLC (Liang, et al., 2009). Interestingly, Dixon and his colleagues showed the mRNA for the A3R was not found in skeletal muscle (Dixon, et al., 1996). Furthermore, it has been shown that both A2bR and A3R are present in the nerve terminal and muscle cells at the neuromuscular junctions (NMJs) (Garcia, et al., 2014).

3.5. Skeletal Muscle Tissue and Anatomy

Skeletal muscle is a vital player in many bodily functions, primarily serving as a mechanical powerhouse, converting chemical energy into force for posture, movement, and overall well-being (Lee & Jun, 2019; Frontera & Ochala, 2015). Skeletal muscle, comprising approximately 40% to 45% of the total body weight, not only constitutes the most significant portion of bodily tissues but also ranks as one of its most versatile and adaptable components (Lee & Jun, 2019; Frontera & Ochala, 2015; Karagounis & Hawley, 2010).

Skeletal muscle, as a composite structure, is primarily constituted by muscle cells and myofibers, accompanied by nerves, blood vessels, and an extracellular connective tissue matrix (Gillies & L. Lieber, 2011). Based on their position within the body's structure, the skeletal muscle extracellular matrix (ECM) is classified into endomysium, perimysium, and epimysium (Chapman, et al., 2016). Individual myofibers are ensheathed by a connective tissue layer termed endomysium. These myofibers are further organized into fascicles, or bundles, which are enveloped by the perimysium. Finally, the outermost layer, known as the epimysium, encircles the entire skeletal muscle (Chapman, et al., 2016; Frontera & Ochala, 2015; Purslow, 2020). A single muscle cell, also called a multinucleated myofiber, is made up of similar contractile units, referred to as sarcomeres, which are predominantly composed of actin (a major component of the thin myofilament) and myosin, found in the thick myofilament protein that collectively account for approximately 80% of the protein content in the sarcomere (Frontera & Ochala, 2015; Squire, 1997) (Figure 5). Satellite cells, positioned within the

interstitial space between the sarcolemma and the basal lamina, serve as the adult stem cells of skeletal muscle, intricately involved in the mechanisms of muscular development, repair, and regeneration (Frontera & Ochala, 2015). Apart from myofibers, skeletal muscle includes different cell types that provide crucial support for tissue structure and health. Among these, fibroblasts are particularly significant. Although they constitute a minority of skeletal muscle cells, fibroblasts are responsible for producing most of the ECM found in the interstitial spaces between muscle fibers. Their role extends beyond structural maintenance and has implications in fibrosis (Chapman, et al., 2016). Skeletal muscle fibroblasts have been actively participating in the development and control of the ECM within skeletal muscle tissue (L.Mendias, 2017).

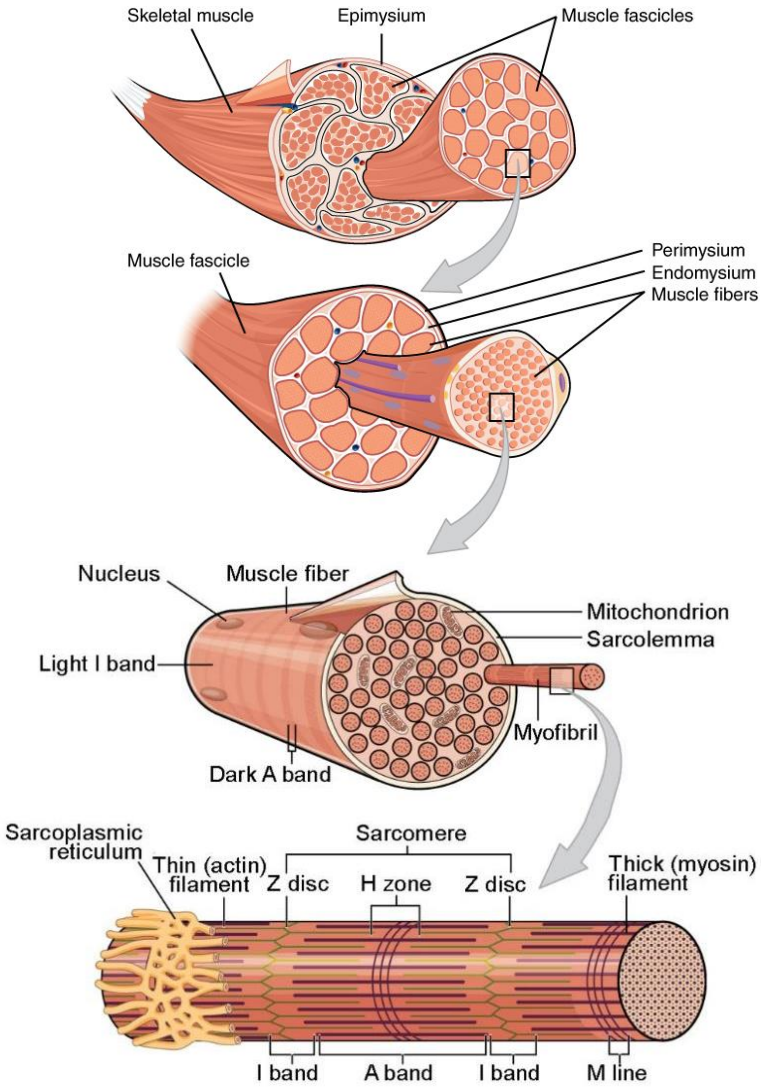

Figure 5: The structure and ultra-structure of skeletal muscle. *This representation diagram illustrates the hierarchical arrangement of structures in skeletal muscles. The standard configuration of individual muscle cells, along with the encompassing layers of connective tissue like epimysium, perimysium, and endomysium, alongside the myofibrils contained within*

the muscle. Myofiber bundles, known as fascicles, merge to form muscle tissue. The illustration depicts a mature muscle fiber as a grouping of myofibrils enveloped by the sarcolemma. The sarcoplasmic reticulum surrounds the fibrils, intertwining with transverse tubules (T-tubules) to form a network. Sarcomeres, the basic functional units of muscle contraction, comprise A-bands, I-bands, H-bands, Z-discs (Z-lines), and M-lines. The central bipolar thick filaments, mainly consisting of myosin, are surrounded by six parallel thin filaments originating from the Z-discs located at both ends of the sarcomere. (Sayed, et al., 2023).

3.6. Injury models

Skeletal muscle, being the primary muscle tissue in the body, is prone to various types of injuries; however, it exhibits a strong inherent ability to self-repair after injury (Laumonier & Menetrey, 2016). The ability to regenerate may be restricted by conditions such as muscular dystrophy or the natural process of aging (Garry, et al., 2016). Studying muscle regeneration *in vivo* frequently involves the application of physical injuries induced by methods like freezing and crushing, as well as chemical injuries inflicted by myotoxic substances like cardiotoxin (CTX) or notexin (NTX), in addition to other chemical compounds like barium chloride (BaCl2). (Forcina, et al., 2020; Hardy, et al., 2016). Among them, CTX injection is a widely used, reproducible method to initiate muscle damage and subsequent regeneration (Musarò, 2014). CTX induces specific damage to muscle fibers while mostly preserving the morphological integrity of satellite cells, nerves, and vascular endothelial cells (Wang, et al., 2022; Hirata, et al., 2003). Structurally, CTXs are composed of short polypeptide chains containing 60–63 amino acid residues, originating from the venom of either the Indian cobra snake “Naja naja” or the African cobra “Naja mossambica” (Forcina, et al., 2020). Regarding its functional role, by serving as a protein kinase C-specific inhibitor, CTX initiates localized myonecrosis and subsequent muscle regeneration (Figure 6). It also disrupts cell membrane integrity, possibly inducing pore formation. These pores could cause membrane depolarization and Ca^{2+} influx, resulting in intense muscle contractions, myofiber breakdown, and acute muscle injury (Musarò, 2014; Fu, et al., 2023). The initiation of necrotic degeneration marks the onset of a cascading process involving the release of DAMPs which attracts inflammatory cells, setting the stage for the initiation of a robust inflammatory response (Zhang, et al., 2010). CTX injury models cause less harm to animals than invasive crushing models, which carry infection risks (Wang, et al., 2022). Observations indicate that CTX exhibits a toxicity level

four times lower than that of NTX (Forcina, et al., 2020). According to Hardy and co-workers, the kinetics of infiltrating cells in the CTX injury model closely resembled those seen in other injury models. Even though, significant differences were observed in cytokine production. In the CTX group, cytokine expression returned to normal after muscle regeneration, whereas in other models, cytokine levels stayed elevated despite normal muscle appearance (Hardy, et al., 2016). Moreover, the appearance of newly regenerating myotubes featuring central nuclei becomes noticeable as early as four days after CTX injection, while the presence induced by NTX is observable only after seven days following the injury (Forcina, et al., 2020). The creation of muscle injury models, such as the CTX model, plays a pivotal role in unraveling the intricate queries and mechanistic intricacies that underlie skeletal muscle regeneration, maintenance of homeostasis, and the remarkable adaptability of these muscular tissues.

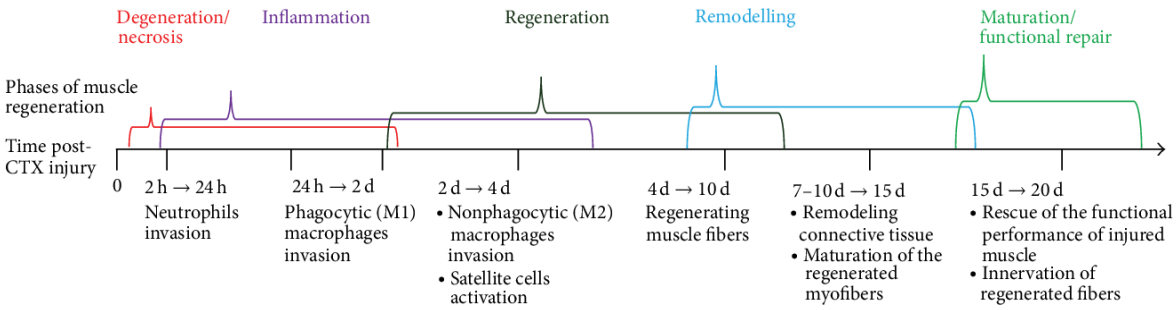

Figure 6: The stages of muscle regeneration and the timing of immune cell influx following CTX injection. *Following the administration of cardiotoxin, neutrophils begin infiltrating between necrotic fibers within a short time frame. By 24 hours post-injection, both neutrophils and macrophages are present in the inflammatory response. During this period, there is heightened phagocytic activity directed towards necrotic myofibers. On the second day after treatment, spindle-shaped mononucleated cells, necrotic debris, leukocytes, and various macrophage types are observable. New myofibers subsequently emerge within the following day, and by 7-10 days post-injection, there is partial restoration of muscle architecture, though most regenerated myofibers are smaller and contain centrally located myonuclei. The progressive maturation of regenerating myofibers continues until approximately 15 days post-injection* (Musarò, 2014).

Muscle injuries can be classified into mild, moderate, or severe depending on the degree of functional impairment they cause. The range of muscle injuries can vary from affecting only some muscle fibers to a complete loss of muscle function (Järvinen, et al., 2005; Fernandes, et

al., 2015). After muscle injury, a complex cascade occurs involving the disruption of the myofiber sarcolemma, leading to heightened myofiber permeability. Consequently, there is an elevation in serum levels of muscle proteins, notably creatine kinase, as these proteins are typically confined to the myofiber cytosol (Karalaki, et al., 2009). Necrosis encompasses the entry of calcium ions, the disintegration of the plasmalemma, the loss of myonuclear and contractile material, and the dissolution of cellular organelles. These processes collectively result in the formation of amorphous debris within the damaged muscle tissue. Necrotic fibers, appearing pale and enlarged, undergo internal structural modifications, including altered architecture and the presence of internal nuclei, potentially indicating invasion of immune cells including neutrophils and Mϕs in conjunction with various other cell types, initiate the recuperative process for the injured muscle, commonly referred to as muscle regeneration. Muscle regeneration is a dynamic process encompassing five interrelated and time-dependent phases: degeneration (myonecrosis), inflammation, regeneration, remodeling, and maturation/functional repair (Musarò, 2014).

3.7. Myogenic and non-myogenic cell involvement in muscle regeneration

3.7.1. Satellite cells and myoblasts

Within muscle tissue, satellite cells make up between 2% and 10% of the total myonuclei population (Dumont, et al., 2015). Despite their relatively small number, these cells are essential for both muscle regeneration and maintenance (Hwang & Brack, 2018; Cutler, et al., 2022). Indeed, the lack of satellite cells leads to the total halt of muscle regeneration (Cutler, et al., 2022). Muscle type, age, and species are the factors that can influence the percentage of satellite cells within muscle tissue (Dumont, et al., 2015). They can be found within an asymmetric environment positioned between the basal lamina and the myofiber membrane throughout the entire length of myofibers (Cutler, et al., 2022; Mauro, 1961). Homeostatic muscles keep satellite cells dormant, but upon injury, satellite cells initially migrate to the damaged area, subsequently leading to increased mitotic activity at that location (Schultz, et al., 1985). Alfaro and colleagues report that the cell surface sialomucin CD34, beyond being a stem cell marker, also assists in their mobility. In mice lacking CD34, satellite cell migration along myofibers is diminished, hampering muscle regeneration (Alfaro, et al., 2011). The activated satellite cells exit the quiescent state, and set in motion a series of events involving proliferation, differentiation, and ultimate fusion, thereby repairing damaged muscle tissue

(Cutler, et al., 2022; Fukada, et al., 2022; Dumont, et al., 2015; Yablonka-Reuveni, et al., 2008; Sousa-Victor, et al., 2022).

In the process of muscle regeneration, not all activated satellite cells undergo full differentiation. Some revert to a dormant state, replenishing the stem cell pool for potential future injuries (Dumont, et al., 2015; Sousa-Victor, et al., 2022; Collins, et al., 2005). Satellite cells can be divided into those committed to myogenic progenitors and those with greater self-renewal potential (Dumont, et al., 2015). Numerous proteins have been identified as markers for satellite cells. These include nuclear proteins like paired type Paired box transcription factor 3 (PAX3) and PAX7 (Kassar-Duchossoy, et al., 2005), as well as specific transcription factors such as Myogenic factor5 (Myf5) and myoblast determination protein1 (MyoD), which are expressed exclusively in myogenic cells but not in quiescent satellite cells (Dumont, et al., 2015). Additionally, various cell surface membrane proteins have been recognized as markers for satellite cells, including M-cadherin, α7- and β1-integrins, c-Met, CXCR4, syndecan-3 and -4, calcitonin receptor, calveolin-1, CD34, VCAM1, and NCAM1 (Gnocchi, et al., 2009; Fukada, et al., 2007).

The embryonic and adult myogenesis during regeneration are orchestrated by common regulatory factors and involve similar signaling pathways (Dumont, et al., 2015). The Myogenic Regulatory Factors (MRFS), including Myf5, MyoD, myogenic factor 6 (Mrf4), and myogenic factor 4 (myogenin) are a group of transcription factors from the basic helix-loop-helix family that play crucial roles in the determination and differentiating of skeletal muscle cells during both embryonic development and postnatal myogenesis (Figure 7). These factors work together at various stages of muscle development to establish the skeletal muscle phenotype, regulating cell proliferation, causing precursor cells to exit the cell cycle permanently, and activating genes necessary for muscle differentiation and sarcomere assembly (Hernández-Hernández, et al., 2017). The initial myogenic transcription factors expressed in muscle progenitors are Pax3 and Pax7 (Buckingham & Relaix, 2015; Soleimani, et al., 2012). Lineage tracing shows Pax3 positive cells are vital for embryonic myogenesis, while Pax7 positive cells are key for late fetal and postnatal myogenesis (Hutcheson, et al., 2009). The regulation of satellite cells' division and differentiation falls under the purview of the Pax7 protein (Seale, et al., 2000). Satellite cells undergoing division produce MRFs (Kaczmarek, et al., 2021). Myf5 deletion doesn't affect initial satellite cell numbers, but *in vivo* studies show these cells are more likely to become fibroblasts or adipocytes rather than

myofibers (Gayraud-Morel, et al., 2007). Myf5 and MyoD are pivotal for determining myogenic cell fate. The simultaneous knocking out of both Myf5 and MyoD in mice results in the lack of myogenin expression and leads to the complete absence of skeletal muscle formation (Dumont, et al., 2015).

Megeney and colleagues found that cell division takes place normally in MyoD-deficient mice, but these myoblasts fail to differentiate and progress into mature muscle cells (Megeney, et al., 1996). Myogenin is crucial for the final differentiation of myogenic cells. Its absence leads to severe muscle deficiency and early death in mice (Hasty, et al., 1993). In the end, myocytes combine to form multi-nucleated myotubes or merge with injured myofibers. This leads to a reduction in MyoD levels and the commencement of myosin heavy chain (MYHC) and other contractile protein expressions, facilitating the maturation phase during muscle regeneration to create the functional units of skeletal muscle (Dumont, et al., 2015). In mice, newly regenerated muscle fibers appear 5-7 days after injury, initially thinner with central nuclei, later moving nuclei to the periphery during maturation (Kaczmarek, et al., 2021).

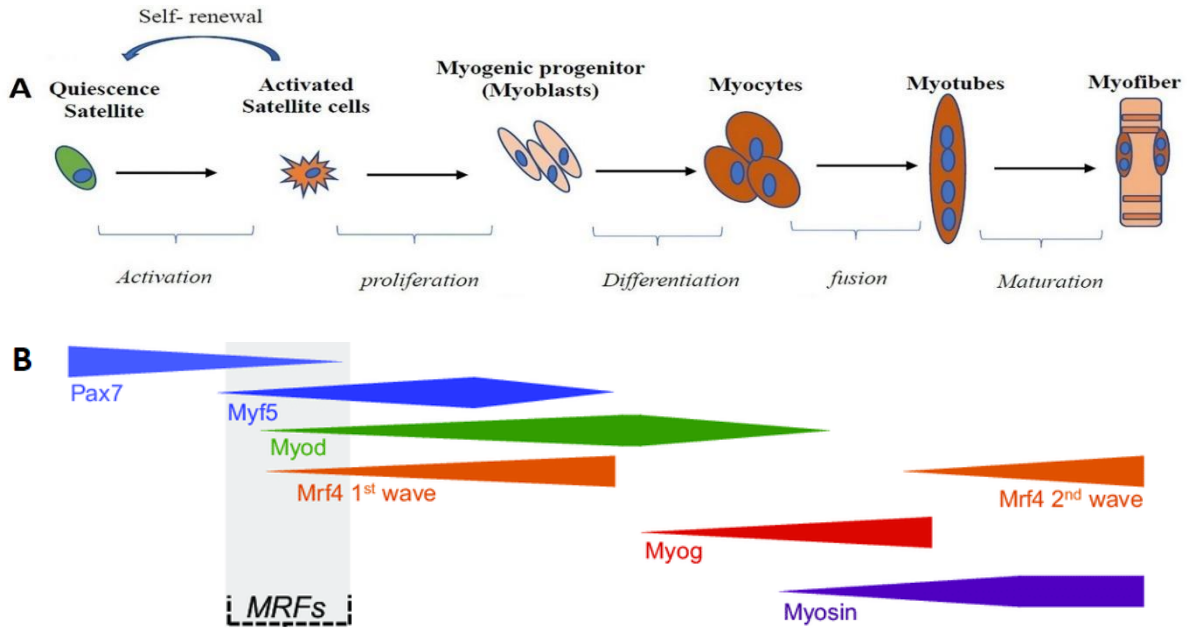

Figure 7: The development of the myogenic lineage and the patterns of expression of crucial myogenic regulators. *(A) The schematic diagram outlines the stages of myogenic lineage development. Following satellite cell activation, cells undergo proliferation, leading to the generation of myogenic progenitor cells. These precursor cells then develop into myocytes, which further merge to create myotubes. Eventually, myotubes mature into myofibers, the fundamental contractile components of skeletal muscle* (Isesele & Mazurak, 2021). *(B) The*

depicted expression profile encompasses major regulators crucial for myogenic lineage development, including myogenic regulatory factors (MRFs) like Myog (myogenic factor 4), Mrf4, Myf5, MyoD, and Pax7 (Sambasivan, et al., 2013).

3.7.2. Myoblast fusion

Cell fusion is a fundamental phenomenon in various biological processes, encompassing sperm-egg fertilization, Mϕ activity, and the formation of bones, placenta, and skeletal muscles (Horsley & Pavlath, 2004; Millay, et al., 2016). The fusion of myoblasts is essential not just for the initial growth and development of muscles in embryos but also for the subsequent regeneration and repair of myofibers following injuries (McColl, et al., 2016; Hindi, et al., 2013). This complex process comprises a sequence of stages, starting with cell recognition, followed by migration, adhesion, signaling, cytoskeletal alterations, and culminating in membrane coalescence (Abmayr & Pavlath, 2012; Lehka & Rędowicz, 2020; Millay, et al., 2016). This process during myogenesis leads to the fusion of mononucleated muscle cells to form multinucleated myofiber (skeletal muscle unit) and the addition of myoblast to existing myofibers thereby increasing the myonuclei pool to facilitate muscle growth (Sampath, et al., 2018). Cell fusion is regulated by several proteins and lipids, which play a crucial role in preparing the cells for fusion (Gamagea, et al., 2022). Myomaker and myomerger regulated by MyoD and myogenin transcription factors, are the two muscle-specific proteins that drive the membrane-remodeling process in myoblast fusion (Sampath, et al., 2018). It is demonstrated that myoblasts from myomaker null mice can differentiate into myocytes but lack the capacity for fusion (Millay, et al., 2016). In addition, the specific elimination of myomaker in satellite cells results in a complete cessation of muscle regeneration (Kim, et al., 2015). Myomaker was found to be essential for the fusion process in both cells involved, while myomerger has a role only in one of the fusing cells (Sampath, et al., 2018).

These membrane-bound proteins work individually to modify cell membranes, facilitating fusion. Myomaker operates at or before the merging of the outer layers of the two membranes (hemifusion), while myomerger regulates pore formation, ensuring the completion of the fusion process (Leikina, et al., 2018; Gamagea, et al., 2022). Defects in myoblast fusion and congenital myopathy are observed in individuals with mutations in the myomaker gene (Sampath, et al., 2018). Among the various factors contributing to fusion, calcium is the key

element whose intracellular concentration significantly impacts myoblast fusion. Studies showed that decreasing the Ca^{2+} level inhibits rat myoblast fusion, potentially disrupting actomyosin contractility and migratory functions regulated through Ca^{2+}-calmodulin pathways (Constantin, et al., 1996; Wakelam, 1985). It's important to note that lipids and their membrane positioning and quantities are vital for fusion (Lehka & Rędowicz, 2020). Among these, phosphatidylserine plays a central role in membrane fusion in myoblasts, osteoclasts, trophoblasts, and HIV virus-cell fusion (Gamagea, et al., 2022). *In vitro* studies in mouse C2C12 myoblast showed that transient exposure of phosphatidylserine on the cell surface is required for proper myoblast fusion (Eijnde, et al., 2001). During the early stages of myoblast fusion, the activation of phosphatidylserine receptors, BAI proteins, and Stabilin-2, leads to actin cytoskeleton remodeling (Gamagea, et al., 2022). BAI-1 and Stabilin-2 have a role in fusion through the activation of the ELMO/Dock180/ Rac1 signaling pathway (Sampath, et al., 2018). In their research, Hochreiter-Hufford and team identified the role of BAI-1 in myoblast fusion *in vivo*. BAI-1 knockout mice were smaller in size and showed reduced muscle repair ability (Hochreiter-Hufford, et al., 2013). Moreover, studies on BAI-3, another member of the BAI family, highlighted its involvement in myoblast fusion during the development of skeletal muscles in chick embryos (Hamoud, et al., 2014).

Additionally, it was demonstrated that annexin isoforms A1 and A5, which are membrane proteins binding to both calcium ions and phosphatidylserine, promote myoblast fusion in culture through a functionally overlapping mechanism. *In vivo* studies highlighted that annexin A5 specifically plays a vital role in cell fusion necessary for myofiber regeneration (Lehka & Rędowicz, 2020). Recent research suggests that blocking the annexins A1 and A5, also hampers the fusion of myoblast (Leikina, et al., 2013).

3.7.3. Fibro-adipogenic progenitors (FAPs) in muscle regeneration

FAPs, a subset of non-myogenic cells, assume a critical role in coordinating the skeletal muscle regeneration process (Molina, et al., 2021). These cells belong to the category of muscle interstitial mesenchymal cells, residing adjacent to blood vessels and situated outside the capillary basement membrane (Biferali, et al., 2019). Identification of FAPs involves assessing the expression of platelet-derived growth factor receptor alpha (PDGFRα, also known as PDGFRA), along with other surface markers such as CD34 and stem cell antigen-1 (Sca1) (Low, et al., 2017; Molina, et al., 2021; Contreras, et al., 2021). When responding to injury,

FAPs become activated, leading to rapid proliferation and expansion (Wang, et al., 2023). Upon activation, FAPs demonstrate their versatile potential by being able to differentiate into adipocytes, fibroblasts, osteoblasts, and chondrocytes (Chen, et al., 2022). However, during the progression of regeneration, FAPs undergo apoptosis and are systematically eliminated by immune cells. In contrast, during chronic injuries or dystrophic muscle degeneration, the main contributors to the accumulation of intramuscular fat and fibrosis are the continuously proliferating FAPs and their resistance to clearance, as elucidated in Lemos et al.'s study (Lemos, et al., 2015). Consequently, it is demonstrated that within skeletal muscles, FAPs are acknowledged as the primary source of infiltrating fibroblasts and adipocytes (Biferali, et al., 2019). Furthermore, FAPs play a crucial role as a primary source of paracrine factors, contributing to muscle regeneration through the secretion of substances like IL-6, insulin-like growth factor-1 (IGF-1), WNT-1, IL-10, and follistatin. (Molina, et al., 2021). In the context of skeletal muscle, FAPs assume a pivotal role in supporting satellite cells, facilitating their differentiation, and maintaining the muscle Stem Cells population during tissue regeneration (Chen, et al., 2022; Sastourné-Arrey, et al., 2023). Interestingly, it is found that the removal of PDGFRα^+ lineage cells leads to impaired muscle stem cell expansion and reduced immune cell infiltration. This results in suboptimal skeletal muscle regeneration after acute chemical injury, ultimately causing neuromuscular issues and muscle atrophy (Contreras, et al., 2021). *In vitro* experiments have demonstrated that FAPs exhibit the capacity to differentiate into fibroblasts when exposed to TGF-β. Moreover, when cultured in a medium containing insulin, 3-isobutyl-1-methylxanthine, and dexamethasone, FAPs can differentiate into adipocytes (Molina, et al., 2021). The faith of their differentiation is also influenced by the type of injury. According to the research by Uezumi and collaborators, when FAPs from CTX-injured muscles, typically characterized by limited adipogenesis, were transplanted into glycerol-injured muscles, they indeed transformed into adipocytes. Conversely, it is found that FAPs from glycerol-injured muscles did not undergo this transformation when transplanted into CTX-injured muscles (Uezumi, et al., 2010).

3.7.4. Immune cells in muscle regeneration

Following muscle injury, a tightly controlled and time-dependent process triggers the rapid activation of immune cells. This orchestrated activation serves the purpose of expeditiously clearing necrotic tissue and facilitating the release of soluble factors. These

soluble factors, in turn, play a major role in overseeing the activation of satellite cells and guiding them through the intricate stages of the differentiation process (Howard, et al., 2020). Neutrophils assume a paramount role as a pivotal immune cell type during the inaugural phase of the pro-inflammatory response after muscle injury (Howard, et al., 2020; Yang & Hu, 2018; Wang & Zhou, 2022). Upon injury, neutrophil recruitment is orchestrated by the neutrophil chemoattractant CXC-chemokine ligand 1 (CXCL1) and CC-chemokine ligand 2 (CCL2), which are synthesized by tissue-resident Mϕs. Concurrently, the presence of DAMPs, exemplified by HMGB1, further contributes to the mobilization and recruitment of neutrophils (Koike, et al., 2022). Neutrophil infiltration commences within a 2-hour window post-injury, peaking around the 24-hour mark. During this period, neutrophils actively phagocytose damaged muscle debris and release ROS, proteases, and inflammatory cytokines, thereby fostering an inflammatory milieu (Wang & Zhou, 2022) to induce the infiltration of various other immune cell types (Koike, et al., 2022). Impairing the presence of neutrophils in the early stages of acute skeletal muscle injury hinders the phagocytosis of necrotic tissue, consequently causing a delay in the regeneration process (Teixeira, et al., 2003; Caballero-Sánchez, et al., 2022). Mϕs play essential roles not only in the inflammatory cascade but also in tissue development, homeostasis, and regeneration. In response to skeletal muscle injury, the recruitment of Mϕs is facilitated by cytokines released by neutrophils that have already infiltrated the site of injury. During the early phase of the injury response, Lymphocyte Antigen 6 Complex Locus C ($Ly6C)^{high}$ C-C chemokine receptor type 2 positive ($CCR2^{+}$) inflammatory monocytes are mobilized and predominantly undergo differentiation into Ly6Chigh Mϕs (Yang & Hu, 2018; Koike, et al., 2022; Al-Zaeed, et al., 2021). $Ly6C^{high}$ $F4/80^{+}$ pro-inflammatory monocyte-derived Mϕs demonstrate heightened expression of TNF-α and IL-1β (Caballero-Sánchez, et al., 2022; Budai, et al., 2021) as well as NO (Zamora, et al., 2000). NO plays a role in the activation of satellite cells (Sakurai, et al., 2013), resulting in morphological hypertrophy and reduced adhesion within the fiber-lamina complex. Research has unveiled that inhibiting NOS activity pharmacologically impeded the immediate release of myogenic cells post-injury and delayed the hypertrophy of satellite cells within the muscle (Anderson, 2000).

Mϕs were first discernible at the lesion site 24 hours following injury. The Mϕ count experiences a notable surge two days post-injury, concurrently with a rapid reduction in neutrophil numbers (Yang & Hu, 2018). During the timeframe of 48 to 72 hours post-injury, pro-inflammatory Mϕs attain their zenith in numbers, engaging in the phagocytosis of debris, preceding the ascendance of anti-inflammatory Mϕs (Khuu, et al., 2023). Sustained signaling

of pro-inflammatory cytokines has the potential to induce muscle wasting by dampening muscle protein synthesis and initiating the breakdown of muscle proteins. This phenomenon is observable in various pathophysiological conditions associated with muscle wasting. As an extreme illustration, burn injuries can result in widespread skeletal muscle breakdown (Howard, et al., 2020). Following the phagocytosis of necrotic muscle debris, intramuscular Ly6C^{high} Mϕs can convert into Ly6C^{low} Mϕs. The shift from Ly6C^{high} to Ly6C^{low} during the repair of skeletal muscle injury implies substantial functional alterations in Mϕs as part of the injury repair process (Wang & Zhou, 2023).

The timely transition between the two primary subsets of Mϕs is crucial for the proper progression of the regeneration process (Howard, et al., 2020; Al-Zaeed, et al., 2021). The process of Mϕ polarization, referred to as the "macrophage switch," initiates on day 2 post-injury and concludes by day 4 post-injury. This results in the acquisition of distinct effector functions by Mϕs (Caballero-Sánchez, et al., 2022). Ly6C^{high} and Ly6C^{low} Mϕs were formerly linked to the binary classification of M1 (pro-inflammatory) and M2 (anti-inflammatory or pro-regenerative) Mϕs, respectively (Wang & Zhou, 2023). Reports are indicating that the M1 phenotype expresses CD68, while M2 Mϕs express CD163 and CD206 (Forcina, et al., 2020). Ly6C^{high} and Ly6C^{low} Mϕs play distinct roles in skeletal muscle regeneration by actively supporting the proliferation and differentiation of satellite cells (Koike, et al., 2022). Several molecular processes intricately regulate the ability of Mϕs to transition from the M1 to M2 phenotype. Notably, the phagocytosis of apoptotic cells leads to the activation of lipid-sensing nuclear receptors, such as LXRs and PPARs, and diminishes pro-inflammatory cytokine production in Mϕs and augments their anti-inflammatory activity (Szondy, et al., 2017).

The transcription factor Nuclear receptor subfamily 4 group A member 1 (NR4A1), also known as Nur77, is expressed as an early response gene and has demonstrated the ability to inhibit the expression of pro-inflammatory genes during efferocytosis (Garabuczi, et al., 2023). In human and mouse macrophages, Nur77 expression is induced by inflammatory signals such as LPS and TNF-α through NF-κB. Despite this induction, Nur77 functions to ease the inflammatory response of macrophages by suppressing NF-κB signaling. Additionally, the deficiency of Nur77 exacerbates several inflammation-related disorders, including atherosclerosis and sepsis triggered by LPS (Koenis, et al., 2018).

Additionally, heightened concentrations of IL-10 promote the M2 phenotype, while interferon-gamma (IFN-γ) signaling hinders the M1 to M2 conversion (Howard, et al., 2020).

The precise timing of the inflammatory response is crucial for coordinating myogenesis and related supportive biological processes. Notably, inhibiting key molecular pathways involved in the shift of Mϕs—such as IGF-1, encodes MAP kinase phosphatase 1 (MKP1)-p38, SRB1-ERK, AMP-activated protein kinase (AMPK), CCAAT/enhancer binding protein β (C/EBPβ), STAT3, nuclear factor I X (NFIX), and the BTB and CNC homology 1(BACH1) leads to a failure to acquire the reparative phenotype, resulting in diminished the growth of muscle fibers and impaired muscle regeneration (Bernard, et al., 2022). A delayed shift from pro-inflammatory to pro-regenerative Mϕs may also contribute to fibrosis. Notably, the concurrent expression of M1-derived TNF-α and M2-derived TGF-β1 has been observed to decrease the apoptosis of FAPs and elevate ECM deposition (Howard, et al., 2020). Ly6C^{low} monocytes, characterized by diminished expression of CCR2, exhibit the capacity to ingress into damaged tissue through a CX3CR1-dependent mechanism. This participation occurs during the third wave of regenerative inflammation, where they assume the role of M2 pro-regenerative/healing Mϕs, actively contributing to tissue repair (Forcina, et al., 2020). M2 Mϕs secrete anti-inflammatory cytokines, exemplified by IL-4, IL-10, along with TGF-β1, growth differentiation factor-3 (GDF3), and IGF-1 (Peake, et al., 2017; Tamas, et al., 2016) (Figure 8). IL-4, IL-10, and TGF-β1 were shown to inhibit the production of NO from macrophages or reduce the expression of iNOS in activated macrophages (Zamora, et al., 2000). It has demonstrated that GDF3 acts as a factor that promotes myoblast fusion and facilitates muscle regeneration (Hays, et al., 2018). In addition, the absence of GDF3 hindered muscle regeneration, while administering recombinant GDF3 improved repair in vivo and promoted the fusion of primary myogenic precursor cells (MPCs) in vitro cultures (Varga, et al., 2016). IGF-1 also boosts skeletal muscle regeneration by activating satellite cells, potentially promoting muscle hypertrophy and preventing atrophy (Yoshida & Delafontaine, 2020). Following cardiotoxin injection-induced acute damage, there is a noted elevation in the overall levels of IGF-I (Bikle, et al., 2015).

Healing Mϕs actively facilitate angiogenesis, stimulate fibroblastic cells to engage in ECM remodeling, and autonomously secrete various ECM components, including proteoglycans, matricellular proteins, and assembly proteins (Bernard, et al., 2022). The infiltrating Mϕs contribute to muscle regeneration by overseeing the fundamental phases of myogenic cell activation, proliferation, differentiation, and fusion following injury. Various macrophage subtypes demonstrate distinct functions in this process. Pro-inflammatory Mϕs play a role in promoting myogenic cell activation and proliferation, whereas anti-inflammatory

Mϕs facilitate myogenic cell differentiation and fusion. Histopathological analysis of injured skeletal muscle corroborates these observations, revealing the co-localization of pro-inflammatory Mϕs with proliferating satellite cells and the co-localization of anti-inflammatory Mϕs with differentiated myoblasts (Wang & Zhou, 2023). During acute muscle injury, there is involvement of self-limiting physiological acute inflammatory responses, while chronic muscle disorders, typified by progressive muscle wasting and including conditions like muscular dystrophies, manifest persistent chronic inflammation. In the mdx mice, a genetic model for Duchenne muscular dystrophy (DMD), the infiltration of neutrophils and activated M1 Mϕs into the muscle and subsequent muscle lysis is observed as early as the 4th weeks after birth (Villalta, et al., 2009).

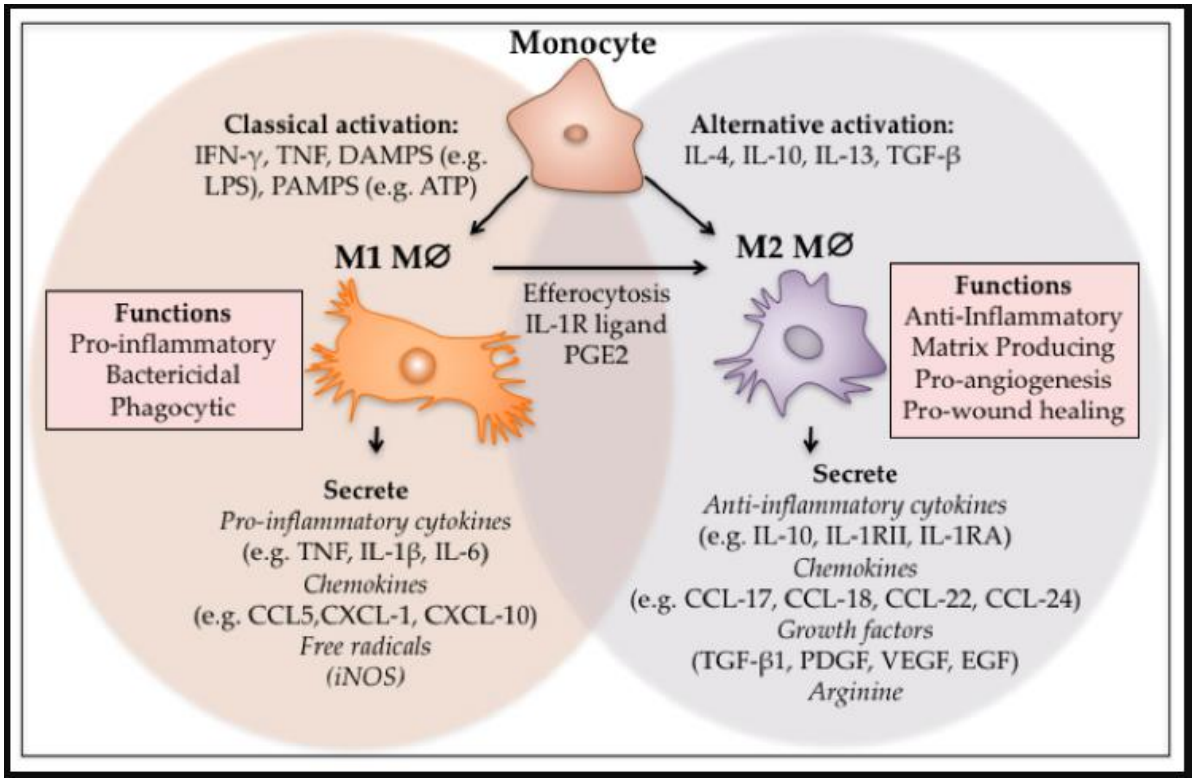

Figure 8: M1 and M2 polarization of Mϕs. Monocytes can be classically or alternatively activated to form M1 and M2 Mϕs respectively. *M1 Mϕs can also differentiate into M2 Mϕs through local cues and after phagocytosis. The M1 phenotype is pro-inflammatory, phagocytic, and bactericidal, while the M2 Mϕs act to switch off inflammation and regulate re-vascularisation, wound closure, and tissue repair.* (Hesketh, et al., 2017)

4. Aim of the study

The primary objective of this study was to examine the effects of the absence of RetSat enzyme and Adenosine A3 receptor on skeletal muscle development and regeneration in mice. The specific objectives of this study were as follows:

- To examine whether these specific genes have any effect on body and muscle weight in non-injected (control) state and after CTX-injection in wild-type and knockout mice;
- To investigate whether the ablation of the genes under study alter the distribution of fiber size either in control or in different time-point after CTX injection muscle;
- to determine whether the ablation of RetSat and A3R genes affects the collagen 1 deposition and the size of the necrotic area in the regenerating muscles;
- to determine whether the ablation of RetSat and A3R genes affects the frequency of satellite cells and FAP cells during muscle regeneration;
- to compare the expression of myogenic genes involved in the myoblast proliferation and differentiation between the knockout and corresponding wild-type mice;
- to assess whether the ablation of RetSat and A3R genes affects the abundance of intramuscular leukocyte infiltration in the regenerating muscles of wild-type and knockout mice;
- to characterize regenerating muscle-derived $CD45^+$ and $F4/80^+$ cells regarding their inflammatory marker expression isolated from knockout and corresponding wild-type mice.

5. Material and Methods

5.1. Reagents

Unless otherwise stated, all reagents used in the experiments were purchased from Merck (Darmstadt, Germany).

5.2. Experimental animals

Experiments were carried out using 2-6 month-young adult male C57BL/6J RetSat$^{+/+}$ and their full body RetSat $^{-/-}$ littermates and 3-6 month-old male C57BL/6J A3R$^{+/+}$ mice and their whole body A3R$^{-/-}$ littermates. Mice were bred in the heterozygous form under specific pathogen-free conditions in the central animal facility of the University of Debrecen. All animal experiments were approved by the Animal Care and Use Committee of the University of Debrecen, with permission numbers 7/2016 and 7/2021/DEMÁB.

5.3. CTX-induced muscle injury model

Mice were placed under anesthesia using a Somno Suite device with 2.5% isoflurane. To induce muscle damage, 50 μL injection of 12 μM CTX (Latoxan, Valence, France) dissolved in phosphate-buffered saline (PBS) was administered directly into the tibialis anterior (TA) muscle. This particular concentration of CTX was chosen as it produces significant muscle injury, allowing for the detection of notable changes in the subsequent regeneration process, even in the absence of regeneration-related genes. However, despite the severity of the injury, full regeneration was observed three months post-injury. At different time points following the injury, the mice were euthanized, and the TA muscles were harvested for further experimentation.

5.4. Hematoxylin/eosin and immunofluorescent staining of the muscles

TA muscles were obtained from either non-injected (control) mice or CTX-injected mice at specified time points following injury for histological evaluation. The muscles were rapidly frozen by immersing them in isopentane cooled with liquid nitrogen and stored at -80°C. Cryosections with a thickness of seven micrometers were cut at -20$^{\circ C}$ using a 2800 Frigocut microtome from Leica (St Jouarre, France) and stored at -20$^{\circ C}$ until further analysis. Hematoxylin and Eosin (H&E) staining was performed to assess the overall morphology and presence of necrotic fibers following the injury. Images of the sections were captured using an AMG EVOS fl microscope from Thermo-Fisher Scientific (Waltham, MA, USA). To determine the cross-sectional area (CSA) and collagen-stained areas, frozen muscle sections

were incubated in a citric acid-sodium citrate buffer (pH 6.0) with a concentration of 10 mM for 15 minutes, followed by blocking in a blocking solution (50% fetal bovine serum (FBS) in PBS) for 1 hour at room temperature. Subsequently, the samples were labeled with Dylight 488-conjugated anti-laminin B antibody (PA5-22901, Invitrogen, Carlsbad, CA, USA) at a dilution of 1:100, and anti-collagen 1 antibody (SAB4500362) at a dilution of 1:100. The samples were incubated overnight at 4°C, followed by labeling with Alexa Fluor 488-conjugated Goat anti-Rabbit IgG secondary antibody. After three washes with PBS, the nuclei were stained with 4 μg/mL 4',6-diamidino-2-phenylindole (DAPI) from Invitrogen (R37606), and the slides were mounted with glass coverslips. Images were captured using a Floid Cell Imaging Station fluorescent microscope from Thermo-Fisher Scientific (4471136), and analysis was performed using ImageJ v1.52 software from the National Institutes of Health (Bethesda, MD, USA) with a muscle morphometry plugin. Regenerating muscle areas were identified by the presence of centrally-located nuclei within the fibers. The CSA values are reported in square micrometers (μm²), while the collagen content is reported as the percentage of the total examined regenerating area.

5.5. Quantification of necrotic area

Necrotic areas were identified based on specific histological characteristics, including blurred cell borders, cytoplasmic fragmentation, variation in fiber diameter, altered cell spacing, loss of nuclei, and increased infiltration of immune cells. Necrotic myofibers were defined as pale, patchy fibers exhibiting a pinkish hue and infiltration by basophilic single cells. Quantification of necrotic myofibers followed a previously described method (Patsalos, et al., 2022). In summary, six to eight H&E-stained sections of the TA muscle were examined under 200-fold magnification. Four non-overlapping microscope fields were digitally captured, and the necrotic area was manually outlined in each section. The percentage of necrotic area in relation to the total regenerating area was calculated.

5.6. Isolation of muscle-derived $CD45^+$ Leukocytes

The TA muscles were excised at 2, 3, and 4 days after the injury. The fascia surrounding the TA muscle was eliminated. The muscles were then dissociated in RPMI 1640 medium containing 0.2% Collagenase II (Thermo-Fisher Scientific) and incubated at $37^{°C}$ for 1 hour. The resulting mixture was passed through a 100-μm filter, followed by a 40-μm filter to obtain a single-cell suspension. $CD45^+$ cells were isolated from this suspension using magnetic sorting

techniques according to manufacturer's instructions (Miltenyi Biotec, Bergisch Gladbach, Germany).

5.7. Generation of bone marrow-derived macrophages (BMDMs) for NEO cassette expression analysis

Bone marrow progenitors were collected from the femur of RetSat $^{+/+}$ and RetSat$^{-/-}$ mice aged between 2 to 4 months through rinsing with sterile physiological saline. The cells were then cultured in DMEM medium supplemented with 10% conditioned medium obtained from L929 cells, which served as a source of macrophage colony-stimulating factor (M-CSF). The culture medium also contained 2 mM glutamine, 100 U/mL penicillin, and 100 mg/mL streptomycin. The cells were incubated at 37$^{\circ C}$ in an environment with 5% CO2 for a period of 5 days. Throughout this time, non-adherent cells were regularly removed by washing every other day.

5.8. Gene expression analysis

RNA was extracted from magnetically separated muscle-derived CD45^{+}cells, BMDMs, as well as different organs, using TRIzol reagent from Invitrogen following the provided instructions. TA muscles and other organs were homogenized using a Shakeman homogenizer from BioMedical Science (USA) with TRIzol. Total RNA was isolated using the TRI reagent, as per the manufacturer's guidelines from Thermo-Fisher Scientific. The isolated total RNA was then reverse transcribed into cDNA using the High Capacity cDNA Reverse Transcription Kit from Thermo-Fisher Scientific following the provided instructions. Quantitative RT-PCR was conducted in triplicates on a Roche LightCycler LC 480 real-time PCR instrument (Roche, Basel, Switzerland) using pre-designed FAM-labeled MGB assays from Thermo-Fisher Scientific and LightCycler 480 Multi-well 384 white plates sealed with adhesive tapes. The relative mRNA levels in the case of CD45^{+} cells were determined using the comparative CT method and normalized to β-actin mRNA. For total muscle samples, gene expressions were normalized to the total RNA content (200 ng) of the samples. The TaqMan assay catalog numbers used are listed in Table 1.

Table 1. Catalog numbers of the TaqMan assays that were used in RT-qPCR.

Gene	Catalog numbers	Gene	Catalog numbers
A3R	Mm07296455_m1	A2bR	Mm00839292_m1
Actb	Mm02619580_g1	Gdf3	Mm00433563_m1
Arg1	Mm00475988_m1	MFG-E8	Mm00500549_m1
eNOS	Mm01164908_m1	iNOS	Mm00440502_m1
IGF1	Mm00439560_m1	Nr4a1/Nur77	Mm01300401_m
MCP-1	Mm00441242_m1	Pax7	Mm00834082_m1
Myhc1	Mm01332489_m1	IL6	Mm00446190_m1
MyoD1	Mm00440387_m1	IL10	Mm01288386_m1
Myog	Mm00446194_m1	IL4	Mm00445259_m1
NEO cassette	NEOCASSETTE	A2aR	Mm00802075_m1
RetSat	Mm00458863_m1	NPY	Mm01410146_m1
Tgf-β 1	Mm01178820_m1	IL1B	Mm00434228_m1
Tnf-α	Mm00443258_m1	PPARg	Mm00440940_m1

5.9. Quantification of satellite and FAP cells in the TA muscle following CTX-induced injury

To detect intramuscular satellite cells and FAP cells the TA muscle was collected on day 4 post-injury. The muscle was dissociated in RPMI medium containing 0.2% collagenase II from Thermo-Fisher Scientific and incubated at 37$^{\circ C}$ for 1 hour. The resulting cell suspension was filtered through a 100 µm filter. Before staining, approximately 225,000 polystyrene microbeads (8 µm, 78511) were added to the muscle cell suspension to facilitate the later determination of absolute cell numbers. The identification of muscle precursor cells involved staining with specific markers. Satellite cells were identified by staining with α7-integrin (PE-conjugated, 130-120-812, Miltenyi Biotec). FAP cells were identified using CD140a (BV711-conjugated, 740740, BD Biosciences, San Jose, CA, USA) and Sca1 (BV605-conjugated, 563288, BD Biosciences). Other cell types present in the muscle tissue were gated out using specific staining with biotin anti-mouse CD45 (103104, BioLegend, San Diego, CA, USA),

biotin anti-mouse CD31 (102404, BioLegend), and biotin anti-mouse Ter119 (79748, BioLegend). APC-conjugated streptavidin (405207, BioLegend) was added as a second step to the cells. Before measurement, cells were washed with 0.5% BSA-physiological saline and suspended in 0.5% BSA-physiological saline supplemented with SYTO16 green-fluorescent nucleic acid stain (S7578, Invitrogen) and 7-AAD non-cell-permeable dead cell stain (A1310, Thermo-Fisher Scientific) to exclude injured and dead cells. The measurement was performed using a FACS Aria III cytometer from Becton, Dickinson, and Company (Franklin Lakes, NJ, USA), equipped with violet (405 nm), blue (488 nm), yellow (561 nm), and red (633 nm) lasers. The microbeads were distinguished based on their intense side scatter properties. Living cells were gated based on their APC fluorescence, distinguishing between CD45/CD31/Ter119 positive and negative populations. The APC non-stained cells primarily consisted of Sca1 bright, CD140a^{+}, integrin-α7^{-} FAP cells, as well as integrin-α7^{+}, Sca1^{-}, CD140a^{-} satellite cells. Absolute cell counts were determined by calculating the ratio of cells of interest to microbeads within the measured samples.

5.10. Single-cell RNA sequencing and analysis of CD45^{+} cells

Data from single-cell gene expression barcodes, features, and count matrices of CD45^{+} cells collected on day 4 post-CTX-induced muscle injury were obtained from dataset GSE161467 (Patsalos, et al., 2022). Subsequent analysis was performed using established methods detailed in a prior study (Garabuczi, et al., 2023).

5.11. Quantification of intramuscular immune cells by flow cytometry

The muscle-derived CD45^{+} cells that were isolated using magnetic sorting underwent staining using a combination of Alexa Fluor 488-conjugated anti-F4/80 antibody (MF48020, Invitrogen) and Alexa Fluor 647-conjugated anti-Lymphocyte Antigen 6 Complex Locus g6d (Ly6G)/Ly6C (GR-1) antibodies (108418, BioLegend). This staining was conducted at room temperature for a duration of 15 minutes. The cells were then analyzed based on their forward and side scatter characteristics. Mϕs were identified as GR-1^{-} and F4/80^{+}, while neutrophils were identified as F4/80^{-} and GR-1^{+} cells. This gating strategy has been previously described in our published work (Al-Zaeed, et al., 2021). F4/80^{+} Mϕs were further analyzed for the expression of Ly6C, CD206, or major histocompatibility complex (MHC) II, using corresponding antibodies: Ly6C percp-Cy5.5 (128012, BioLegend), CD206-PE (141705, BioLegend), or MHCII-FITC (107605, BioLegend), respectively. Fluorescent intensity was detected using a Becton Dickinson FACSCalibur instrument.

5.12. C2C12 cell culture

The murine myoblast C2C12 cell line (ATCC, CRL-1772) was obtained and cultured following the manufacturer's instructions. Briefly, cells were maintained in DMEM supplemented with 10% FBS, 100 U/ml penicillin, and 100 μg/ml streptomycin (growth medium) at 37$^{\circ C}$ in a humidified atmosphere containing 5% CO_2 and 95% air. The absence of mycoplasma contamination was confirmed using PCR Mycoplasma Test Kit I/C (PromoCell, Heidelberg, Germany).

5.13. In vitro phagocytosis assay by F4/80^{+} cells

Phagocytosis experiments were conducted following previously established protocols (Budai, et al., 2019). In summary, C2C12 cells were subjected to necrosis by heating them at 65$^{\circ C}$ for 10 minutes. Some of the C2C12 cells were labeled with 1 μM CellTracker Deep Red Dye from Thermo-Fisher Scientific, while others were left unlabeled. Based on our previous findings indicating a reduced efferocytosis capability of RetSat$^{-/-}$ Mϕs associated with decreased production of MFG-E8 during long-term efferocytosis (Sarang, et al., 2019), To stimulate the generation of MFG-E8, the unlabeled cells were initially added to F4/80^{+} cells isolated from collagenase-treated TA muscles on day 4 post-CTX injury. The F4/80^{+} cells were isolated using magnetic beads (Miltenyi Biotec) and stained with 6 μm 5-carboxyfluorescein diacetate (CFDA) (Thermo-Fisher Scientific). F4/80^{+} cells were plated in 8-well chamber slides (Gräfelfing, Germany) at a density of 3 × 105 cells per well, and unlabelled necrotic C2C12 cells were added to them at 5:1 macrophage:C2C12 cell ratio. After 5 hours of co-culture, the F4/80^{+} cells were washed and further incubated with CFDA-labeled necrotic C2C12 cells for an additional 2 hours. Subsequently, the target cells were extensively washed away. In some cultures, Mϕs were detached by trypsinization, and the percentage of engulfing cells was determined using a Becton Dickinson FACSCalibur flow cytometer. Other cultures were fixed using 1% paraformaldehyde, and representative fluorescent images were captured using a Floid Cell Imaging Station.

5.14. *In vivo* assessment of muscle force

The strength of the forepaw was assessed using established methods (Sztretye, et al., 2020). Briefly, A3R$^{+/+}$ and A3R$^{-/-}$ animals were trained to grasp a meter bar in the grip test. They were then gently pushed horizontally, and the maximum force applied before releasing the bar was measured and digitized at 2 kHz. Each mouse provided one data point, obtained

from 10 to 15 repetitions of the test. Grip strength measurements were taken on the day of sacrifice for all animal groups.

5.15. Voluntary activity wheel measurement

Individual control $A3R^{+/+}$ and $A3R^{-/-}$ mice were placed in separate cages equipped with running wheels (Campden Instruments Ltd., Loughborough, UK). The wheels were linked to a computer, which continuously recorded revolutions in 20-minute intervals over a period of 14 days. Daily calculations were made for each mouse, including average and maximum speed, distance covered, and duration of running. These individual data points were then averaged for each group.

5.16. Forced treadmill running measurement

Control $A3R^{+/+}$ and $A3R^{-/-}$ mice were assessed for the duration and distance they could sustain on a motor-driven wheel-track treadmill. The running speed began at 1 km/h and increased by 0.1 km/h every 2 minutes on a flat surface until the mice reached exhaustion.

5.17. *Ex vivo* assessment of muscle force

Extensor digitorum longus (EDL) and soleus (SOL) muscle contractions were assessed following established procedures (Sztretye, et al., 2020). In summary, the muscles under study were manually dissected and placed horizontally in an experimental chamber. They were continuously perfused with Krebs solution (composition: NaCl 135 mM, KCl 5 mM, $CaCl_2$ 2.5 mM, $MgSO_4$ 1 mM, Hepes 10 mM, $NaHCO_3$ 10 mM, and glucose 10 mM; pH 7.2; at room temperature) at a flow rate of 10 ml/min. The chamber was equilibrated with 95% O_2 and 5% CO_2. One end of the muscle was attached to a rod and the other end to a capacitive mechano-electric force transducer. Two platinum electrodes placed beneath the muscle delivered brief, supramaximal pulses lasting 2 ms to induce single twitches. The force responses were digitized at 2 kHz using the Digidata 1200A/D interface and analyzed with AxoTape software (Axon Instruments, Foster City, CA, USA). The muscles were stretched by adjusting the transducer to a length that elicited the maximum force response and were allowed to stabilize for 5 minutes. Single twitches were induced at a frequency of 0.5 Hz, and a minimum of ten twitches were recorded from each muscle under these conditions. The amplitude of individual force transients within the train varied by less than 3%; thus, the mean amplitude of all transients was used to characterize the muscles. Tetanus was induced using single pulses at 200 Hz for 200 ms (for EDL) or 100 Hz for 500 ms (for SOL). The duration of individual twitches and

tetani was calculated based on the time from the onset of the transient to the relaxation to 10% of the maximal force.

5.18. Statistical analysis

The data presented in this study are derived from a minimum of three distinct experimental replicates, and all numerical values are reported as either mean or median ± SEM or SD. Statistical analysis was conducted using a two-tailed, unpaired Student's t-test and ANOVA, accompanied by a post-hoc Tukey HSD test. The homogeneity of variances among the samples was assessed using an F-test. The symbol "*" denotes a significance level of $p < 0.05$, while "**" signifies a significance level of $p < 0.01$. The presence of asterisks indicates a statistically significant difference compared to the corresponding wild-type counterparts unless stated otherwise by significance brackets.

6. Results

6.1. Part I: Role of RetSat in skeletal muscle regeneration

6.1.1. The regeneration program in the TA muscle remains unchanged in the absence of RetSat

In order to investigate the potential involvement of RetSat in skeletal muscle development and regeneration, we formulated a plan to gather samples from both non-injected mice and those injected with CTX at different time points. This strategy was designed to allow for the examination of development, early (2, 3, and 4 days post-injury) and late phases (10 and 22 days post-injury) of regeneration. Throughout the thesis, samples from non-injected mice are referred to as "control" and are represented as "0 day" in the figures (Figure 9 A). Throughout the study, it is important to highlight that each muscle was treated as an individual sample. However, in instances where experiments required a greater number of cells, the combination of two muscles was treated as a unified sample. We then analyzed the muscle weights and myofiber CSAs of untreated and CTX-treated TA muscles in both $RetSat^{+/+}$ and $RetSat^{-/-}$ mice. The observations showed there are no significant differences in the body and TA muscle weights/body weight ratio between $RetSat^{+/+}$ and $RetSat^{-/-}$ mice (Figure 9 B, C). Likewise, the evaluation of TA muscle weight/body weight ratios in response to induced muscle damage showed similar values between the two strains (Figure 9 D).

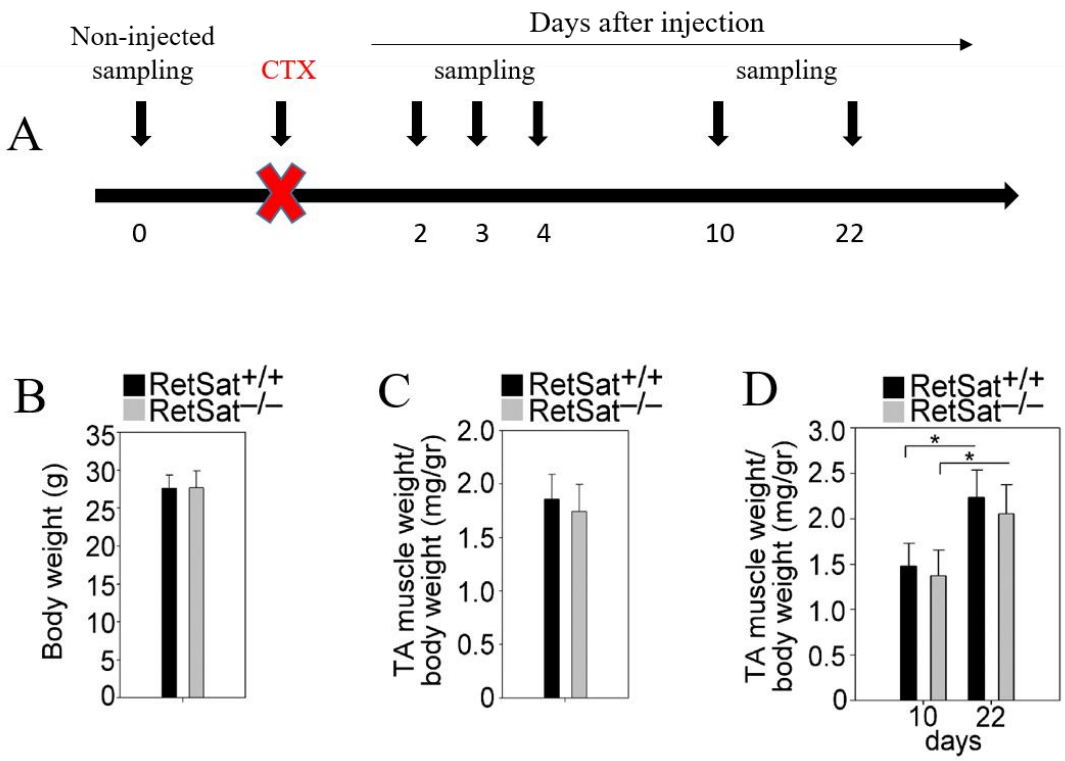

Figure 9: Normal body and muscle weight in Retsat$^{-/-}$ mice. *(A)The experimental design established for studying RetSat ablation's impact on skeletal muscle regeneration in mice. (B) Assessment of body weights in untreated RetSat$^{-/-}$ and RetSat$^{+/+}$ mice. (C)TA muscle weight/body weight ratios were measured in untreated RetSat$^{+/+}$ and RetSat$^{-/-}$ mice. (D) The TA muscle weight/body weight ratio weight was assessed in RetSat$^{+/+}$ and RetSat$^{-/-}$ mice at 10 and 22 days after injury. The data are presented as a mean ± SEM (n=6). Asterisks indicate statistical significance (* p< 0.05, ** p< 0.01, Student's t-test).*

To further examine the impact of RetSat ablation on skeletal muscle regeneration, we conducted an experimental study on fiber size distribution in control and CTX-damaged TA muscles. The fiber size distribution in the muscles before and after injury exhibited similar patterns in both RetSat$^{+/+}$ and RetSat$^{-/-}$ mice. Subsequently, we evaluated the mean and median CSAs of the myofibers in untreated and at 10 and 22 days post-injury mice. There were no significant differences in CSAs between RetSat$^{+/+}$ and RetSat$^{-/-}$ mice (Figure 10 A, B, C, and D). The process of myoblast fusion during muscle regeneration was evaluated by counting myofibers with two or more central nuclei. In the control muscles of both RetSat$^{+/+}$ and RetSat$^{-/-}$ mice, there were no central nucleated fibers observed in the histological images.

Furthermore, the analysis of newly formed fibers at 10 and 22 days post-injury muscles, characterized by the presence of 2 or more central nuclei, and the mean number of central nuclei per fiber, indicative of myoblast fusion during muscle regeneration, also revealed no notable distinctions between RetSat$^{+/+}$ and RetSat$^{-/-}$ mice at both 10 and 22 days after injury (Figure 10 E). Overall, these findings suggest that the absence of RetSat does not significantly affect skeletal muscle regeneration in terms of muscle weights, myofiber CSAs, and myoblast fusion.

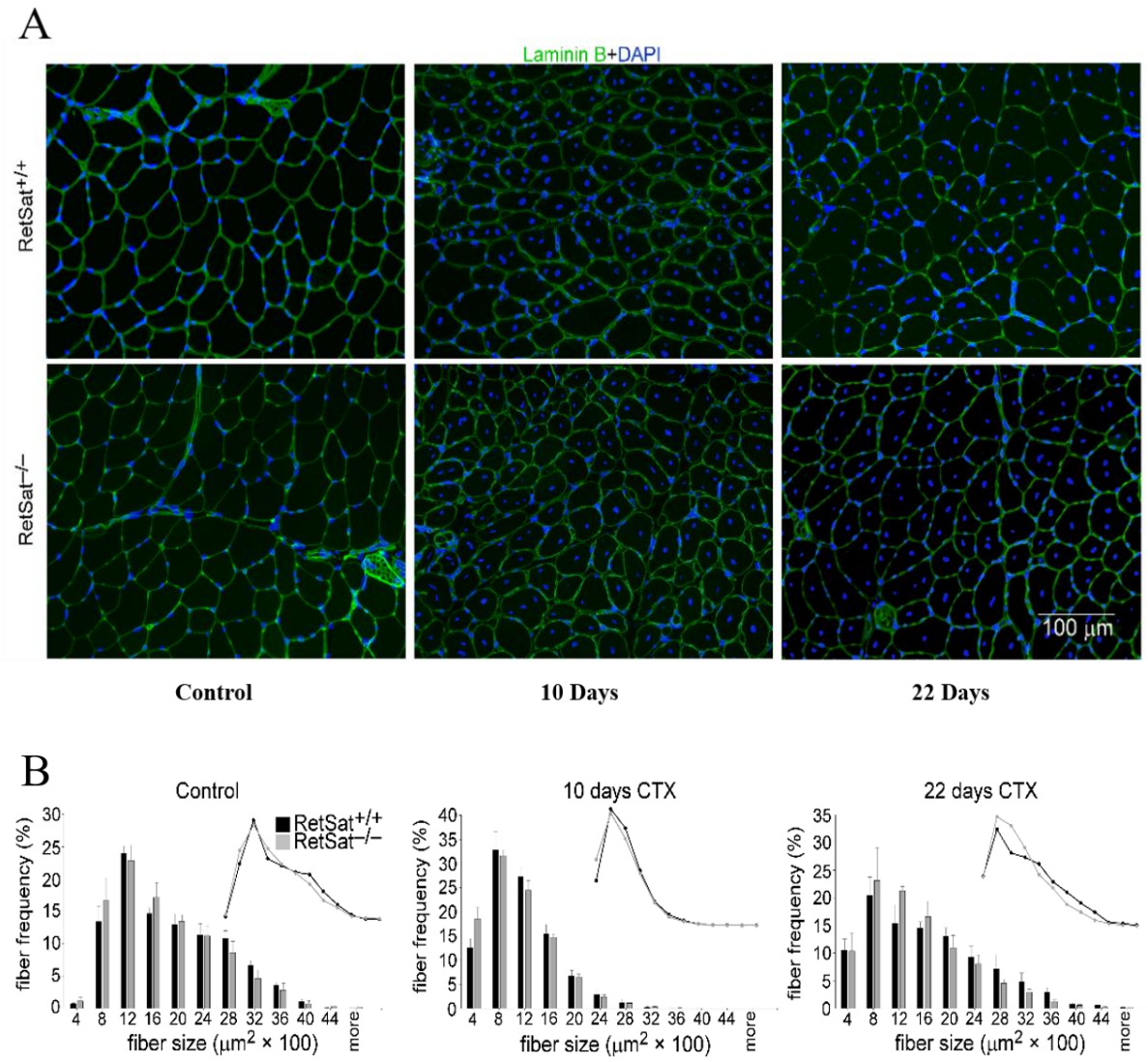

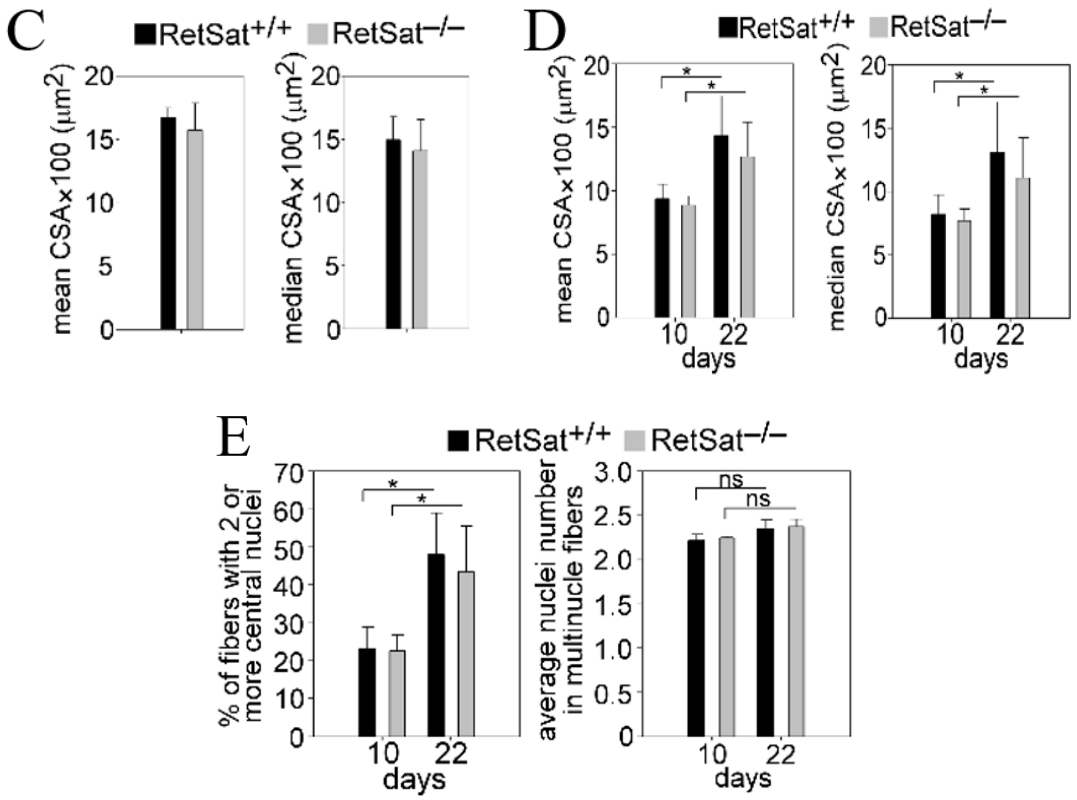

Figure 10: Normal skeletal muscle regeneration in RetSat$^{-/-}$ mice. *(A) representative immunofluorescence staining of laminin (green) and DAPI (blue) in muscle cryosections from TA muscles of control and 10- and 22-day regenerating muscles of RetSat$^{+/+}$ and RetSat$^{-/-}$ mice. (B, C, and D) distribution of myofiber size, mean and median CSA values in control and regenerating TA muscles of RetSat$^{+/+}$ and RetSat$^{-/-}$ mice. (E) The proportion of recently developed myofibers with two or more central nuclei, as well as the average number of central nuclei per fiber, was assessed on days 10 and 22 following CTX-induced injury in both RetSat$^{+/+}$ and RetSat$^{-/-}$ mice. Scale bar, 100 μm. Data are expressed as mean or median ± SEM (n=4 in control and 22 days and n=6 in 10 days samples). Asterisks indicate statistical significance (* p< 0.05, ** p< 0.01, Student's t-test).*

Microscopic analysis did not reveal any apparent morphological differences between the control muscles of RetSat$^{+/+}$ and RetSat$^{-/-}$ mice. On day 4 post-injury, both RetSat$^{+/+}$ and RetSat$^{-/-}$ mice exhibited local necrosis and a significant presence of leukocytes infiltrating the regenerating muscles (Figure 11). By day 10, the necrotic tissue had mostly been cleared, and by day 22 post-injury, the overall histological structure of the muscles in both RetSat$^{+/+}$ and RetSat$^{-/-}$ mice had been mostly restored, with no visible signs of necrotic fibers.

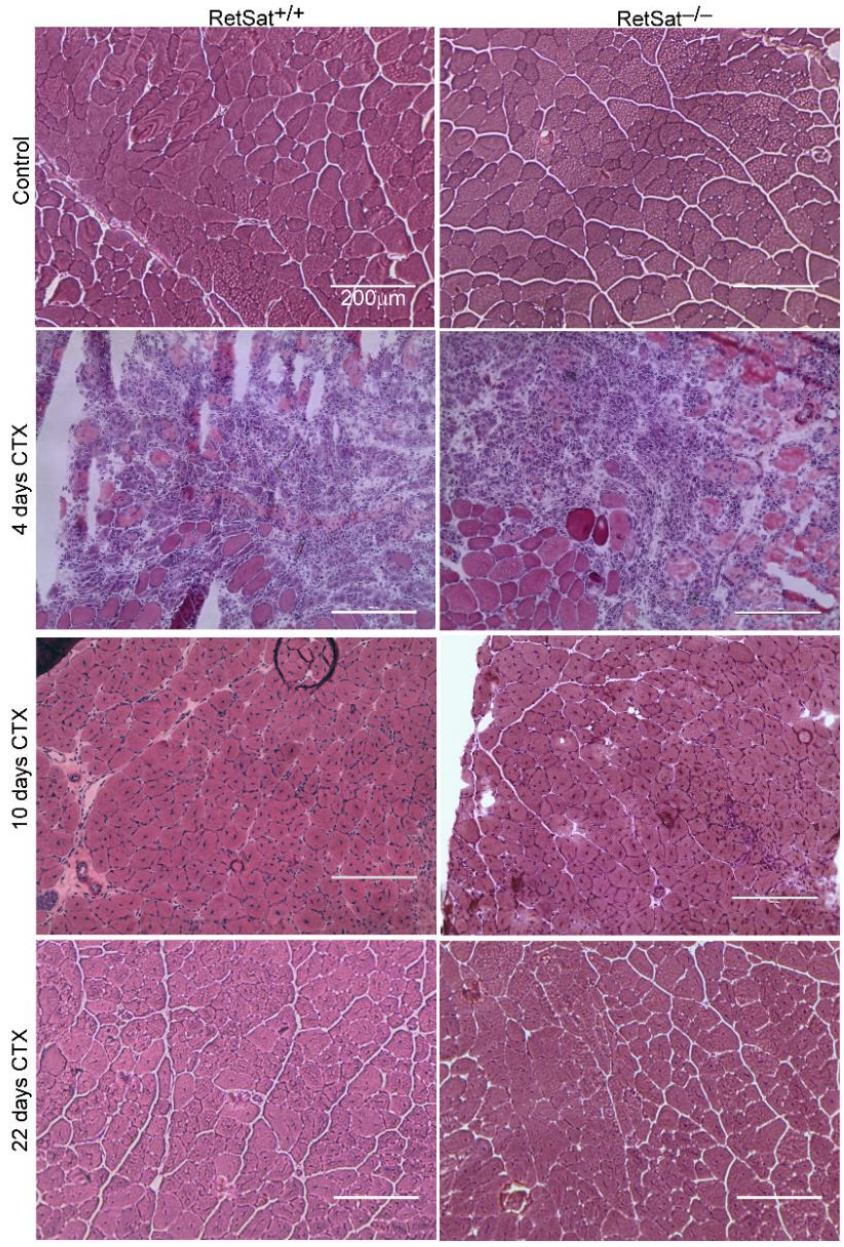

Figure 11: The histological changes over time in TA muscles of RetSat$^{+/+}$ and RetSat$^{-/-}$ mice were examined after CTX-induced injury. *Muscle damage was induced by injecting 50 μL of 12 μM CTX into the TA muscles. Representative cross-sections of TA muscles were stained with H&E and observed before, as well as 4, 10, and 22 days after CTX treatment (n=4). Scale bars represent 200 μm*

In our previous study, we identified a decreased phagocytic capacity in RetSat$^{-/-}$ mice (Sarang, et al., 2019). Consistently, when we conducted an *in vitro* phagocytosis assay using muscle-derived Mϕs and necrotic myoblasts as target cells, we observed a similar reduction in

phagocytic activity (Figure 12 A, B). To further investigate the impact of RetSat loss, we evaluated the sizes of necrotic areas in both control and regenerating TA muscles. Remarkably, our findings demonstrated comparable necrotic area sizes between the two mouse strains (Figure 12 C), indicating that the *in vivo* clearance of dead fibers remains unaffected by the absence of RetSat. In the process of muscle repair, there is a temporary rise in the deposition of ECM proteins, essential for regulating satellite cells and promoting myoblast proliferation and differentiation (Zhang, et al., 2021). Consequently, we aimed to assess the levels of collagen 1 in both control and regenerating TA muscles. In both mouse strains, there was a temporary increase in collagen 1 deposition observed at day 10 post-injury, which subsequently decreased by day 22. However, there was no significant difference observed between the two strains (Figure 12 D, E).

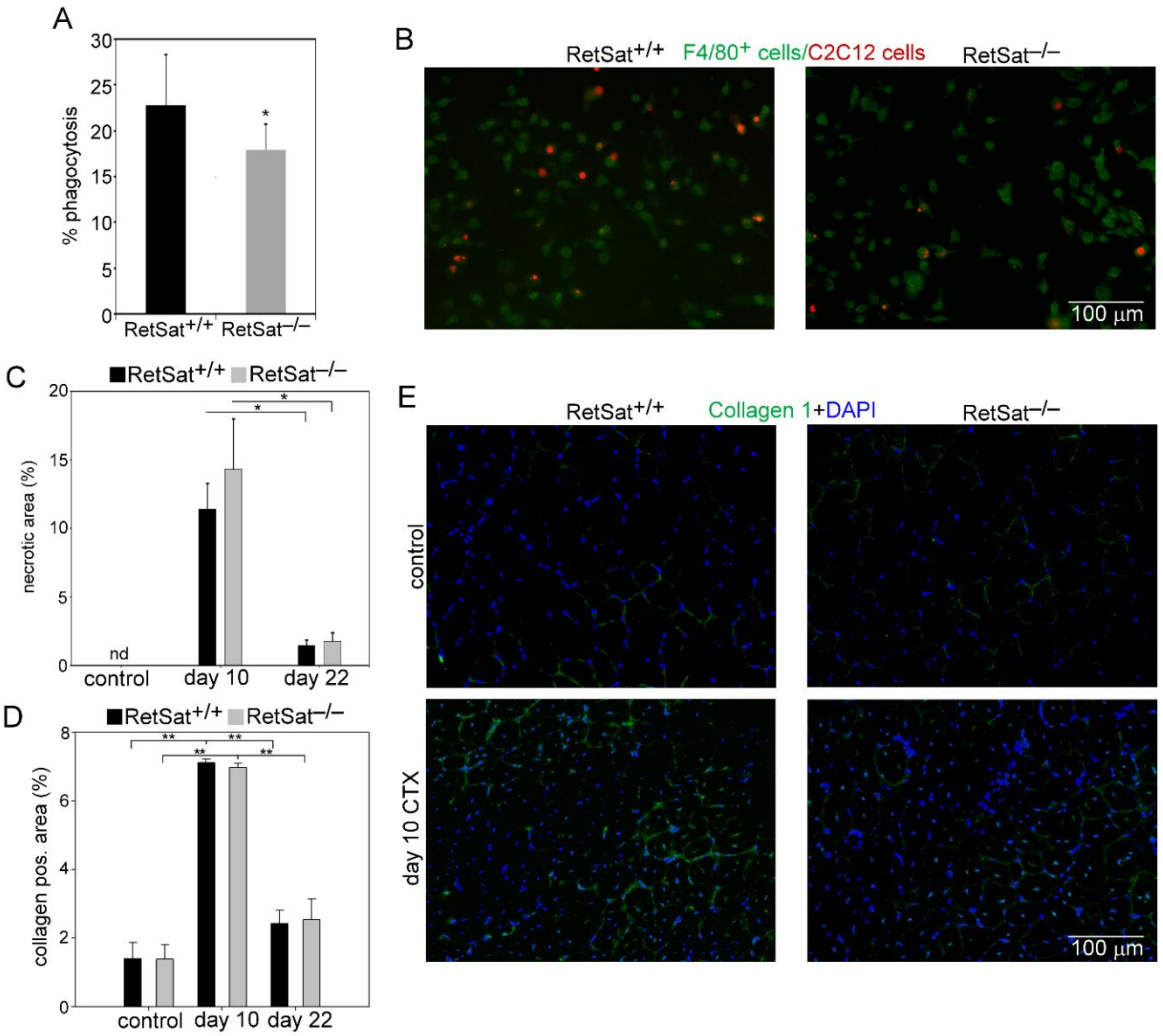

Figure 12: Normal elimination of necrotic cells and collagen 1 deposition in the TA muscles of RetSat$^{-/-}$ mice after CTX-induced damage. *Muscle-derived RetSat$^{-/-}$ F4/80^{+} cells exhibited reduced in vitro phagocytosis of necrotic C2C12 myoblasts, as demonstrated by (A) FACS*

analysis and (B) cell engulfment visualization. (C) Necrotic regions were examined in control and regenerating muscles of RetSat$^{+/+}$ and RetSat$^{-/-}$ mice on days 0, 10, and 22 post-CTX injury. (D) Collagen 1-positive regions were quantified in control and 10- and 22-day regenerating muscles of RetSat$^{+/+}$ and RetSat$^{-/-}$ mice. (E) Immunofluorescence images depicted type 1 collagen (in green) and DAPI (in blue) nuclear staining in control and 10-day regenerating TA muscles of RetSat$^{+/+}$ and RetSat$^{-/-}$ mice. Scale bars represent 100 µm. All data are presented as mean ± SD (n=4). Significant differences are denoted by asterisks (p < 0.05, ** p < 0.01, Student's t-test); 'nd' indicates not detected.*

To investigate the potential influence of RetSat ablation on gene expression, satellite cell proliferation, and differentiation in both normal and regenerating TA muscles, we examined the satellite cell count (as shown in Figure 13A) and the expression levels of myogenic genes such as Pax7, MyoD, and myogenin. These genes are associated with myoblast proliferation and differentiation, as well as the MHC1 differentiation marker. Throughout the muscle regeneration process, the mRNA expression of Pax7, MyoD, and myogenin exhibited temporary increases, while RetSat and MYHC1 expressions showed temporary decreases in TA muscles. However, except for the RetSat mRNA, there were no significant differences observed in their expression between the two mouse strains (depicted in Figure 13B). In summary, the data strongly indicate that the absence of RetSat has no significant impact on satellite cell numbers in skeletal muscle. Furthermore, it does not affect the developmental processes or the regeneration of skeletal muscle tissue.

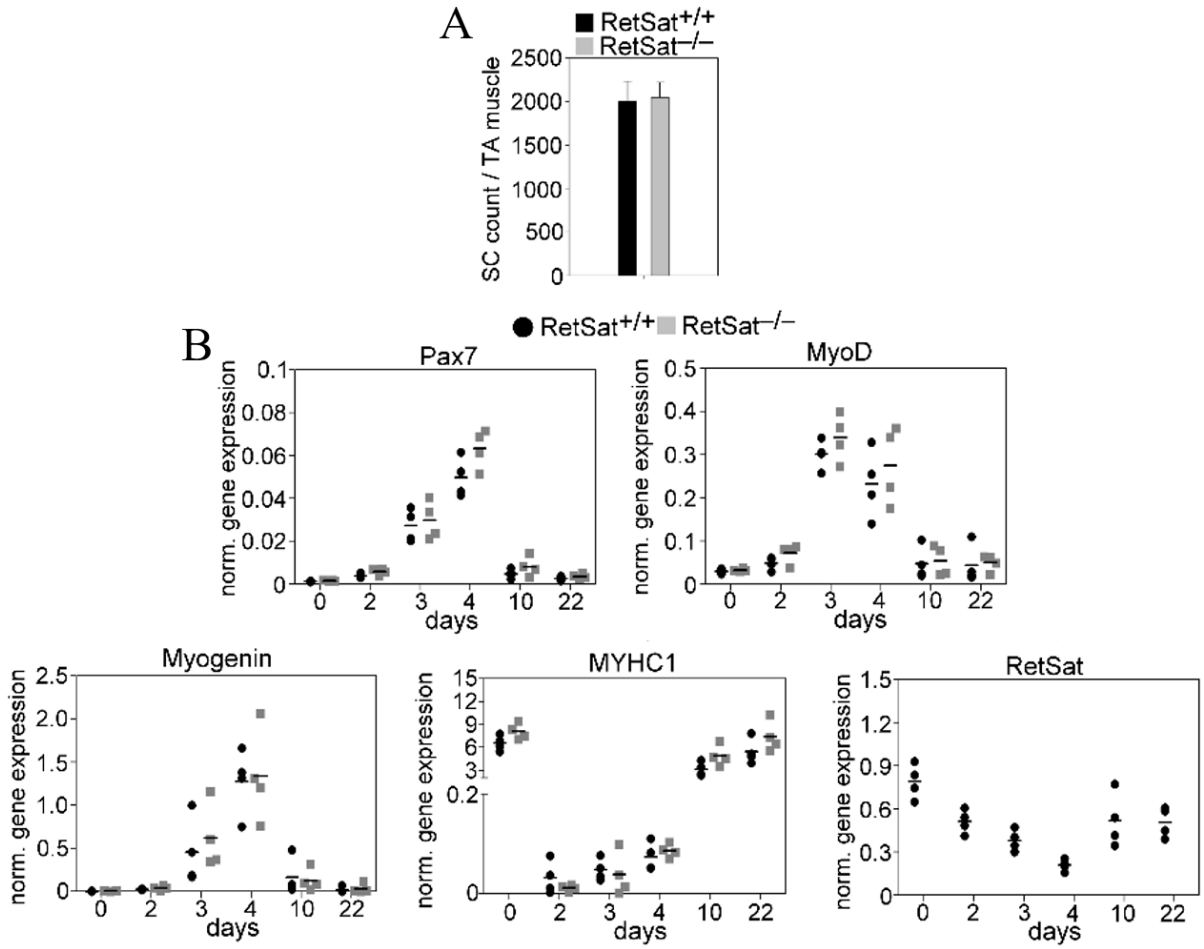

Figure 13: Normal satellite cell number and myogenic gene expression in the regenerating TA muscle of RetSat$^{-/-}$mice. *(A) The count of satellite cells in TA muscles on day 4 post-CTX-induced injury, and (B) the mRNA expression levels of several myogenic marker genes and RetSat in both control and regenerating TA muscles of RetSat$^{+/+}$ and RetSat$^{-/-}$ mice were analyzed using qRT-PCR (n=4). Significance was tested by Student's t-test.*

6.1.2. In the absence of RetSat, there is reduced recruitment of Mϕs and neutrophils following injury

After injury, muscle repair initiates with the migration of inflammatory cells to the site of injury. To understand the leukocyte composition in the early phase of muscle regeneration, we conducted a flow cytometry analysis of CD45$^+$ cells isolated from collagenase-digested muscles. Consistent with previous findings, we observed early neutrophil infiltration at day 2 post-injury, followed by an increasing number of Mϕs at days 3 and 4 in RetSat$^{+/+}$ mice. However, in the absence of RetSat, there was a significantly reduced influx of CD45$^+$ cells into the injured muscle (Figure 14A). Moreover, at day 2 post-injury, a markedly decreased

expression of monocyte chemoattractant protein-1 (MCP-1) was detected (Figure 14 B), while the neutrophil/Mϕ ratios remained unchanged (Figure 14 C).

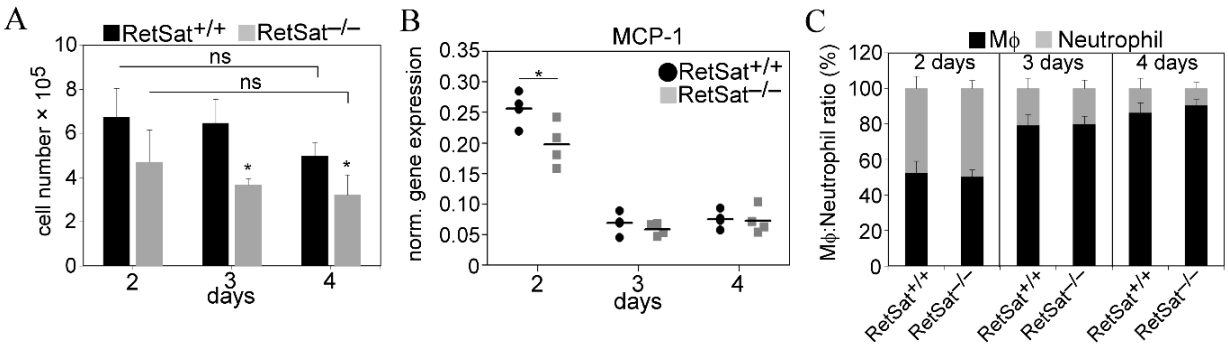

Figure 14: Diminished Mϕ and neutrophil recruitment in the regenerating TA muscle of RetSat$^{-/-}$mice. *(A) The quantity of CD45^{+} leukocytes per injured muscle and (B) MCP-1 mRNA expression levels in muscle-derived CD45^{+} leukocytes from RetSat$^{+/+}$ and RetSat$^{-/-}$ mice were determined through qRT-PCR after CTX-induced injury (n=4). (C) The ratio of anti-F4/80 antibody-stained Mϕs to anti-Ly6G/Ly6C (GR-1)-stained neutrophils within the CD45^{+} leukocyte populations in TA muscles from RetSat$^{+/+}$ and RetSat$^{-/-}$ mice was assessed during the initial 4 days of regeneration following CTX-induced injury (n=3). Significant differences are denoted by asterisks (* p < 0.05, ANOVA test); 'ns' is non-significant.*

6.1.3. Myoblasts compensate for diminished MFG-E8 levels in RetSat$^{-/-}$ mice Mϕs

To explore the influence of RetSat ablation on Mϕ polarization and gene expressions, CD45^{+} cells from collagenase-digested regenerating muscles were isolated at days 2, 3, and 4 post-injury and labeled with surface markers F4/80, Ly6C, CD206, and MHCII. Their gene expressions were analyzed using quantitative PCR. Surprisingly, despite the reduction in necrotic areas (Figure 12C), RetSat loss *in vivo* didn't seem to impact efferocytosis during skeletal muscle regeneration. Initially, we examined whether muscle-derived CD45^{+} cells from RetSat$^{-/-}$ mice showed altered MFG-E8 levels. As depicted in Figure 15, the expression of MFG-E8 mRNA within CD45^{+} cells gradually increased until day 4 following CTX-induced injury in both mouse strains. However, in line with our previous findings (Sarang, et al., 2019), muscle-derived CD45^{+} cells in RetSat$^{-/-}$ mice exhibited significantly lower MFG-E8 expression. This observation was consistent with the results of the *in vitro* phagocytosis assay, indicating a reduced long-term efferocytosis capacity of muscle-derived RetSat$^{-/-}$ Mϕs (Figure 12 A, B).

Despite the absence of RetSat in regenerating muscles, we observed no changes in MFG-E8 mRNA levels in RetSat$^{-/-}$ mice compared to their RetSat$^{+/+}$ counterparts (Figure 15). This suggests that myoblasts, the only other cell type besides Mϕs known to produce MFG-E8 in regenerating skeletal muscle, likely compensate for the reduced MFG-E8 production in Mϕs of RetSat$^{-/-}$ mice. Our analysis of NPY mRNA expression in CD45^{+} cells and total muscle (Figure 16) allowed us to estimate that in RetSat$^{+/+}$ regenerating muscles, less than 1% of MFG-E8 originates from CD45^{+} cells. Since MFG-E8 is released into the tissue environment, myoblast-derived MFG-E8 is likely accessible to phagocytic cells.

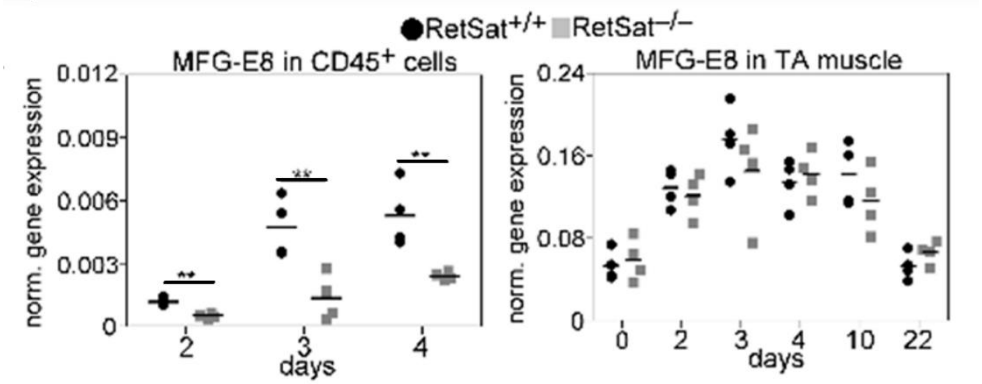

Figure 15: Myoblasts offset the reduced MFG-E8 production of RetSat$^{-/-}$ Mϕs. *MFG-E8 mRNA expression was analyzed in muscle-derived CD45^{+} leukocytes, total TA muscles of RetSat$^{+/+}$ and RetSat$^{-/-}$ mice using qRT-PCR after CTX-induced injury (n=4). Statistical significance was denoted by asterisks (* $p < 0.05$, ** $p < 0.01$, Student's t-test).*

6.1.4. Altered NPY levels in the Mϕs and skeletal muscle of RetSat$^{-/-}$ mice

Subsequently, we examined the expression of NPY in muscle-derived CD45^{+} cells. NPY is known for its anti-inflammatory properties (Dimitrijević, et al., 2008; Singer, et al., 2013) and its role in promoting angiogenesis (Lee, et al., 2003). In RetSat$^{+/+}$ mice, NPY mRNA levels in CD45^{+} cells from muscles increased until day 3 post-CTX-induced injury, after which they began to decline. In contrast, as previously observed (Sarang, et al., 2019), CD45^{+} cells from RetSat$^{-/-}$ mice exhibited negligible NPY expression (Figure 16). While skeletal muscle itself doesn't express NPY mRNA or protein in mice (Expression Atlas database (https://www.ebi.ac.uk/gxa/); MGI database (https://www.informatics.jax.org/)), sympathetic neurons, which co-release NPY with noradrenaline upon stimulation, do (Lundberg, et al., 1989). Notably, sympathetic neurons, regulate immune functions via NPY (Farzi, et al., 2015) and facilitate muscle repair (Yuan, et al., 2021). As shown in Figure 16, we found NPY mRNA

expression only in control muscles and muscles at day 10 and 22 post-injury in both RetSat$^{+/+}$ and RetSat$^{-/-}$ mice (Figure 16) concomitant with significantly elevated NPY mRNA levels in control muscles and 22 days regenerating RetSat$^{-/-}$ muscles. This pattern was consistent across various organs, except for the brain, where NPY mRNA expression was similar between the two strains. These results suggest that the loss of RetSat not only impacts NPY mRNA expression in Mϕs but also in sympathetic neurons innervating different tissues. Furthermore, in RetSat$^{+/+}$ mice, NPY mRNA expression in muscles peaked at day 3 post-injury, gradually declining afterward. In contrast, RetSat$^{-/-}$ mice showed no NPY mRNA expression during this period. Given the absence of NPY expression in CD45^{+} cells of RetSat$^{-/-}$ mice, the temporary increase in NPY expression in RetSat$^{+/+}$ muscle might be attributed to infiltrating NPY-expressing CD45^{+} cells.

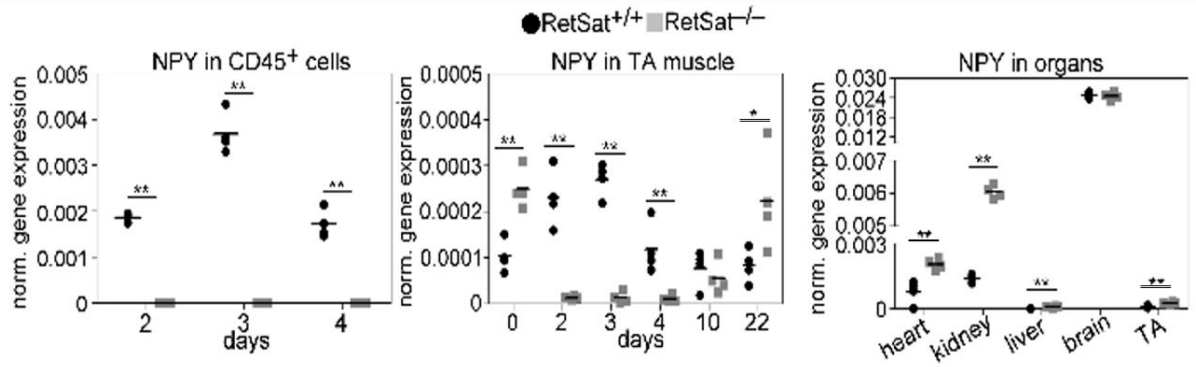

Figure 16: Altered NPY levels in Mϕs and skeletal muscle of RetSat$^{-/-}$ mice. *NPY mRNA expression was assessed in muscle-derived CD45^{+} leukocytes, total TA muscles, and various organs of RetSat$^{+/+}$ and RetSat$^{-/-}$ mice using qRT-PCR after CTX-induced injury (n=4). Statistical significance was denoted by asterisks (* $p < 0.05$, ** $p < 0.01$, Student's t-test).*

6.1.5. Altered M1/M2 phenotypic switch in the regenerating muscle of RetSat$^{-/-}$ mice

The precise orchestration of M1/M2 Mϕ phenotypic changes is crucial for effective muscle regeneration. To closely track this process, we analyzed the evolving expression of M1- and M2-specific surface markers on Mϕs and examined the gene expression profiles of CD45^{+} cells. Even though the loss of RetSat did not impact *in vivo* phagocytosis, regulating the normal Mϕ polarization, we observed a delay in the formation of Ly6C^{low} CD206^{+} Mϕs derived from Ly6C^{high} RetSat$^{-/-}$ NPY deficient pro-inflammatory cells on post-injury day 3 (Figure 17). However, by day 4, this delay dissipated, possibly due to elevated myoblast-derived MFG-E8

levels, facilitating M1/M2 conversion, in conjunction with the emergence of CD206^{+} Mϕs (Laplante, et al., 2017). Notably, the development of MHCII^{high}-expressing cells proceeded unaffected during this intricate temporal process.

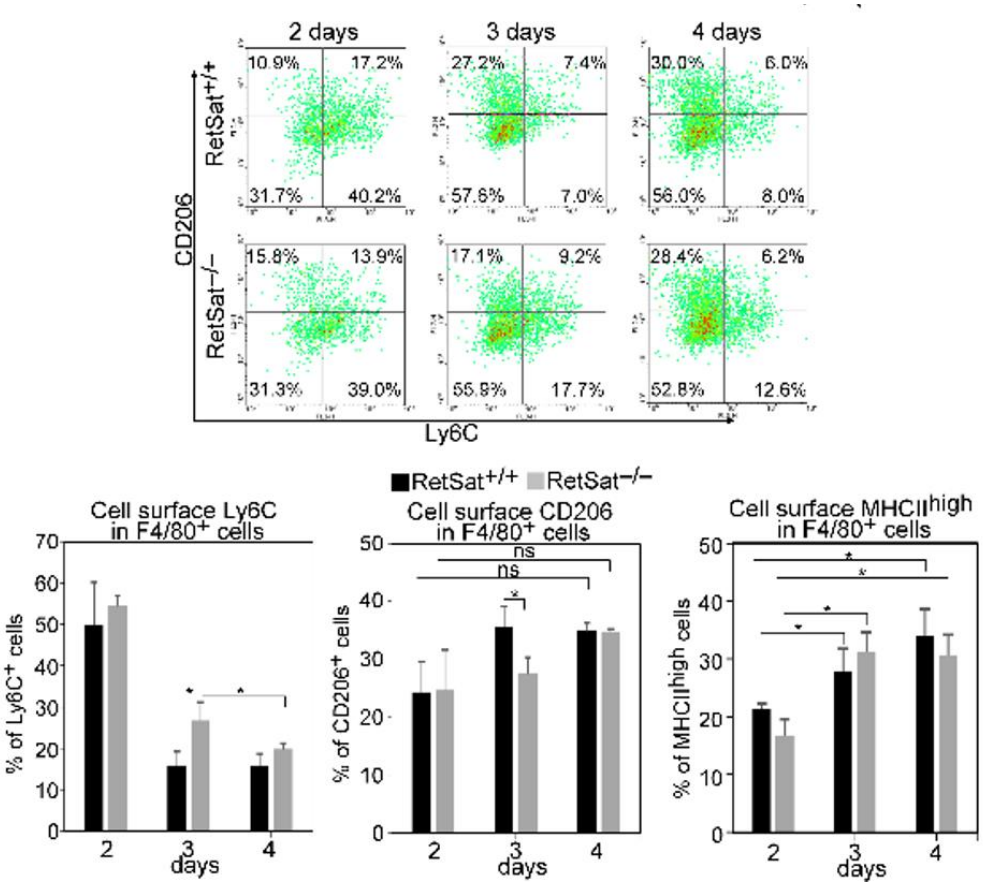

Figure 17: M1/M2 transition delay in RetSat$^{-/-}$ mice's Mϕs during muscle regeneration. *Scatter plots representing CD206- and Ly6C-stained muscle-derived F4/80^{+} cells were analyzed, determining the proportions of Ly6C^{high}, CD206^{+}, and MHCII^{high} cells within the muscle-derived F4/80^{+} population on specific days following CTX-induced injury in TA muscles of RetSat$^{+/+}$ and RetSat$^{-/-}$ mice (n=3). Statistical significance was denoted by asterisks (* p < 0.05, ** p < 0.01, ANOVA); 'ns' indicates non-significant results.*

6.1.6. Gene expression profiling of muscle-infiltrating CD45^{+} cells in RetSat $^{+/+}$ and RetSat$^{-/-}$ mice

In line with our earlier findings (Sarang, et al., 2014), there was an observed increase in RetSat mRNA expression within muscle-derived CD45^{+} cells involved in engulfing (Figure 18 A). Upon further examination, it was found that at day 2 post-injury, there was an elevated production of IL-1β in RetSat$^{-/-}$ cells, while other pro-inflammatory markers such as TNFα

and IL-6 showed no significant differences between the two strains. Additionally, the expression of anti-inflammatory markers, IL-10, and TGF-β1 displayed an increasing pattern from day 2 to 4, with only TGF-β1 showing alterations at day 2 post-injury. Noteworthy changes were observed in Arg1, NOS3, and the inducible iNOS, all known regulators of NO level. Interestingly, our study unveiled a significantly increased mRNA expression level of IL-4 in RetSat$^{-/-}$ CD45^{+} cells at post-injury day 2. Moreover, we compared the amount of FAP cells at day 4 post-injury in the TA muscle and found similar cell numbers between the two strains (Figure 18 B).

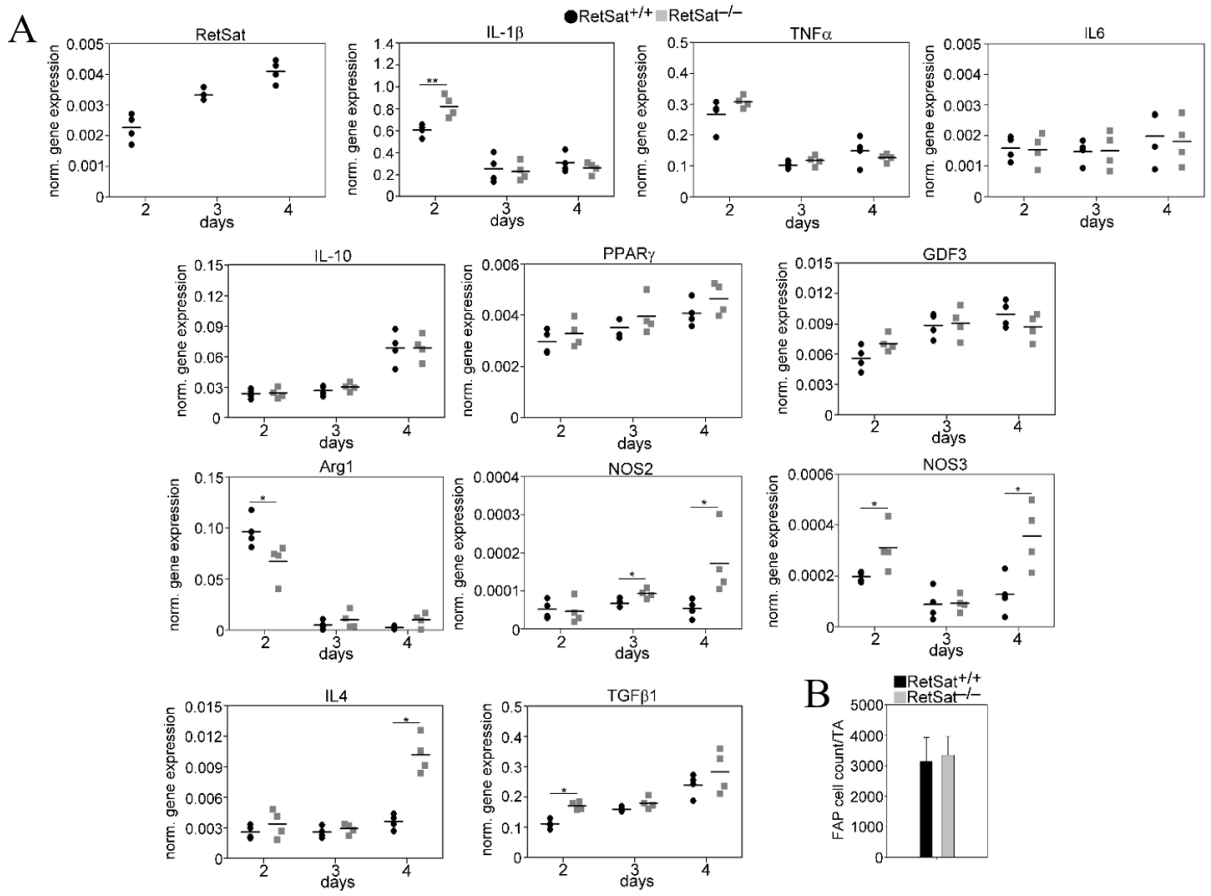

Figure 18: The mRNA expression of RetSat, cytokines, and growth factors in CD45^{+} Mϕs from regenerating TA muscles in RetSat$^{+/+}$ and RetSat$^{-/-}$ mice. *(A) Quantification of RetSat mRNA expression and various M1 and M2 marker genes in CD45^{+} cells isolated from TA muscles at post-injury days 2, 3, and 4 using qRT-PCR (n=4). Statistical significance is denoted by asterisks (* $p < 0.05$, ** $p < 0.01$, Student's t-test). (B) FAP cells count in TA muscles injected with CTX on day 4 after injury. Data presented as mean ± SD.*

6.2. Part II: Role of Adenosine A3 Receptor in skeletal muscle regeneration.

6.2.1. The lack of A3R does not affect skeletal muscle function in the knockout mice

In our next set of experiments, we set a goal to study the possible role of A3R in muscle homeostasis. Initially, we compared the characteristics of the TA, EDL, and SOL muscles in $A3R^{+/+}$ and $A3R^{-/-}$ mice. Interestingly, we found no significant disparities in body weights and muscle weights, including TA, EDL, and SOL muscles, between the two groups (Figure 19 B, C). However, a notable trend emerged: the fast twitch muscles (TA, EDL) of $A3R^{-/-}$ mice exhibited a tendency towards larger mean and median fiber CSA compared to their $A3R^{+/+}$ counterparts (Figure 19 D). Furthermore, our analysis revealed a higher proportion of larger fibers in the fast twitch muscles of $A3R^{-/-}$ mice in comparison to the $A3R^{+/+}$ mice (Figure 19 E-G). These intriguing findings shed light on the potential influence of A3 receptors on muscle fiber characteristics.

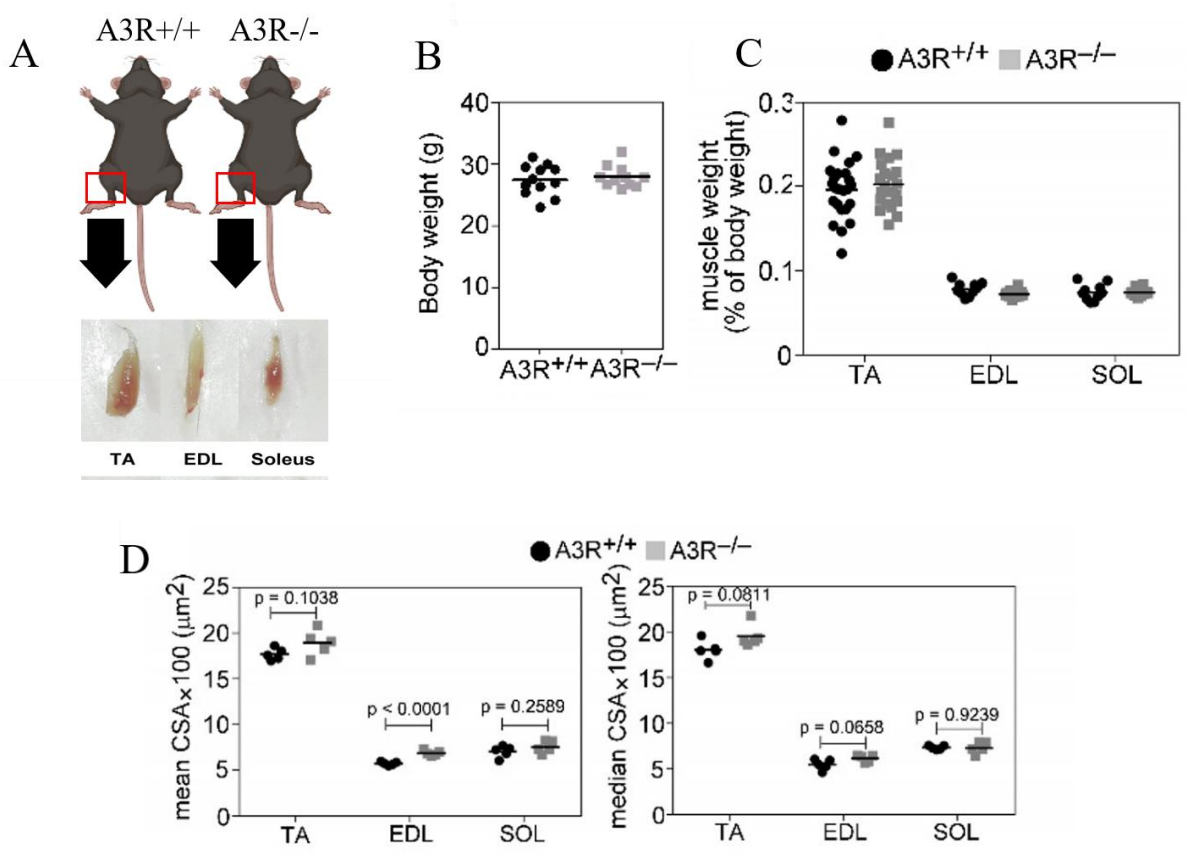

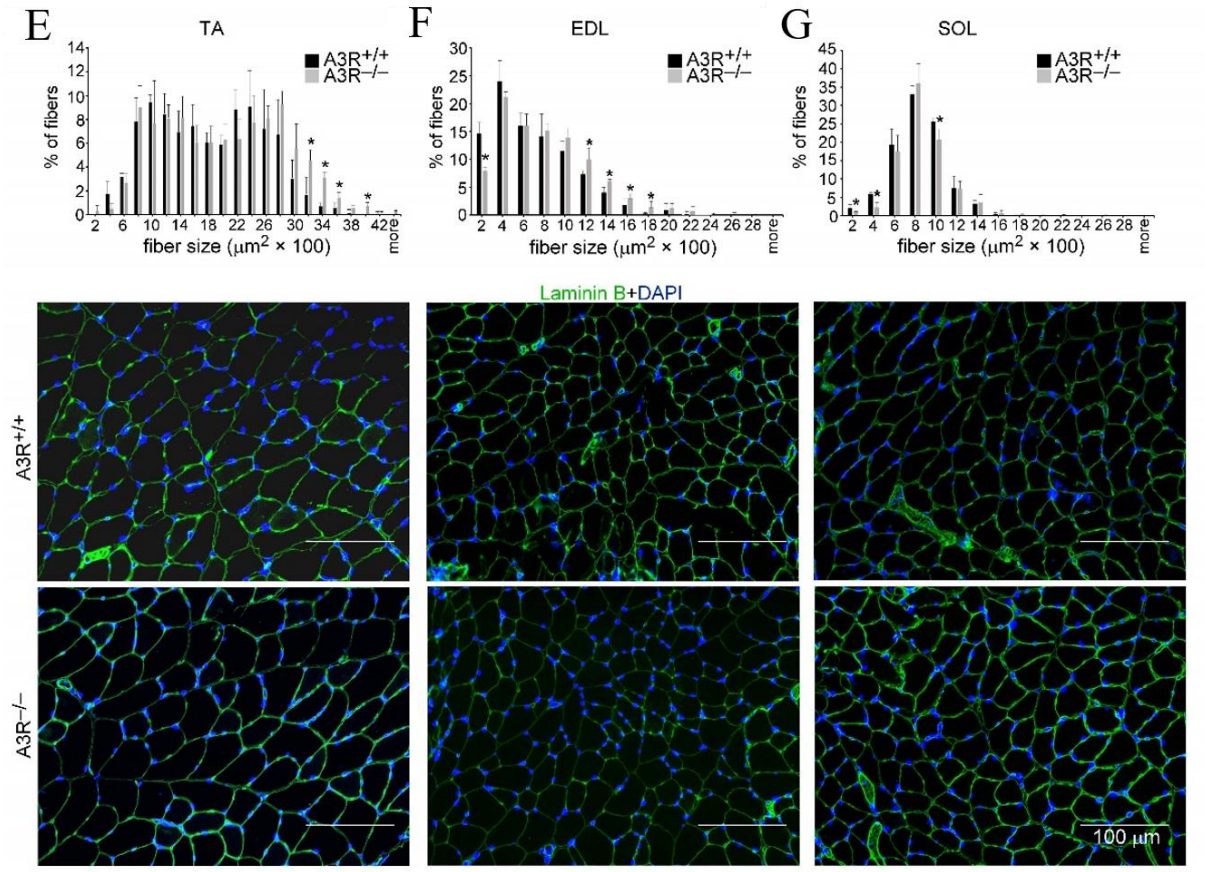

Figure 19: The phenotypic characteristics of TA, EDL, and SOL muscles of A3R$^{+/+}$ and A3R$^{-/-}$ mice. *(A) Schematic representation illustrating the three types of leg muscles (TA, EDL, SOL) that were isolated and utilized in the physiological experiments and laminin staining. (B) The body weight and (C) muscle weight/body weight ratios were compared between A3R$^{+/+}$ and A3R$^{-/-}$ mice. (D) Mean and median myofiber CSA of the TA, EDL, and SOL muscles in A3R$^{+/+}$ and A3R$^{-/-}$ untreated mice were analyzed. The data were expressed as mean and individual values, and statistical significance was determined by two-tailed Student's t-test (n= at least 4 samples). Myofiber size distribution in (E) TA, (F) EDL, and (G) SOL muscles of A3R$^{+/+}$ and A3R$^{-/-}$ mice was examined. Representative immunofluorescence pictures of laminin (green) and DAPI (blue) nuclear staining were captured, and ImageJ software was used to analyze 500 or more myofibers in each sample. Scale bars, 100 μm. Mean values ± SD are shown, and statistical significance was determined by two-tailed Student's t-test. *p < 0.05. (n=4 samples).*

We also conducted an in-depth analysis to assess the influence of A3R deficiency on the physical abilities of A3R$^{-/-}$ mice (Table 2). In our study, we specifically focused on evaluating their *in vivo* grip strength, a crucial metric used to gauge upper body and overall

muscular power. This assessment was meticulously performed in mice aged 18 to 20 weeks, encompassing both $A3R^{+/+}$ and $A3R^{-/-}$ mice. We observed a substantial reduction in the maximal grip force of $A3R^{-/-}$ mice compared to their $A3R^{+/+}$ counterparts, with values of 161.94 ± 7.13 mN in $A3R^{+/+}$ mice versus 122.79 ± 3.44** mN in $A3R^{-/-}$ mice, indicating a significant difference at ** $p < 0.01$ ($N = 5$). This disparity remained consistent even after accounting for the identical average body weight between the two groups: 5.80 ± 0.27 mN/g in $A3R^{+/+}$ vs. 4.57 ± 0.07 mN/g in $A3R^{-/-}$ mice. Consequently, we observed a significant reduction in the voluntary running activity of $A3R^{-/-}$ mice in comparison to their $A3R^{+/+}$ counterparts. Although the daily running distance remained unchanged, both the average and maximal speeds were considerably decreased in the $A3R^{-/-}$ mice. However, upon evaluating their performance during forced treadmill running, there was no discernible difference between the two groups.

Table 2: Grip force and voluntary running measurement in $A3R^{+/+}$ and $A3R^{-/-}$ mice.

Grip force	$A3R^{+/+}$ (N=5)	$A3R^{-/-}$ (N=5)
Body weight (g)	27.96 ± 0.28	26.9 ± 0.74
Maximal force (mN)	161.94 ± 7.13	122.79 ± 3.44**
Force normalized to body weight (mN/g)	5.8 ± 0.27	4.57 ± 0.07**
Voluntary running	$A3R^{+/+}$ (N=4)	$A3R^{-/-}$ (N=5)
Distance (m/day)	7805 ± 262.6	8002.8 ± 201.7
Average speed (m/min)	13.2 ± 0.5	11.6 ± 0.2*
Max speed (m/min)	24.9 ± 0.8	19.3 ± 0.4***
Forced running	$A3R^{+/+}$ (N=5)	$A3R^{-/-}$ (N=5)
Time (min)	15.55 ± 0.48	16.8 ± 1.0
Distance (m/day)	347.6 ± 13.6	386.5 ± 31.3

Mean values ± SD are shown, and statistical significance was determined by two-tailed Student's t-test. *p < 0.05, ** p < 0,01, and *** p < 0.001. N= number of animals.

We also observed no reduction in the maximum force capacity of the isolated EDL or SOL muscles (Table 3). These findings strongly suggest that the inferior grip force and voluntary running results in $A3R^{-/-}$ mice can be attributed to altered neurological functions (Wei, et al., 2011) rather than any changes in skeletal muscle function (Table 3).

Table 3: Muscle force measurement of EDL and SOL in $A3R^{+/+}$ and $A3R^{-/-}$ mice.

	TWITCH		TETANUS	
	$A3R^{+/+}$ (n=10)	$A3R^{-/-}$ (n=10)	$A3R^{+/+}$ (n=10)	$A3R^{-/-}$ (n=10)
EDL Force (mN/mm^2)	1.6 ± 0.19	1.59 ± 0.12	7.24 ± 0.76	7.35 ± 0.47
SOL Force (mN/mm^2)	1.87 ± 0.16	2.46 ± 0.21*	9.21 ± 0.64	12.22 ± 1.14*

Mean values ± SD are shown, and statistical significance was determined by two-tailed Student's t-test. *$p < 0.05$. n= number of muscles.

6.2.2. Faster regeneration of the TA muscle in $A3R^{-/-}$ mice

To investigate the potential role of A3Rs in skeletal muscle regeneration, we conducted a histological examination of TA muscles from both $A3R^{+/+}$ and $A3R^{-/-}$ mice, both in control conditions and after CTX injection. The gross appearance of the control muscles was unchanged, (Figure 20 A). On days 2, 3, and 4 post-injury, both $A3R^{+/+}$ and $A3R^{-/-}$ regenerating muscles similarly exhibited local necrosis and a substantial influx of inflammatory cells. Previous research has indicated that impaired phagocytosis can lead to delayed clearance of necrotic areas (Al-Zaeed, et al., 2021). Surprisingly, even though the Mϕs' ability to engulf dead cells remained unaffected by the absence of A3Rs (Duró, et al., 2014), the $A3R^{-/-}$ muscles demonstrated a more efficient clearance of necrotic fibers by day 8 after CTX-induced injury (Figure 20 A and B).

This observation suggests that there might be compensatory mechanisms or alternative pathways at play in $A3R^{-/-}$ mice, leading to enhanced necrotic tissue clearance despite the lack of A3Rs. By day 22 post-injury, both $A3R^{+/+}$ and $A3R^{-/-}$ muscles exhibited a largely restored histological structure, indicating that the regenerative processes had effectively taken place, and necrotic fibers were no longer visible (Figure 20 A and B).

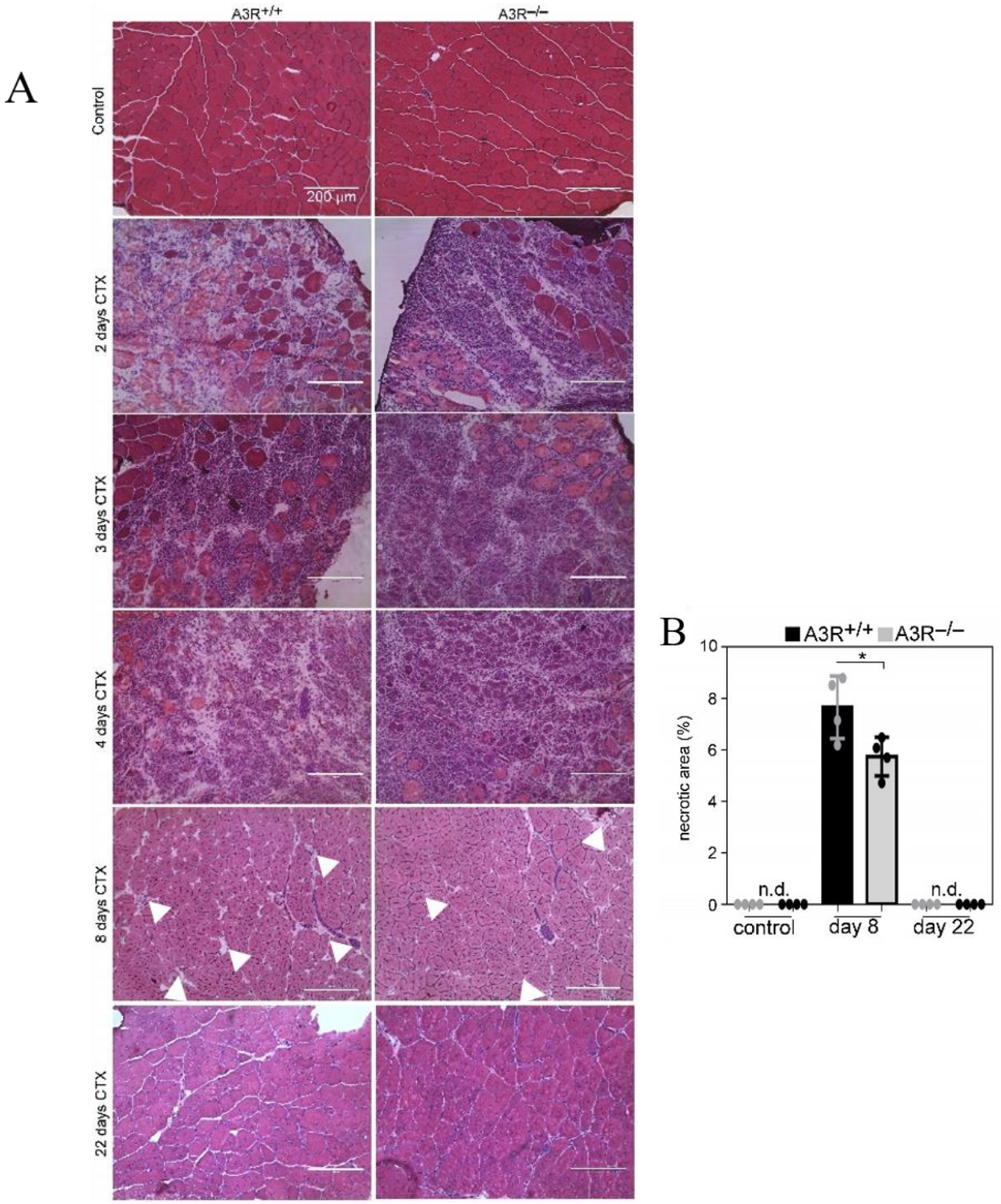

Figure 20: Histological changes in TA muscles of A3R$^{+/+}$ and A3R$^{-/-}$ mice post-CTX injury, showing improved dead cell clearance in regenerating A3R$^{-/-}$ TA muscles over time. *(A)Muscle damage was induced by injecting 50 µl of 12 µM CTX into the TA muscles. Cross-sections of TA muscles from both A3R$^{+/+}$ and A3R$^{-/-}$ mice were stained with H&E to observe changes before (control) and at days 2, 3, 4, 8, and 22 following CTX treatment (n=4). Necrotic areas are marked with arrows. The scale bars represent 200 µm. (B) Necrotic areas in the*

*muscles of both A3R$^{+/+}$ and A3R$^{-/-}$ mice were examined in both the control, 8 and 22-day regenerating muscle tissues. The results are presented as the mean values along with individual data points. Statistical significance was assessed using a two-tailed Student's t-test. *p < 0.05. The study involved a sample size of n=4. In cases where values were not detected, it is denoted as n.d*

Apart from immune cells and satellite cells, successful muscle regeneration requires the presence of fibroblasts. These cells create a provisional ECM, stabilizing the healing tissue and offering support for growing muscle fibers. Initially, collagen 1 deposition rises, peaking before gradually declining over time (Mann, et al., 2011). By the tenth day after CTX-induced injury, regenerating muscles in both A3R$^{+/+}$ and A3R$^{-/-}$ mice displayed elevated collagen I levels compared to their non-regenerating counterparts. Interestingly, A3R$^{-/-}$ muscles exhibited significantly reduced collagen deposition at this stage. However, by the 22nd day post-injury, collagen levels had almost returned to normal, and there was no significant difference in collagen deposition between the two mouse strains, indicating only a temporary disparity in collagen production during the regenerative process (Figure 21 A and B).

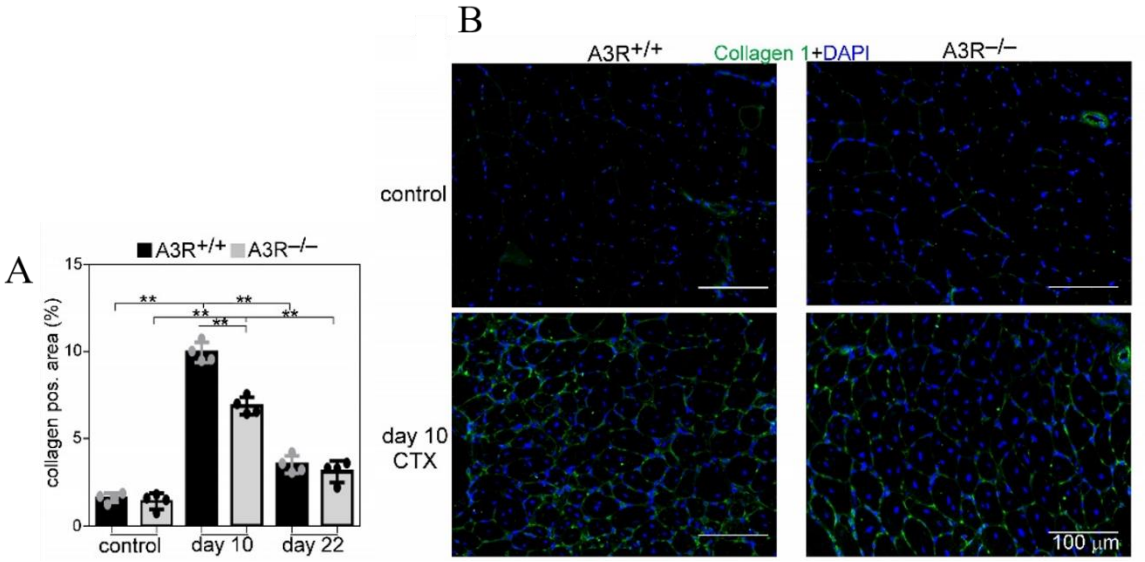

Figure 21: Reduced collagen 1 accumulation in the regenerating TA muscles of A3R$^{-/-}$ mice. *(A) Calculation of collagen 1-positive areas in the muscles that were regenerating for 10 and 22 days, as well as in the control muscles of both A3R$^{+/+}$ and A3R$^{-/-}$ mice. The results are presented as mean values along with individual data points. Statistical significance was determined using a two-tailed ANOVA test. **p < 0.01. The study included a sample size of n=4. (B) Illustrative immunofluorescence images displaying type 1 collagen (green) and DAPI*

(blue) nuclear staining in the control and 10-day regenerating TA muscles of both A3R$^{+/+}$ and A3R$^{-/-}$ mice. The scale bars represent 100 μm.

To delve deeper into the muscle regeneration process in the absence of A3Rs, we examined the muscle weights and myofiber CSAs of TA muscles treated with CTX in A3R$^{+/+}$ and A3R$^{-/-}$ mice. Notably, TA muscle weights did not display any noticeable differences between A3R$^{-/-}$ mice and their A3R$^{+/+}$ counterparts at various time points post-injury with CTX (Figure 22A). In A3R$^{-/-}$ mice, the mean and median CSAs of newly formed myofibers with central nuclei were comparable to the A3R$^{+/+}$ at day 10 (Figure 22 B, C) but notably larger than those in A3R$^{+/+}$ mice at day 22 post-injury (Figure 22 B, D). Examination of CSA frequency distribution revealed a similar fiber size distribution in control A3R$^{+/+}$ and A3R$^{-/-}$ mice. However, at day 22 of regeneration, the A3R$^{-/-}$ muscles exhibited a significantly reduced frequency of smaller fibers and a marked increase in the frequency of larger fibers compared to the A3R$^{+/+}$ counterparts (Figure 22 D). The presence of myofibers containing multiple central nuclei is a marker of myoblast fusion during muscle regeneration. As demonstrated in Figure 22E, the count of newly formed fibers with two or more central nuclei was significantly higher in A3R$^{-/-}$ mice compared to their A3R$^{+/+}$ counterparts at both day 10 and day 22 post-injury, as depicted in the provided data (Figure 22 E). Collectively, these findings suggest an expedited skeletal muscle regeneration in the absence of A3Rs, marked by swifter elimination of necrotic regions, earlier reduction or lesser accumulation of collagen, increased myoblast fusion, and the generation of larger myofibers.

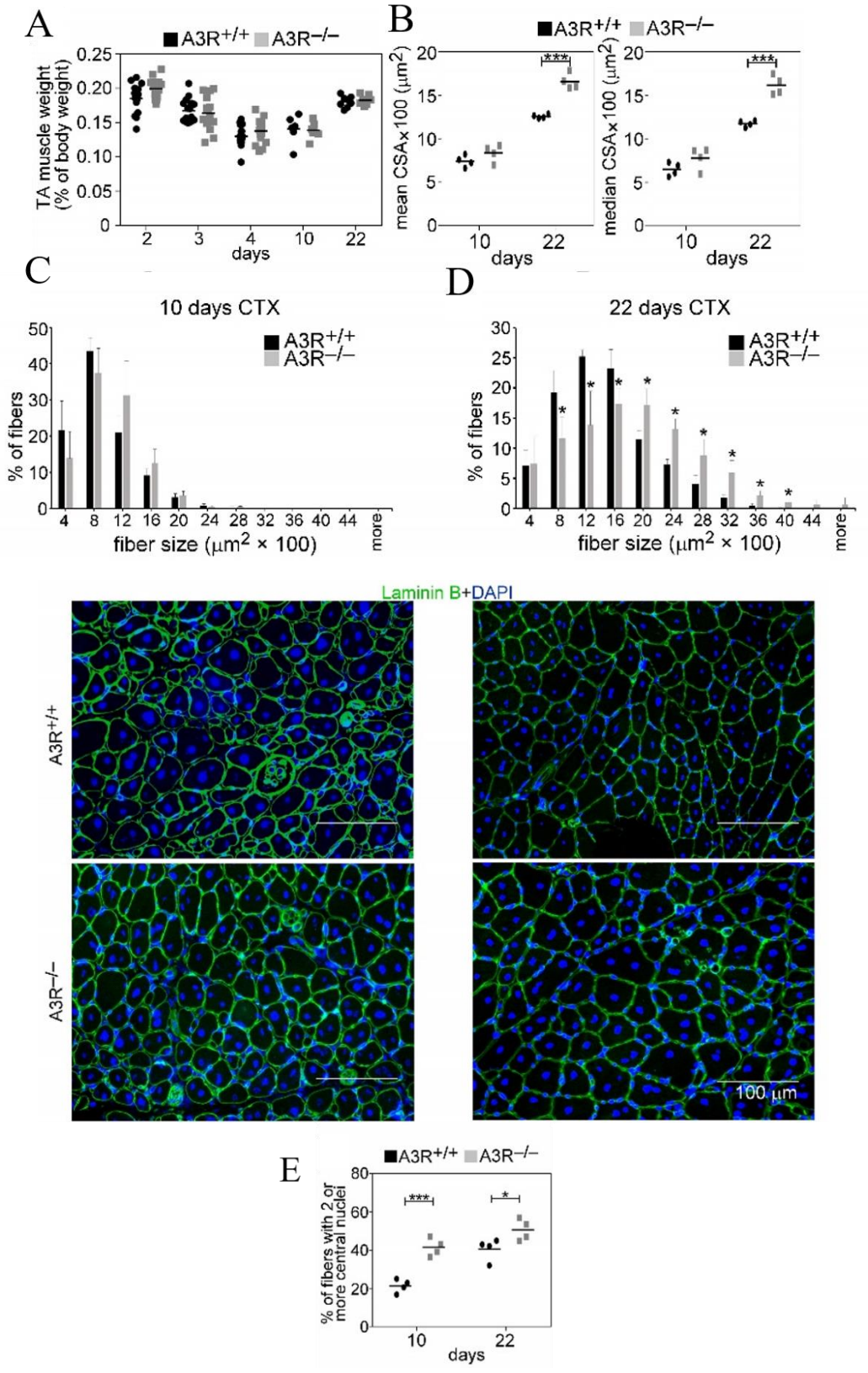

Figure 22: Enlarged muscle fiber size observed in the regenerating muscles of A3R$^{-/-}$ mice. *(A) Weights of muscles relative to body weight, (B) mean and median myofiber cross-sectional area (CSA) of the TA muscles, (C) and (D) myofiber size distribution in TA muscles of A3R$^{+/+}$ and A3R$^{-/-}$ mice at days 10 and 22 after CTX-induced injury, along with corresponding*

*immunofluorescence images showing laminin (green) and DAPI (blue) nuclear staining. Scale bars, 100 μm. More than 500 myofibers were analyzed in each sample using ImageJ software. Data are presented as mean or median ± SD. (E) Percentage of newly formed myofibers containing two or more central nuclei in TA muscles of A3R$^{+/+}$ and A3R$^{-/-}$ mice at days 10 and 22 post-CTX injury. Mean or median values are shown along with individual data points in panels (A, B, and E) (n= at least 15 samples in panel (A) and n=4 in panels (B and E)), whereas mean ± SD (n=4) is presented in panels (C and D). Statistical significance was determined using a Student's t-test. *p < 0.05, ***p < 0.001*

6.2.3. The absence of A3Rs leads to higher recruitment of CD45$^+$ cells to the site of injury

The absence of A3Rs in skeletal muscle tissues, as indicated by previous research (Gnad, et al., 2020), suggests that the observed changes are not directly linked to muscle cells themselves. Considering the pivotal role of inflammatory cell migration and tissue inflammation in the muscle regeneration process following injury, our attention was directed towards understanding the impact of A3Rs on these inflammatory cells, vital components of the regenerative response.

To quantify leukocyte, count and assess the proportion of Mϕs within the recruited cells during the initial stages of muscle regeneration, we conducted flow cytometric analysis on magnetically isolated CD45$^+$ cells obtained from collagenase-digested muscles. Consistent with prior findings, we observed early infiltration of CD45$^+$ cells at day 2 post-injury (Figure 23 A) and a progressive increase in the percentage of MΦs within this cell population at days 3 and 4 in A3R$^{+/+}$ mice (Figure 23 B). Deletion of A3Rs had no impact on the MΦ/CD45$^+$ ratios (Figure 23 B), but it led to a notable rise in both the number of infiltrating CD45$^+$ cells (Figure 23 A) and the expression level of monocyte chemoattractant protein-1 (MCP-1), a chemoattractant signal crucial for neutrophil and MΦ recruitment (Metzemaekers, et al., 2020; Martinez, et al., 2010) (Figure 23 C), in the regenerating muscles of A3R$^{-/-}$ mice.

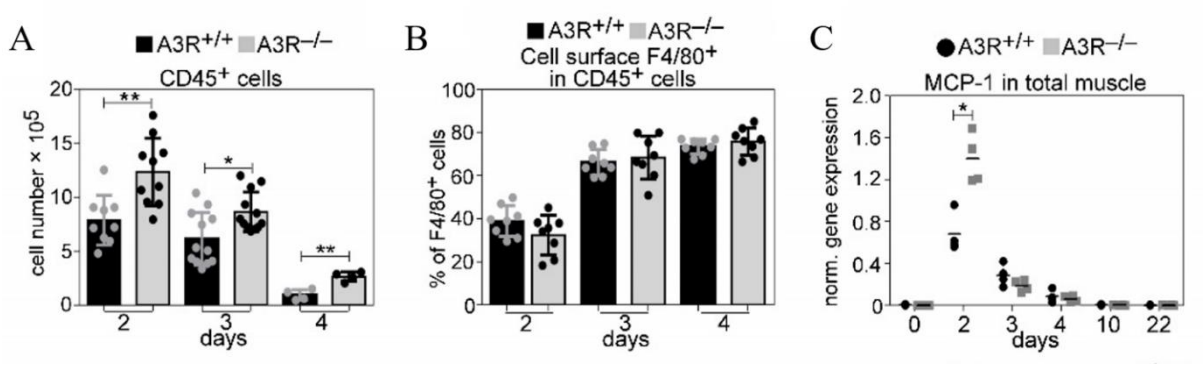

Figure 23: Increased leukocyte number in the regenerating TA muscles of A3R$^{-/-}$ mice. *(A) Changes in the number of CD45$^+$ leukocytes per injured muscle and (B) the percentage of anti-F4/80 antibody-stained Mϕs within the CD45$^+$ leukocyte population in A3R$^{+/+}$ and A3R$^{-/-}$ TA muscles during the initial 4 days of regeneration after CTX-induced injury (n= at least 4 samples). (C) mRNA expression levels of MCP-1 in A3R$^{+/+}$ or A3R$^{-/-}$ TA muscles determined by RT-qPCR following CTX-induced injury (n=4). The data are presented as mean values along with individual data points, and statistical significance was assessed using a Student's t-test. *p < 0.05, **p < 0.01 (n=4).*

6.2.4. Altered M1/M2 Mϕ phenotypic switch in the regenerating muscles of A3R$^{-/-}$ mice

In light of adenosine's known role in modulating the phenotypic shift of Mϕs toward M1/M2 states (Pinhal-Enfield, et al., 2003), which is integral for effective tissue regeneration, our study delved into understanding the phenotypic dynamics of A3R$^{-/-}$ MΦs during skeletal muscle regeneration. As depicted in Figure 24 A-C, our findings revealed a delayed disappearance of the M1-specific marker (Arnold, et al., 2007; Saclier, et al., 2013; Bosurgi, et al., 2012) Ly6C^{high} and a postponed appearance of M2-specific marker CD206 phagocytic receptor (Chávez-Galán, et al., 2015) on F4/80$^+$ MΦs in A3R$^{-/-}$ muscles. Notably, the presence of MHCII^{high}-expressing A3R$^{-/-}$ F4/80$^+$ MΦs, indicative of a distinct activation state (Panduro, et al., 2018), was heightened during this process. Considering our earlier research, which indicated that the absence of Nur77 transcription factor, selectively expressed by a subset of reparative Mϕs can disrupt their phenotypic transition (Garabuczi, et al., 2023), we investigated A3R expression in distinct subpopulations of isolated CD45$^+$ cells at day 4 post-CTX injury (Figure 24 D). Our analysis revealed low A3R expression in pro-inflammatory Mϕs but selective upregulation in resolution-related and antigen-presenting reparative Mϕ subgroups. Furthermore, high expression levels were observed in CD8$^+$ Clec9a$^+$ dendritic cells and

neutrophils. A3R expression was detected in muscle-specific $CD45^+$ cells at both day 2 and day 3 post-injury (Figure 24 E). Notably, as the proportion of Mϕs within the $CD45^+$ cell population increased, A3R expression levels also rose. Concurrently, A2aR expression within the $CD45^+$ cell population exhibited a temporal increase (Figure 24 E). Given that A2aR was more prominently expressed in pro-inflammatory Mϕs, this rise could reflect its heightened expression in lymphoid $CD8a^+$ dendritic cells (Figure 24 D). The absence of A3Rs had no significant impact on the expression of A2aRs, but a notable compensatory increase was observed in A2bRs (Figure 24 E). Unlike A3Rs, A2bRs were prominently expressed in pro-inflammatory Mϕs and neutrophils (Figure 24 D), and as the proportions of both neutrophils and pro-inflammatory Mϕs diminished throughout regeneration, the expression of A2bRs also declined. These findings underscore the signaling roles of A2Rs in pro-inflammatory processes, with A3Rs being particularly implicated in neutrophils and resolution-related and antigen-presenting Mϕs. In line with the muscle gene expression data (Figure 23 C), MCP-1 expression in $CD45^+$ cells was notably elevated at day 2 post-injury (Figure 24 E), indicating that the increased number of migrating cells contributed to the heightened MCP-1 expression in the total muscle (Figure 23 C). Notably, the absence of A3Rs did not significantly alter the temporal expression patterns of the pro-inflammatory cytokines IL-1β and TNF-α, although there was a tendency for higher mRNA levels at day 2 post-injury. These findings underscore the intricate regulation of cytokine dynamics during muscle regeneration, suggesting that the influence of A3Rs on the inflammatory response may involve intricate signaling pathways yet to be fully comprehended. Because past research suggested that the Nur77 transcription factor can dampen pro-inflammatory reactions in monocytes and Mϕs (McMorrow & Murphy, 2011), and adenosine was demonstrated to induce Nur77 expression (Crean, et al., 2015), we assessed Nur77 mRNA expression. On day 2 post-injury, $A3R^{-/-}$ $CD45^+$ cells exhibited significantly reduced Nur77 mRNA levels compared to their $A3R^{+/+}$ counterparts, although this distinction vanished by day 3, as illustrated in Figure 24 E. On the contrary, the mRNA levels of M2-associated cytokines IGF-1 and TGF-β remained unchanged, while the expression of GDF3 notably decreased from day 3 post-injury in $A3R^{-/-}$ cells compared to the $A3R^{+/+}$ cells. These findings collectively indicated a postponed shift from pro-inflammatory to reparative Mϕs during skeletal muscle regeneration in $A3R^{-/-}$ mice. More prominently, an early intensified pro-inflammatory response was observed, marked by a diminished Nur77 upregulation.

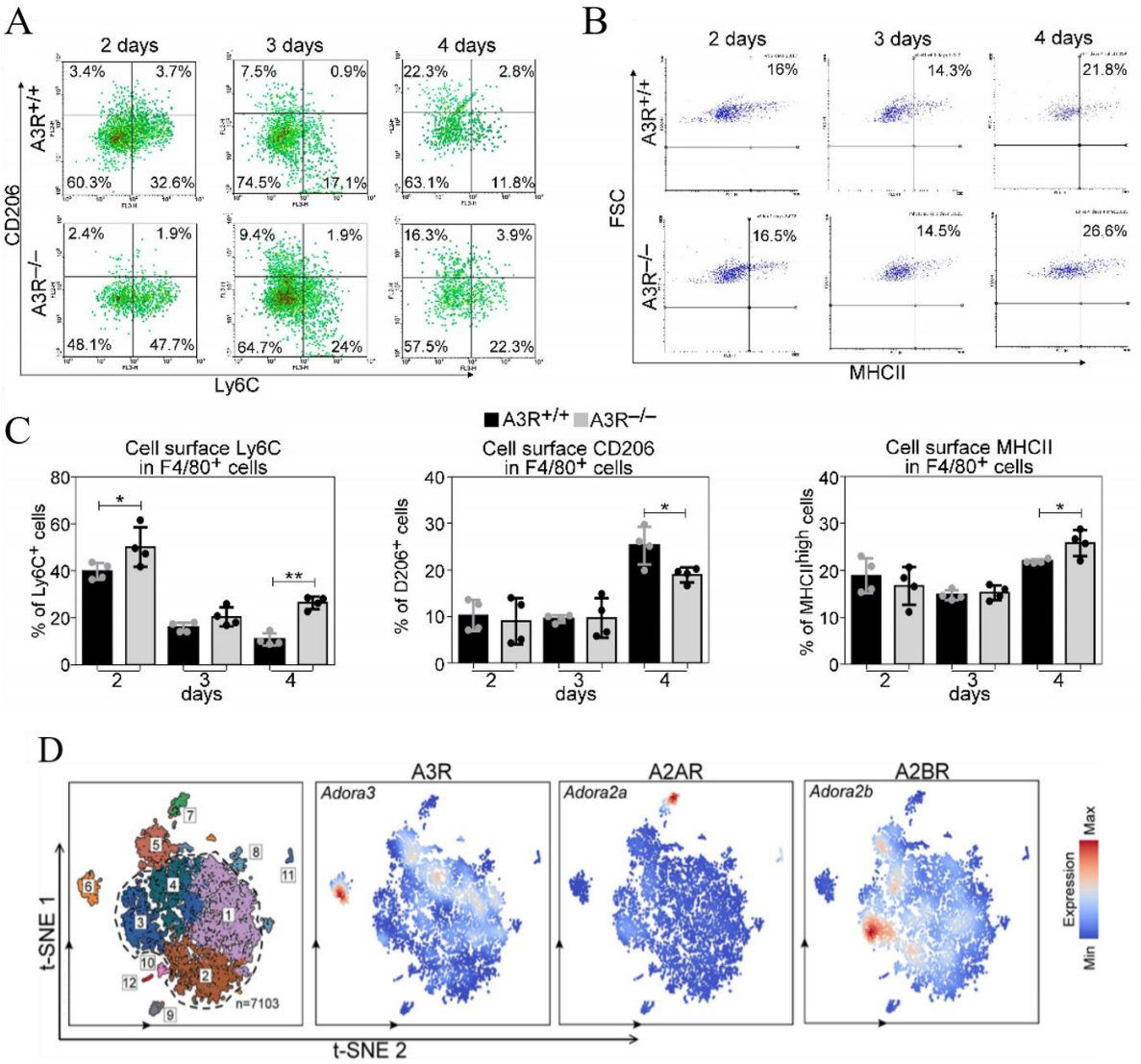
A
2 days
3 days
4 days
A3R+/+
A3R−/−
CD206
Ly6C
3.4%
3.7%
60.3%
32.6%
7.5%
0.9%
74.5%
17.1%
22.3%
2.8%
63.1%
11.8%
2.4%
1.9%
48.1%
47.7%
9.4%
1.9%
64.7%
24%
16.3%
3.9%
57.5%
22.3%
B
2 days
3 days
4 days
16%
14.3%
21.8%
16.5%
14.5%
26.6%
FSC
MHCII
C
A3R+/+ A3R−/−
Cell surface Ly6C in F4/80+ cells
% of Ly6C+ cells
Cell surface CD206 in F4/80+ cells
% of D206+ cells
Cell surface MHCII in F4/80+ cells
% of MHCIIhigh cells
days
D
A3R
A2AR
A2BR
Adora3
Adora2a
Adora2b
t-SNE 1
t-SNE 2
n=7103
Expression
Max
Min

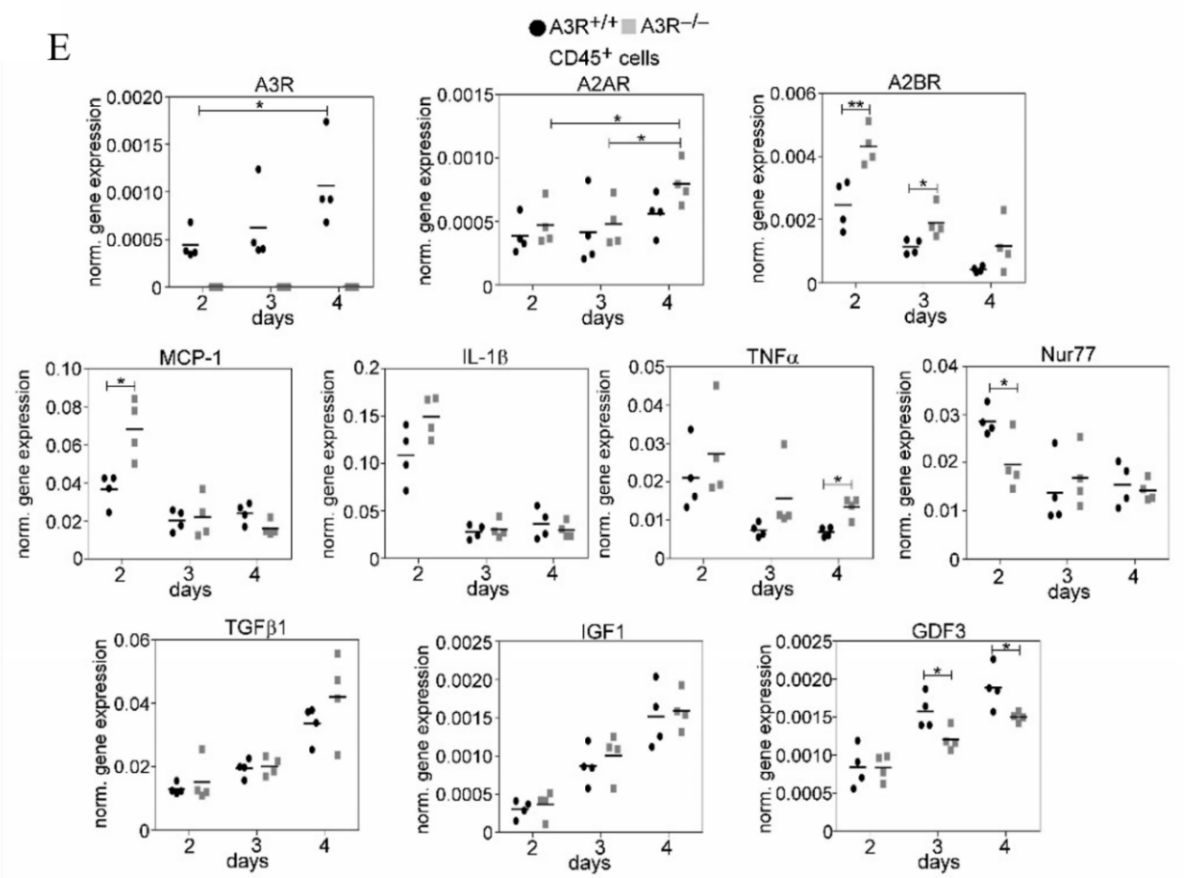

Figure 24: The regenerating A3R$^{-/-}$ TA muscles display altered Mϕ polarization, and the absence of A3R affects the gene expression pattern in muscle-derived CD45^{+} cells. *(A) Sample scatter plots illustrating CD206/Ly6C-stained and (B) MHCII^{high} muscle-derived F4/80^{+} cells observed on specified days following CTX-induced injury in TA muscles of both A3R$^{+/+}$ and A3R$^{-/-}$ mice. (C)Percentages of Ly6C^{high}, CD206^{+}, and MHCII^{high} cells within the muscle-derived F4/80^{+} population assessed on the indicated days post-CTX-induced injury in TA muscles of A3R$^{+/+}$ and A3R$^{-/-}$ mice (n = 4). Additionally, (D) a single-cell analysis depicted the expression patterns of various ARs in CD45^{+} cells isolated from TA muscles of* A3R$^{+/+}$ *mice at day 4 post-CTX-induced injury, (colored by 12 clusters defined using cluster resolution 0.4; the dotted line indicates the four Mϕ clusters 1-4; 1: Resolution-related, 2: Growth Factors-Expressing, 3: Pro-inflammatory, 4: Antigen-presenting Mϕs, 5: myeloid CD8a^{+} dendritic cells, 6: CD8a^{+} Clac9a^{+} dendritic cells, 7: Lymphoid CD8a^{+} dendritic cells, 8: Fibroblast-like cells, 9: Neutrophils, 10: Endothelial cells, 11: T-cell/NK T cells, 12: Fibroblasts). (E) mRNA expressions of various ARs and inflammatory markers in muscle-derived CD45^{+} cells isolated at different time points post-CTX injury were determined by RT-qPCR. The data are presented as mean and individual values and statistical significance was determined using a Student's t-test and ANOVA. *p < 0.05, **p < 0.01 (n=4).*

6.2.5. Improved proliferation and accelerated differentiation of satellite cells in the healing skeletal muscle of mice lacking A3Rs

To further explore the impact of A3R depletion on skeletal muscle regeneration, we evaluated the number of satellite cells and analyzed the mRNA expression levels of myogenic genes, including Pax7 and MyoD transcription factors that govern satellite cell proliferation and differentiation (Zammit, et al., 2006). Additionally, we examined myogenin, a marker indicative of myoblast differentiation that orchestrates myoblast fusion by transcribing crucial elements (Ganassi, et al., 2018), in both control and regenerating TA muscles. The transcription factor Pax7 is a vital marker indicating quiescent satellite cells, with its expression persisting during satellite cell activation and proliferation but diminishing when myogenic differentiation commences (Rudnicki, et al., 2008). Consequently, its mRNA levels directly reflect the quantity of satellite cells. As depicted in Figure 25 A, by day 4 post-injury, there was a notable increase in the number of satellite cells in the $A3R^{-/-}$ TA muscle compared to their $A3R^{+/+}$ counterparts. Furthermore, compared to $A3R^{+/+}$ muscle, an elevated Pax7 mRNA expression was evident in the $A3R^{-/-}$ muscles by day 3 following injury (Figure 25 B). These findings underscore an augmented satellite cell response in the absence of A3Rs during skeletal muscle regeneration. The expression of MyoD exhibited a proportional increase with Pax7 by day 3 in $A3R^{-/-}$ muscles, suggesting that its heightened expression is linked to the increased numbers of satellite cells rather than an amplified expression within individual satellite cells. In contrast, myogenin mRNA expression, previously observed to peak at day 4 post-injury in $A3R^{+/+}$ muscles (Tarban, et al., 2022), reached its zenith by day 3 in the $A3R^{-/-}$ muscles. These findings point to an accelerated proliferation and an earlier onset of satellite cell differentiation into myoblasts in $A3R^{-/-}$ muscles, accompanied by a premature decline in Pax7 gene mRNA expression. In the subsequent analysis, we assessed the mRNA levels of cytokines and growth factors with known effects on satellite cell proliferation and differentiation. This examination aimed to capture their expression in the entire muscle, representing the *in vivo* milieu influencing myoblasts. On day 2 post-injury, $A3R^{-/-}$ muscles exhibited significantly elevated mRNA expression of pro-inflammatory cytokines such as TNF-α, and IL-6, which are also produced by neutrophils (Tecchio, et al., 2014). Notably, IL-1β expression was also increased in the knockout muscles but it did not reach a significant level. This heightened expression aligns with the increased influx of inflammatory cells and is indicative of an accelerated pro-inflammatory response in $A3R^{-/-}$ muscles. Notably, these signaling molecules are recognized for their role in promoting satellite cell proliferation (Otis, et al., 2014; Tidball & Welc, 2015). By the third day post-injury, a decline in the mRNA expression levels of pro-inflammatory

cytokines was observed. Concurrently, the expression of GDF3, an early regulator of myoblast differentiation and fusion (Ge, et al., 2013), significantly decreased, facilitating the early onset of differentiation. By day 3 post-injury, the mRNA levels of differentiation-promoting factors, including TGF-β and IGF-1, peaked. Particularly, IGF-1, which regulates myogenin expression (Rudnicki, et al., 2008), was significantly elevated in $A3R^{-/-}$ muscles compared to $A3R^{+/+}$ counterparts. These time shifts in cytokine expressions likely contribute to the accelerated proliferation, earlier differentiation of satellite cells, and enhanced myoblast fusion observed in $A3R^{-/-}$ muscles.

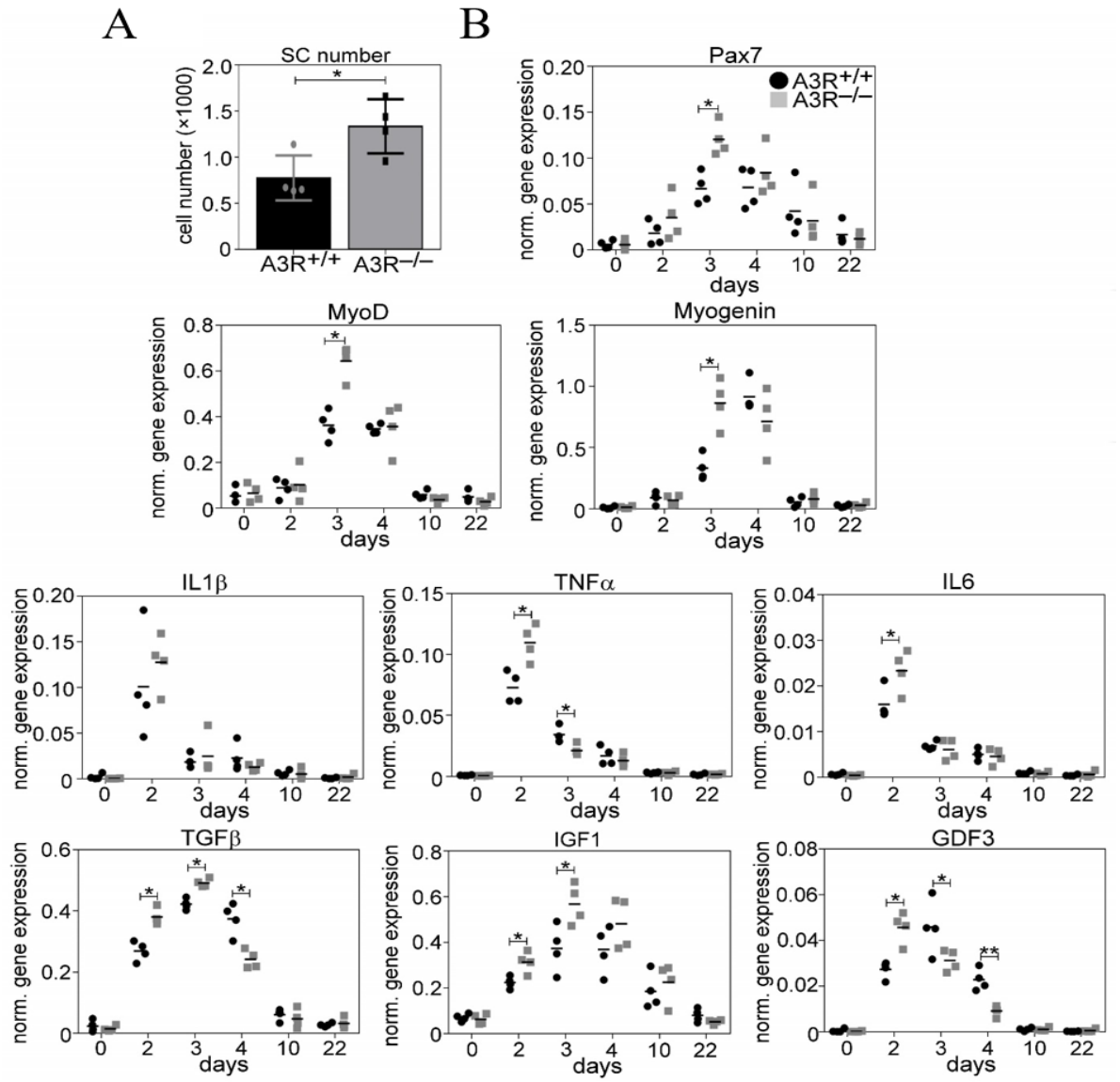

Figure 25: Regenerating skeletal muscle in $A3R^{-/-}$ mice shows increased proliferation and earlier differentiation of satellite cells. *(A) Number of satellite cells from regenerating TA muscles of $A3R^{+/+}$ and $A3R^{-/-}$ mice, and expression of Pax7 in control and regenerating TA*

*muscles detected through RT-qPCR. (B) Expression levels of myogenic and inflammatory markers in control and regenerating TA muscles from A3R$^{+/+}$ and A3R$^{-/-}$ mice at different post-injury time points, determined by RT-qPCR. Data are presented as mean and individual values and statistical significance was determined using a Student's t-test. *$p < 0.05$, n=4.*

7. Discussion

Prior studies have established the significance of robust intercellular communication among diverse cell populations during the process of skeletal muscle repair, ensuring a delicate balance in the regeneration process. Our current research builds upon this foundation, revealing that in the regenerating muscles of RetSat$^{-/-}$ mice, intricate crosstalk mechanisms come into play to compensate for the compromised functions of Mϕs. This compensation is attributed to the diminished production of MFG-E8 and the absence of NPY expression in RetSat$^{-/-}$ CD45^{+} cells. Notably, the regenerating muscles themselves exhibit elevated levels of MFG-E8, rendering the release of MFG-E8 by Mϕs less critical for proper efferocytosis, independently of RetSat loss. Our findings revealed an intriguing pattern of altered cytokine expression in RetSat$^{-/-}$ mice. The increased IL-1β levels at day 2 post-injury might play a pivotal role in promoting satellite cell activation and differentiation due to its known stimulatory effects (Chaweewannakorn, et al., 2018). The increase of Il-1β expression was also accompanied by the delay in the decrease of Ly6C^{high} CD45^{+} cell population among the infiltrating leukocytes. Surprisingly, this elevation occurred alongside a lack of changes in other key pro-inflammatory cytokines such as TNF-α or IL-6. This unique cytokine profile suggests a complex interplay of immune responses within the absence of RetSat. Intriguingly, the expression patterns of specific enzymes involved in NO production were altered in a way that could potentially lead to prolonged NO release. Arg1, NOS3, and the inducible iNOS, all known regulators of NO, displayed changes that might sustain NO production over an extended period. The prolonged NO presence, in conjunction with heightened IL-1β levels, could potentially enhance satellite cell activation in the reduced Mϕ environment (Anderson, 2000), further supporting angiogenesis initiation in the absence of NPY (Morbidelli, et al., 2003). Additionally, the elevated NO production favors cysteine nitrosylation and was shown to inhibit the aminophospholipid translocase leading to phosphatidylserine exposure on apoptotic cell surfaces, promoting their swift clearance by Mϕs (Tyurina, et al., 2007). This intricate gene expression alteration in RetSat$^{-/-}$ mice sheds light on the nuanced mechanisms underlying muscle regeneration in the absence of RetSat, revealing a finely tuned balance of pro-inflammatory factors and their impact on satellite cell activation and tissue repair (Figure 26).

Moreover, the heightened production of IL-1β and NO by CD45^{+} cells in RetSat$^{-/-}$ muscles serves as a substitute for NPY, promoting sufficient satellite cell proliferation, even in the presence of fewer neutrophils and Mϕs at the regeneration sites.

Prior research has underscored the crucial role of eosinophils, in addition to Mϕs, in facilitating proper muscle repair through IL-4 production during regeneration (Heredia, et al., 2013). IL-4 not only aids in the correct M2-like polarization of Mϕs (Gordon, 2003) but, more importantly, triggers the proliferation of FAP cells (Heredia, et al., 2013). FAP cells collaborate with Mϕs to effectively clear necrotic cells and contribute to myogenesis (Heredia, et al., 2013; Theret, et al., 2021). Apart from IL-4, macrophage-derived TGF-β1 also participates in generating FAP cells, with FAP numbers correlating with TGF-β1 levels (Contreras, et al., 2019). Remarkably, our study revealed significantly increased mRNA expression levels of TGF-β1 and IL-4 in RetSat$^{-/-}$ CD45^{+} cells at post-injury days 2 and 4, respectively. Consequently, we observed unchanged FAP cell numbers in RetSat$^{-/-}$ muscle during regeneration which might further contribute to the observed normal dead cell clearance in the knockout muscles. This observation highlights the intricate regulatory processes wherein elevated expression of pivotal regulatory factors compensates for the absence of RetSat, ensuring a balanced environment conducive to efficient muscle repair. It remains unclear whether these adaptations are specific to RetSat ablation or if they could be induced under other circumstances with reduced infiltration of neutrophils and Mϕs in damaged skeletal muscle areas. Notably, our laboratory found a similar elevated Ly6C^{high} CD45^{+} cell population in two other phagocytosis-deficient and autoimmune-prone mouse strains. The MerTK and transglutaminase 2 knockout mice were also characterized by altered M1-M2 Mϕ conversion and decreased Arg1 expression by the infiltrating leukocytes (Al-Zaeed, et al., 2021; Budai, et al., 2021) indicating that the decreased Mϕ phagocytic capacity results in similar gene expression alterations regardless of the cause. Although the lack of compensatory mechanisms leads to impaired muscle regeneration in these strains the described adaptive crosstalk mechanisms observed in RetSat$^{-/-}$ mice result in the restoration of normal skeletal muscle repair following CTX-induced injury. This highlights the resilience and flexibility of the cellular interactions involved in muscle regeneration, providing valuable insights into potential therapeutic strategies for enhancing muscle repair processes. In addition, although the expression of RetSat was detected by us by qPRC in C2C12 myoblast cells (not shown) and total TA muscle and by others by RNA sequencing (data series GSE220249) its metabolic function has not been investigated previously in the skeletal muscle. Interestingly, the SRP-35 enzyme, a recently identified all-trans-retinol dehydrogenase, has been shown to enhance skeletal muscle glucose metabolism and performance *in vivo* by activating mTORC2 signaling in muscle cells (Ruiz, et al., 2018). This underscores the direct involvement of retinol derivatives in skeletal muscle metabolism.

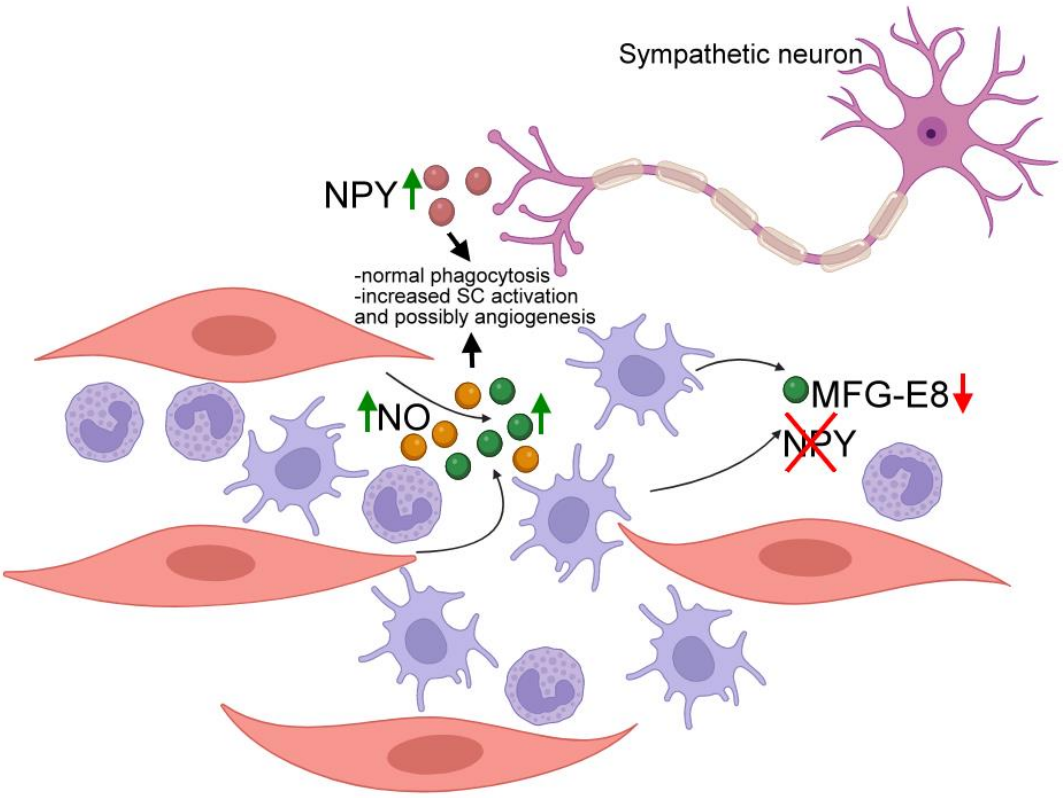

Figure 26: The proposed effect of RetSat gene ablation on skeletal muscle regeneration. *The absence of RetSat results in impaired macrophage function, leading to decreased levels of MFG-E8 and the absence of NPY expression. Consequently, elevated levels of MFG-E8 produced by regenerating muscles generally compensate for the lack of MFG-E8 release by macrophages, ensuring proper efferocytosis even in the absence of RetSat. Additionally, increased levels of IL-1β and NO produced by CD45^{+} cells serve to substitute for NPY, which may also be present at the site of repair from sympathetic neurons, promoting sufficient proliferation of satellite cells despite the reduced presence of neutrophils and macrophages at the regeneration sites of RetSat$^{-/-}$ muscles (Created in BioRender).*

For an extensive period, adenosine has been recognized as an endogenously produced signaling molecule with the ability to negatively regulate inflammation (Haskó & Cronstein, 2013). Given the pivotal role of regenerative inflammation in orchestrating tissue regeneration after injury, our study delves into the involvement of A3Rs in the regeneration of the TA muscle following CTX-induced injury. Despite the absence of A3Rs in skeletal muscle cells (Gnad, et al., 2020), our data reveal that their loss accelerates muscle regeneration, resulting in a regenerated skeletal muscle characterized by larger myofibers. The deficiency of A3Rs

induces an early and heightened pro-inflammatory environment in the TA muscle post-CTX injury. This environment is marked by increased transmigration of inflammatory cells, elevated pro-inflammatory cytokines, earlier IGF-1 production at the muscle level, and a delayed transition of Mϕs from the M1 to M2 phenotype characterized by increased $Ly6C^{high}$ and decreased $CD206^{+}$ $CD45^{+}$ cell population. In the injured muscles of $A3R^{-/-}$ mice, the augmented presence of transmigrating cells enhances the efficient clearance of cell debris compared to their $A3R^{+/+}$ counterparts. This heightened phagocytic activity proves crucial, as necrotic myofibers can either act as atrophic factors suppressing myoblast growth or serve as physical barriers hindering myoblast fusion. As our laboratory found previously in the MerTK receptor-deficient mice, the decreased Mϕ phagocytic capacity leads to impaired muscle regeneration (Al-Zaeed, et al., 2021) and conversely, the enhanced engulfment of dead cells by phagocytes facilitates a more efficient skeletal muscle regeneration, allowing for earlier initiation of the repair processes (Tidball, et al., 2014). These events collectively contribute to increased satellite cell proliferation, early and heightened expression of myogenin (responsible for initiating myoblast fusion machinery) (Ganassi, et al., 2018), and consequently, augmented myoblast fusion leading to the generation of larger myofibers. Our findings align with previous reports indicating the influence of inflammation on tissue regeneration following injury (Sugimoto, et al., 2016). However, it is crucial to maintain a proper balance between the magnitude of inflammation and the tissue regeneration response to avoid exacerbating injury (Tu & Li, 2023; Yang & Hu, 2018). Notably, our data underscore that, in the context of skeletal muscle regeneration, A3Rs exhibit an anti-inflammatory role. Interestingly, the heightened inflammatory response observed in the absence of A3Rs falls within a range where it paradoxically promotes regeneration. Given prior research suggesting that A3Rs have an anti-inflammatory impact on both Mϕs (Jacobson, et al., 2018) and neutrophils (Hoeven, et al., 2008), either these muscle-infiltrating myeloid cells or tissue-resident cells, such as capillary endothelial cells, tissue-resident Mϕs, and mast cells, which play a crucial role in recruiting inflammatory cells following injury, can be responsible for the observed accelerated regeneration in the A3R knockout mice. Among these, the inflammatory response was shown to be negatively regulated by A3Rs in tissue-resident Mϕs (Jacobson, et al., 2018) and/or mast cells (Zhang, et al., 2021). Apart from creating an enhanced inflammatory milieu, these cells might contribute to increased satellite cell proliferation by interacting with quiescent satellite cells and promoting their activation (Ratnayake, et al., 2021; Bentzinger, et al., 2013). The further dissection of these cells' contribution to the regeneration process is the topic of another Ph.D. work. Moreover, the evaluation of the impact of A3R deficiency on physiological

performance suggests that the deteriorated grip force and voluntary running outcomes in $A3R^{-/-}$ animals are primarily attributed to altered neurological function rather than skeletal muscle function. Additionally, since the *ex vivo* muscle contraction was induced by direct electric stimulation of the muscles ruling out that properties of the neuromuscular junctions contribute to the elicited contraction, the increased *ex vivo* $A3R^{-/-}$ soleus muscle twitch and tetanus force might arise from different fiber compositions compared to the wild-type mice. The soleus is a slow type muscle and an increase in the type II fast fibers might lead to observed increased force but we have not investigated this in detail.

In conclusion, our comprehensive data underscore the role of A3Rs as negative regulators of injury-related regenerative inflammation and, consequently, muscle fiber growth in the TA muscle. The potential therapeutic value of inhibiting A3Rs emerges as a promising avenue for enhancing skeletal muscle regeneration following injury.

8. Summary

Muscle regeneration is a dynamic process orchestrated by the coordinated efforts of various cell types, with the phenotypic shift of infiltrating monocyte-derived Mϕs playing a pivotal role. The repair program is initiated by the pro-inflammatory M1 Mϕs that subsequently transform into a phenotype that supports tissue repair through the secretion of growth factors. Early inflammation governs the activation, proliferation, and differentiation of myogenic stem cells. Mϕs infiltrating the injury site are crucial for this process, contributing to the removal of necrotic cell debris and apoptotic neutrophils, as well as producing cytokines and other factors that guide myogenesis. The phagocytosis of apoptotic cells facilitates the transition from the pro-inflammatory M1 phenotype to the anti-inflammatory/healing M2 Mϕ phenotype.

The versatile enzyme RetSat and the A3R both influence inflammation. In our current research, we explored the roles of RetSat and A3R in the *in vivo* development and regeneration of skeletal muscle in mice lacking these, utilizing the CTX injury model in the TA muscle. Our findings indicated that although the loss of RetSat impacted the conversion of M1 to M2 Mϕ phenotypes, the complex interplay between the cells at the injury site, ultimately led to a normal muscle regeneration program in the knockout mice. $A3R^{-/-}$ mice also exhibited an altered Mϕ phenotypes transition of Mϕ phenotypes, leading to an accelerated muscle regeneration characterized by an increased initial inflammatory response, elevated number of tissue-infiltrating $CD45^{+}$ and satellite cells, and augmented size of newly formed myofibers.

Therefore, regulation of A3R signaling could hold therapeutic potential for enhancing skeletal muscle regeneration after injury.

9. Acknowledgments

The accomplishment of this project is indebted to the steadfast backing of numerous individuals. I extend my deep appreciation to my supervisor Dr. Zsolt Sarang, and Prof. Dr. Zsuzsa Szondy for welcoming me into their lab as a Ph.D. student and for their enduring patience, unwavering support, and invaluable guidance.

I am sincerely grateful to Prof. Dr. Jozsef Tozser, the Head of the Department of Biochemistry and Molecular Biology, for welcoming me into this department. And I would also like to express my heartfelt appreciation to Prof. Dr. Fésüs László for his invaluable guidance and support.

I'd like to express my gratitude to my colleagues at Prof. Dr. Zsuzsa Szondy's lab, and I want to give special recognition to Dr. Nour Al-Zeed for her invaluable guidance and support throughout my academic journey. Last but not least, I extend my heartfelt appreciation to my family for their unwavering emotional support.

10. References

Abmayr, S. M. & Pavlath, G. K., 2012. Myoblast fusion: lessons from flies and mice. Development, pp. 641-656.

Alfaro, L. A. S. et al., 2011. CD34 Promotes Satellite Cell Motility and Entry into Proliferation to Facilitate Efficient Skeletal Muscle Regeneration. *Stem Cells,* p. 2030–2041.

Al-Zaeed, N., Budai, Z., Szondy, Z. & Sarang, Z., 2021. TAM kinase signaling is indispensable for proper skeletal muscle regeneration in mice. *cell death & disease.*

Anderson, J. E., 2000. A role for nitric oxide in muscle repair: nitric oxide-mediated activation of muscle satellite cells. *Mol Biol Cell,* pp. 1859-74.

Anderson, J. E., 2000. A Role for Nitric Oxide in Muscle Repair: Nitric Oxide–mediated Activation of Muscle Satellite Cells. *Mol Biol Cell,* p. 1859–1874.

Arnold, L. et al., 2007. Inflammatory monocytes recruited after skeletal muscle injury switch into antiinflammatory macrophages to support myogenesis. *J Exp Med,* p. 1057–1069.

Beitzel, F., Sillence, M. N. & Lynch, G. S., 2007. beta-Adrenoceptor signaling in regenerating skeletal muscle after beta-agonist administration. *Am J Physiol Endocrinol Metab,* pp. E932-40.

Bentzinger, C., Wang, Y., NA, D. & MA., R., 2013. Cellular dynamics in the muscle satellite cell niche. *EMBO Rep,* pp. 1062-1072.

Berghe, T. V. et al., 2010. Necroptosis, necrosis and secondary necrosis converge on similar cellular disintegration features. *Cell Death Differ,* pp. 922-30.

Bernard, C. et al., 2022. Role of macrophages during skeletal muscle regeneration and hypertrophy-Implications for immunomodulatory strategies. *Physiol Rep.*

Biferali, B., Proietti, D., Mozzetta, C. & Madaro, L., 2019. Fibro–Adipogenic Progenitors Cross-Talk in Skeletal Muscle: The Social Network. *Frontiers in Physiology.*

Bikle, D. D. et al., 2015. Role of IGF-I Signaling in Muscle Bone Interactions. *Bone,* p. 79–88.

Blume, K. E. et al., 2009. Cell surface externalization of annexin A1 as a failsafe mechanism preventing inflammatory responses during secondary necrosis. *J Immunol,* pp. 8138-47.

Borea, P. A. et al., 2015. The A3 adenosine receptor: history and perspectives. *Pharmacol Rev,* pp. 74-102.

Bosurgi, L. et al., 2012. Transplanted mesoangioblasts require macrophage IL-10 for survival in a mouse model of muscle injury. *J Immunol,* pp. 6267-77.

Bournazou, I. et al., 2009. Apoptotic human cells inhibit migration of granulocytes via release of lactoferrin. *J Clin Invest,* p. 20–32.

Brown, G. C., 2023. Cell death by phagocytosis. *Nat Rev Immunol.*

Bryan, p. T. & Marshall, J. M., 1999. Adenosine receptor subtypes and vasodilation in rat skeletal muscle during systemic hypoxia: a role for A1 receptors. *The Journal of Physiology,* Volume 514.

Buckingham, M. & Relaix, F., 2015. PAX3 and PAX7 as upstream regulators of myogenesis. *Semin Cell Dev Biol,* pp. 115-25.

Budai, Z. et al., 2021. Impaired Skeletal Muscle Development and Regeneration in Transglutaminase 2 Knockout Mice. *Cells.*

Budai, Z. et al., 2019. Macrophages engulf apoptotic and primary necrotic thymocytes through similar phosphatidylserine-dependent mechanisms. *FEBS Open Bio.*

Buttari, B. et al., 2017. Neuropeptide Y as regulator of macrophage phenotype and functions: a neuroimmune CUE in atherosclerosis regression?. Volume 263.

Bynoe, M. S., Viret , C., Yan, A. & Kim , D.-G., 2015. Adenosine receptor signaling: a key to opening the blood-brain door. *Fluids Barriers CNS.*

Caballero-Sánchez, N., Alonso-Alonso, S. & Nagy , L., 2022. Regenerative inflammation: When immune cells help to re-build tissues. *FEBS J.*

Chapman, M. A., Meza, R. & Lieber, R. L., 2016. Skeletal Muscle Fibroblasts in Health and Disease. *Differentiation.*

Chávez-Galán, L., Olleros, M. L., Vesin, D. & Garcia, I., 2015. Much More than M1 and M2 Macrophages, There are also CD169+ and TCR+ Macrophages. *Front Immunol.*

Chaweewannakorn, C. et al., 2018. Roles of IL-1α/β in regeneration of cardiotoxin-injured muscle and satellite cell function. *Am J Physiol Regul Integr Comp Physiol.*

Chen, J.-F., Eltzschig, H. K. & Fredholm, B. B., 2013. Adenosine receptors as drug targets — what are the challenges?. *Nat Rev Drug Discov,* p. 265–286.

Chen, L. et al., 2018. Inflammatory responses and inflammation-associated diseases in organs. *Oncotarget,* Volume Vol. 9, pp. 7204-7218.

Chen, Q., Kang, . J. & Fu , C., 2018. The independence of and associations among apoptosis, autophagy, and necrosis. *Signal Transduct Target Ther.*

Chen, W.-c.et al., 2020. Neuropeptide Y Is an Immunomodulatory Factor: Direct and Indirect. *Front. Immunol,* Volume 11.

Chen, W., You, W., Valencak, T. G. & Shan, T., 2022. Bidirectional roles of skeletal muscle fibro-adipogenic progenitors in homeostasis and disease.

Chen, Y. et al., 2006. ATP release guides neutrophil chemotaxis via P2Y2 and A3 receptors. *Science,* pp. 1792-5.

Chung, E. Y., Kim, S. J. & Ma, X. J., 2006. Regulation of cytokine production during phagocytosis of apoptotic cells. *Cell Res,* pp. 154-61.

Cicchese, J. M. et al., 2018. Dynamic balance of pro- and anti-inflammatory signals controls disease and limits pathology. *Immunol Rev,* p. 147–167.

Cockram, T. O. J., M. Dundee, J. M., Popescu, A. S. & Brown, G. C., 2021. The Phagocytic Code Regulating Phagocytosis of Mammalian Cells. *Front Immunol.*

Cohen, S. & Fishman, P., 2019. Targeting the A3 adenosine receptor to treat cytokine release syndrome in cancer immunotherapy. *Drug Des Devel Ther,* p. 491–497.

Collins, C. A. et al., 2005. Stem cell function, self-renewal, and behavioral heterogeneity of cells from the adult muscle satellite cell niche. *Cell,* pp. 289-301.

Constantin, B., Cognard, C. & Raymond, G., 1996. Myoblast fusion requires cytosolic calcium elevation but not activation of voltage-dependent calcium channels. *Cell Calcium,* pp. 365-74.

Contreras, O. et al., 2019. Cross-talk between TGF-β and PDGFRα signaling pathways regulates the fate of stromal fibro-adipogenic progenitors. *J Cell Sci.*

Contreras, O., Rossi, F. M. V. & Theret, M., 2021. Origins, potency, and heterogeneity of skeletal muscle fibro-adipogenic progenitors—time for new definitions. *Skeletal Muscle.*

Crean, D. et al., 2015. Adenosine Modulates NR4A Orphan Nuclear Receptors To Attenuate Hyperinflammatory Responses in Monocytic Cells. *J Immunol,* pp. 1436-48.

Cutler, A. A. et al., 2022. The regenerating skeletal muscle niche drives satellite cell return to quiescence. *cell press.*

Dimitrijević, M. et al., 2008. The anti-inflammatory effect of neuropeptide Y (NPY) in rats is dependent on dipeptidyl peptidase 4 (DP4) activity and age. *Peptides,* pp. 2179-87.

Dixon, A. K. et al., 1996. Tissue distribution of adenosine receptor mRNAs in the rat. *Br J Pharmacol,* pp. 1461-8.

Dumont, N. A., Bentzinger, C. F., Sincennes, M.-C. & Rudnicki, M. A., 2015. Satellite Cells and Skeletal Muscle Regeneration. *Comprehensive Physiology,* pp. 1027-1059.

Duró, E. et al., 2014. Adenosine A3 receptors negatively regulate the engulfment-dependent apoptotic cell suppression of inflammation. *Immunol Lett,* pp. 292-301.

Eijnde, S. M. v. d. et al., 2001. Transient expression of phosphatidylserine at cell-cell contact areas is required for myotube formation. *J Cell Sci,* pp. 3631-42.

Farzi, A., Reichmann, F. & Holzer, P., 2015. The homeostatic role of neuropeptide Y in immune function and its impact on mood and behaviour. *Acta Physiol (Oxf),* p. 603–627.

Fernandes, T. L., Pedrinelli, A. & Hernandez, . A. J., 2015. Muscle Injury – Physiopathology, diagnosis,treatment and clinical presentation. *Rev Bras Ortop,* pp. 247-55.

Forcina, L., Cosentino, M. & Musarò, A., 2020. Mechanisms Regulating Muscle Regeneration: Insights into the Interrelated and Time-Dependent Phases of Tissue Healing. *Cells.*

Frontera, W. R. & Ochala, J., 2015. Skeletal Muscle: A Brief Review of Structure and Function. *Calcified Tissue International,* p. 183–195.

Fukada, S., Higashimoto, T. & Kaneshige, A., 2022. Differences in muscle satellite cell dynamics during muscle hypertrophy and regeneration. *Skeletal Muscle.*

Fukada, S.-i.et al., 2007. Molecular signature of quiescent satellite cells in adult skeletal muscle. *Stem cells,* pp. 2448-2459.

Fu, X. et al., 2023. Induction of Skeletal Muscle Injury by Intramuscular Injection of Cardiotoxin in Mouse. *Bio Protoc.*

Fu, Y. L. & E. Harrison, R., 2021. Microbial Phagocytic Receptors and Their Potential Involvement in Cytokine Induction in Macrophages. *Front Immunol.*

Galan-Caridad, J. M. et al., 2007. Zfx controls the self-renewal of embryonic and hematopoietic stem cells. *Cell,* pp. 345-57.

Gamagea, D. G. et al., 2022. Phosphatidylserine orchestrates Myomerger membrane insertions to drive myoblast fusion. *PNAS.*

Ganassi, M. et al., 2018. Myogenin promotes myocyte fusion to balance fibre number and size. *Nat Commun.*

Garabuczi, É. et al., 2023. Nur77 and PPARγ regulate transcription and polarization in distinct subsets of M2-like reparative macrophages during regenerative inflammation. *Front Immunol.*

Garcia, N. et al., 2014. Adenosine A2B and A3 receptor location at the mouse neuromuscular junction. *Journal of Anatomy.*

Garry, G. A., Antony , M. L. & Garry , D. J., 2016. Cardiotoxin Induced Injury and Skeletal Muscle Regeneration. *Methods Mol Biol,* pp. 61-71.

Gayraud-Morel, B. et al., 2007. A role for the myogenic determination gene Myf5 in adult regenerative myogenesis. *Dev. Biol,* p. 13–28.

Ge, Y. et al., 2013. RNAi screen reveals potentially novel roles of cytokines in myoblast differentiation. *PLoS One.*

Gillies, A. R. & L. Lieber, R., 2011. Structure and Function of the Skeletal Muscle Extracellular Matrix. *Muscle Nerve,* pp. 318-331.

Gnad, T. et al., 2020. Adenosine/A2B Receptor Signaling Ameliorates the Effects of Aging and Counteracts Obesity. *Cell Metab,* pp. 56-70.

Gnocchi, V. F. et al., 2009. Further Characterisation of the Molecular Signature of Quiescent and Activated Mouse Muscle Satellite Cells. *Plos One.*

Gordon, S., 2003. Alternative activation of macrophages. *Nat Rev Immunol,* pp. 23-35.

Hamoud, N. et al., 2014. G-protein coupled receptor BAI3 promotes myoblast fusion in vertebrates. *Proc Natl Acad Sci U S A,* pp. 3745-50.

Hardy, D. et al., 2016. Comparative Study of Injury Models for Studying Muscle Regeneration in Mice. *PLoS One.*

Haskó, G. & Cronstein, B., 2013. Regulation of Inflammation by Adenosine. *Front Immunol.*

Haskó, G., Linden, J., Cronstein, B. & Pacher, P., 2008. Adenosine receptors: therapeutic aspects for inflammatory and immune diseases. *Nat Rev Drug Discov,* pp. 759-70.

Hasty, P. et al., 1993. Muscle deficiency and neonatal death in mice with a targeted mutation in the myogenin gene. *Nature,* pp. 501-506.

Hays, T. T. et al., 2018. A Novel Role of Growth Differentiation Factor 3 for the Regulation of Muscle Metabolism. *Diabetes.*

Heidenreich, S. et al., 2017. Retinol saturase coordinates liver metabolism by regulating ChREBP activity. *Nat Commun.*

Heredia, J. E. et al., 2013. Type 2 innate signals stimulate fibro/adipogenic progenitors to facilitate muscle regeneration. *cell,* pp. 376-88.

Hernández-Hernández, J. M., García-González, E. G., E Brun, C. & A Rudnicki , M., 2017. The myogenic regulatory factors, determinants of muscle development, cell identity and regeneration. *Semin Cell Dev Biol.*

Hesketh, M., Sahin, K. B., West , Z. E. & Murray, R. Z., 2017. Macrophage Phenotypes Regulate Scar Formation and Chronic Wound Healing. *Int J Mol Sci.*

Hindi, S. M., Tajrishi, M. M. & Kumar, A., 2013. Signaling Mechanisms in Mammalian Myoblast Fusion. *Sci Signal,* Volume 6.

Hirata, A. et al., 2003. Expression Profiling of Cytokines and Related Genes in Regenerating Skeletal Muscle after Cardiotoxin Injection. *Am J Pathol.*

Hochreiter-Hufford, A. E. et al., 2013. Phosphatidylserine receptor BAI1 and apoptotic cells as new promoters of myoblast fusion. *Nature*, pp. 263-7.

Hochreiter-Hufford, A. & Ravichandran, K. S., 2013. Clearing the dead: apoptotic cell sensing, recognition, engulfment, and digestion. *Cold Spring Harb Perspect Biol.*

Hoeven, D. v. d., Wan, T. C. & Auchampach, J. A., 2008. Activation of the A(3) adenosine receptor suppresses superoxide production and chemotaxis of mouse bone marrow neutrophils. *Mol Pharmacol*, pp. 685-96.

Horsley, V. & Pavlath, G. K., 2004. Forming a Multinucleated Cell: Molecules That Regulate Myoblast Fusion. *Cells Tissues Organs*, pp. 67-78.

Howard, E. E. et al., 2020. Divergent Roles of Inflammation in Skeletal Muscle Recovery From Injury. *Front Physiol.*

Hutcheson, D. A. et al., 2009. Embryonic and fetal limb myogenic cells are derived from developmentally distinct progenitors and have different requirements for beta-catenin. *Genes Dev*, pp. 997-1013.

Huynh, M.-L. N., Fadok, V. A. & Henson, P. M., 2002. Phosphatidylserine-dependent ingestion of apoptotic cells promotes TGF-beta1 secretion and the resolution of inflammation. *J Clin Invest*, pp. 41-50.

Hwang, A. B. & Brack, A. S., 2018. Muscle Stem Cells and Aging. *Current Topics in Developmental Biology*, pp. 299-322.

Isesele, P. O. & Mazurak, V. C., 2021. Regulation of Skeletal Muscle Satellite Cell Differentiation by Omega-3 Polyunsaturated Fatty Acids: A Critical Review. *Front Physiol.*

Jacobson, K. A. et al., 2018. A3 Adenosine Receptors as Modulators of Inflammation: From Medicinal Chemistry to Therapy. *Med Res Rev*, p. 1031–1072.

Järvinen, T. A. H. et al., 2005. Muscle Injuries Biology and Treatment. *The American Journal of Sports Medicine*, Volume 33.

Jiang, X. et al., 2021. RETSAT Mutation Selected for Hypoxia Adaptation Inhibits Tumor Growth. *Front Cell Dev Biol.*

Joós, G. et al., 2017. Involvement of adenosine A3 receptors in the chemotactic navigation of macrophages towards apoptotic cells. *Immunol Lett*, pp. 62-72.

Kaczmarek, A. et al., 2021. The Role of Satellite Cells in Skeletal Muscle Regeneration—The Effect of Exercise and Age. *Biology.*

Karagounis, L. G. & Hawley, J. A., 2010. Skeletal muscle: increasing the size of the locomotor cell. *Int J Biochem Cell Biol*, pp. 1376-9.

Karalaki, M., Fili, S., Philippou, A. & Koutsilieris, M., 2009. Muscle Regeneration: Cellular and Molecular Events. *In Vivo*, pp. 779-796.

Kassar-Duchossoy, L. et al., 2005. Pax3/Pax7 mark a novel population of primitive myogenic cells during development. *Genes & Dev*, pp. 1426-1431.

Khuu, S., Fernandez , J. W. & Handsfield, G. G., 2023. Delayed skeletal muscle repair following inflammatory damage in simulated agent-based models of muscle regeneration. *PLoS Comput Biol.*

Kim, J. H., Jin, P., Duan, R. & Chen, E. H., 2015. Mechanisms of myoblast fusion during muscle development. *Curr Opin Genet Dev,* p. 162–170.

Koenis, D. S. et al., 2018. Nuclear Receptor Nur77 Limits the Macrophage Inflammatory Response through Transcriptional Reprogramming of Mitochondrial Metabolism. *Cell Rep,* p. 2127–2140.

Koike, H., Manabe, I. & Oishi, . Y., 2022. Mechanisms of cooperative cell-cell interactions in skeletal muscle regeneration. *Inflamm Regen.*

Kojima, Y. et al., 2016. CD47 blocking antibodies restore phagocytosis and prevent atherosclerosis. *Nature.*

Krüger, M. & Richter, P., 2022. To Die or Not to Die: Cell Death in Biology and Disease. *Int J Mol Sci.*

L.Mendias, C., 2017. Fibroblasts take the centre stage in human skeletal muscle regeneration. *The Journal of Physiology,* p. 5005.

Laplante, P. et al., 2017. MFG-E8 Reprogramming of Macrophages Promotes Wound Healing by Increased bFGF Production and Fibroblast Functions. *J Invest Dermatol,* pp. 2005-2013.

Laumonier, T. & Menetrey, J., 2016. Muscle injuries and strategies for improving their repair. *J Exp Orthop.*

Lee, E. W. et al., 2003. Neuropeptide Y induces ischemic angiogenesis and restores function of ischemic skeletal muscles. *J Clin Invest,* pp. 1853-62.

Lee, J. H. & Jun, H.-S., 2019. Role of Myokines in Regulating Skeletal Muscle Mass and Function. *Frontiers in Physiology.*

Lehka, L. & Rędowicz, M. J., 2020. Mechanisms regulating myoblast fusion: A multilevel interplay. *Semin Cell Dev Biol,* pp. 81-92.

Leikina, E. et al., 2018. Myomaker and Myomerger Work Independently to Control Distinct Steps of Membrane Remodeling during Myoblast Fusion. *Dev Cell,* pp. 767-780.

Leikina, E. et al., 2013. Extracellular annexins and dynamin are important for sequential steps in myoblast fusion. *J Cell Biol,* pp. 109-23.

Lemos, D. R. et al., 2015. Nilotinib reduces muscle fibrosis in chronic muscle injury by promoting TNF-mediated apoptosis of fibro/adipogenic progenitors. *Nature Medicine,* pp. 786-794.

Levin, R., Grinstein, S. & Canton, J., 2016. The life cycle of phagosomes: formation, maturation, and resolution. *Immunol Rev,* pp. 156-79.

Liang, B. T., Urso, . M., Zambraski, E. & Jacobson , K. A., 2009. Adenosine A3 Receptors in Muscle Protection. In: *A3 Adenosine Receptors from Cell Biology to Pharmacology and Therapeutics.* s.l.:s.n., pp. 257-280.

Low, M., Eisner, C. & Rossi, F., 2017. *Fibro/Adipogenic Progenitors (FAPs): Isolation by FACS and Culture.* s.l.:s.n.

Lundberg, J. M. et al., 1989. Co-release of neuropeptide Y and noradrenaline from pig spleen in vivo: importance of subcellular storage, nerve impulse frequency and pattern, feedback regulation and resupply by axonal transport. *Neuroscience,* pp. 475-86.

Lynge, J. & Hellsten, Y., 2000. Distribution of adenosine A1, A2A and A2B receptors in human skeletal muscle. *Acta Physiol Scand,* pp. 283-90.

Mann, C. J. et al., 2011. Aberrant repair and fibrosis development in skeletal muscle. *Skelet Muscle.*

Martinez, C. O. et al., 2010. Regulation of skeletal muscle regeneration by CCR2-activating chemokines is directly related to macrophage recruitment. *Am J Physiol Regul Integr Comp Physiol.*

Martinez, F. O., Gordon, S., Locati, M. & Mantovani, A., 2006. Transcriptional Profiling of the Human Monocyte-to-Macrophage Differentiation and Polarization: New Molecules and Patterns of Gene Expression. *The Journal of Immunology.*

Mauro, A., 1961. Satellite cell of skeletal muscle fibers. *The Journal of Biophysical and Biochemical Cytology,* pp. 493-495.

Mazziotta, C. et al., 2022. Cancer biology and molecular genetics of A3 adenosine receptor. *Oncogene,* pp. 301-308.

McColl, R., Nkosi, . M., Snyman, C. & Niesler, C., 2016. Analysis and quantification of in vitro myoblast fusion using the LADD Multiple Stain. *BioTechniques,* Volume 61, pp. 323-326.

McMorrow, J. P. & Murphy, E. P., 2011. Inflammation: a role for NR4A orphan nuclear receptors?. *Biochem Soc Trans,* pp. 688-93.

Megeney, L. A. et al., 1996. MyoD is required for myogenic stem cell function in adult skeletal muscle. *Genes Dev,* pp. 1173-83.

Metzemaekers, M., Gouwy, M. & Proost, P., 2020. Neutrophil chemoattractant receptors in health and disease: double-edged swords. *cellular & molecular immunology.*

Millay, D. P. et al., 2016. Structure–function analysis of myomaker domains required for myoblast fusion. *PNAS,* pp. 2116-21.

Moise, A. R. et al., 2009. Activation of Retinoic Acid Receptors by Dihydroretinoids. *Mol Pharmacol,* p. 1228–1237.

Moise, A. R., Kuksa, V., Imanishi, Y. & Palczewski, K., 2004. Identification of All-trans-Retinol:All-trans-13,14-dihydroretinol Saturase. *J Biol Chem,* p. 50230–50242.

Molina, T., Fabre, P. & A. Dumont, N., 2021. Fibro-adipogenic progenitors in skeletal muscle homeostasis, regeneration and diseases. *open biology.*

Morbidelli, L., Donnini, S. & Ziche, M., 2003. Role of nitric oxide in the modulation of angiogenesis. *Curr Pharm Des,* pp. 521-30.

Musarò, A., 2014. The Basis of Muscle Regeneration. *Hindawi Publishing Corporation Advances in Biology.*

Nagaoka-Yasuda, R. et al., 2007. An RNAi-based genetic screen for oxidative stress resistance reveals retinol saturase as a mediator of stress resistance. *Free Radic Biol Med,* pp. 781-8.

Neurath, M. F., 2019. Resolution of inflammation: from basic concepts to clinical application. *Semin Immunopathol,* pp. 627-631.

Nishat, S., Khan, L. A., Ansari, Z. M. & Basir, S. F., 2016. Adenosine A3 Receptor: A promising therapeutic target in cardiovascular disease. *Curr Cardiol Rev,* pp. 18-26.

Oldenborg, P. A. et al., 2000. Role of CD47 as a marker of self on red blood cells. *Science,* pp. 2051-4.

Ortega-Gómez, A., Perretti, M. & Soehnlein, O., 2013. Resolution of inflammation: an integrated view. *EMBO Mol Med*, pp. 661-74.

Otis, J. S. et al., 2014. Pro-inflammatory mediation of myoblast proliferation. *PLoS One.*

Panduro, M., Benoist, C. & Mathis, D., 2018. Treg cells limit IFN-γ production to control macrophage accrual and phenotype during skeletal muscle regeneration. *Proc Natl Acad Sci U S A.*

Pang, X.-Y.et al., 2017. Retinol saturase modulates lipid metabolism and the production of reactive oxygen species. *Arch Biochem Biophys*, pp. 93-102.

Park, P. J. et al., 2009. Integration of heterogeneous expression data sets extends the role of the retinol pathway in diabetes and insulin resistance. *Bioinformatics.*

Park, S.-Y.et al., 2016. Stabilin-2 modulates the efficiency of myoblast fusion during myogenic differentiation and muscle regeneration. *Nat Commun.*

Park, S.-Y. & Kim, I.-S., 2017. Engulfment signals and the phagocytic machinery for apoptotic cell clearance. *Exp Mol Med.*

Patsalos, A. et al., 2022. A growth factor-expressing macrophage subpopulation orchestrates regenerative inflammation via GDF-15. *J Exp Med*, Jan.

Peake, J. M., Neubauer , O., Gatta, P. A. D. & Nosaka, K., 2017. Muscle damage and inflammation during recovery from exercise. *J Appl Physiol (1985).*

Pinhal-Enfield, G. et al., 2003. An Angiogenic Switch in Macrophages Involving Synergy between Toll-Like Receptors 2, 4, 7, and 9 and Adenosine A2A Receptors. *Am J Pathol.*

Purslow, P. P., 2020. The Structure and Role of Intramuscular Connective Tissue in Muscle Function. *Front Physiol.*

Rai, V., Mathews, G. & Agrawal, D. K., 2022. Translational and Clinical Significance of DAMPs, PAMPs, and PRRs in Trauma-induced Inflammation. *Arch Clin Biomed Res.*

Ramkumar, V., Stiles, G. L., Beaven, M. A. & Ali, H., 1993. The A3 adenosine receptor is the unique adenosine receptor which facilitates release of allergic mediators in mast cells. *J Biol Chem.*

Ratnayake, D. et al., 2021. Macrophages provide a transient muscle stem cell niche via NAMPT secretion. *Nature*, pp. 281-287.

Rayavarapu, S., Coley, W., Kinder , T. B. & Nagaraju, K., 2013. Idiopathic inflammatory myopathies: pathogenic mechanisms of muscle weakness. *Skeletal Muscle.*

Riegman, M., Bradbury, M. S. & Overholtzer, M., 2019. Population Dynamics in Cell Death: Mechanisms of Propagation. *Trends Cancer*, pp. 558-568.

Roh, J. S. & Sohn, D. H., 2018. Damage-Associated Molecular Patterns in Inflammatory Diseases. *Immune Netw.*

Rosales, C. & Uribe-Querol, E., 2017. Phagocytosis: A Fundamental Process in Immunity. *Biomed Res Int.*

Rudich, N., Ravid, K. & Sagi-Eisenberg, R., 2012. Mast cell adenosine receptors function: a focus on the a3 adenosine receptor and inflammation. *Front Immunol.*

Rudnicki, M. A., Grand, F. L., McKinnell, I. & Kuang, S., 2008. The molecular regulation of muscle stem cell function. *Cold Spring Harb Symp Quant Biol*, pp. 323-31.

Ruiz, A. et al., 2018. Over-expression of a retinol dehydrogenase (SRP35/DHRS7C) in skeletal muscle activates mTORC2, enhances glucose metabolism and muscle performance. *Sci Rep.*

Sachet, M., Liang, Y. Y. & Oehler, R., 2017. The immune response to secondary necrotic cells. *Apoptosis,* p. 1189–1204.

Saclier, M. et al., 2013. Differentially activated macrophages orchestrate myogenic precursor cell fate during human skeletal muscle regeneration. *Stem Cells,* pp. 384-96.

Saini, A. et al., 2022. Adenosine receptor antagonists: Recent advances and therapeutic perspective. *Eur J Med Chem.*

Sakurai, T. et al., 2013. Role of nitric oxide in muscle regeneration following eccentric muscle contractions in rat skeletal muscle. *J Physiol Sci,* pp. 263-70.

Sambasivan, R. et al., 2013. Embryonic founders of adult muscle stem cells are primed by the determination gene Mrf4. *Dev Biol,* pp. 241-55.

Sampath, S. C., Sampath, S. C. & Millay, D. P., 2018. Myoblast fusion confusion: the resolution begins. *Skeletal Muscle.*

Sarang, Z. et al., 2014. Macrophages engulfing apoptotic cells produce nonclassical retinoids to enhance their phagocytic capacity. *J Immunol,* pp. 5730-8.

Sarang, Z. et al., 2019. Retinol Saturase Knock-Out Mice are Characterized by Impaired Clearance of Apoptotic Cells and Develop Mild Autoimmunity. *Biomolecules.*

Saraste, A. & Pulkki, K., 2000. Morphologic and biochemical hallmarks of apoptosis. *Cardiovasc Res,* pp. 528-37.

Sastourné-Arrey, Q. et al., 2023. Adipose tissue is a source of regenerative cells that augment the repair of skeletal muscle after injury. *Nature Communications.*

Sayed, R. K. A., Hibbert, J. E., Jorgenson, K. W. & Hornberger, T. A., 2023. The Structural Adaptations That Mediate Disuse-Induced Atrophy of Skeletal Muscle. *Cells.*

Schultz, E., Jaryszak, D. L. & Valliere, C. R., 1985. Response of satellite cells to focal skeletal muscle injury. *Muscle Nerve,* pp. 217-222.

Schupp, M. et al., 2009. Retinol saturase promotes adipogenesis and is downregulated in obesity. *Proc Natl Acad Sci U S A.*

Seale, P. et al., 2000. Pax7 Is Required for the Specification of Myogenic Satellite Cells.. *Cell,* p. 777–786.

Sepand, M.-R.et al., 2020. Mechanisms and pathogenesis underlying environmental chemical-induced necroptosis. *Environ Sci Pollut Res Int,* pp. 37488-37501.

Sheth, S. et al., 2014. Adenosine receptors: expression, function and regulation. *Int J Mol Sci,* pp. 2024-52.

Singer, K. et al., 2013. Neuropeptide Y is produced by adipose tissue macrophages and regulates obesity-induced inflammation. *PLoS One.*

Soleimani, V. D. et al., 2012. Transcriptional Dominance of Pax7 in Adult MyogenesisIs Due to High-Affinity Recognition of Homeodomain Motifs. *Dev Cell,* pp. 1208-20.

Sousa-Victor, P., García-Prat2, L. & Muñoz-Cánoves, P., 2022. Control of satellite cell function in muscle regeneration and its disruption in ageing. *Nature Reviews Molecular Cell Biology,* Volume 23.

Squire, J. M., 1997. Architecture and function in the muscle sarcomere. *Current Opinion in Structural Biology,* pp. 247-257.

Straub, R. H. et al., 2000. Neuropeptide Y cotransmission with norepinephrine in the sympathetic nerve-macrophage interplay. *J Neurochem,* pp. 2464-71.

Sugimoto, M. A. et al., 2016. Resolution of Inflammation: What Controls Its Onset?. *Front Immunol.*

Szondy, Z. et al., 2017. Anti-inflammatory Mechanisms Triggered by Apoptotic Cells during Their Clearance. *Front Immunol.*

Sztretye, M. et al., 2020. Improved Tetanic Force and Mitochondrial Calcium Homeostasis by Astaxanthin Treatment in Mouse Skeletal Muscle. *Antioxidants (Basel).*

Tajbakhsh, A. et al., 2020. Regulation of efferocytosis by caspase-dependent apoptotic cell death in atherosclerosis. *The International Journal of Biochemistry & Cell Biology,* Volume 120.

Tamas, V. et al., 2016. Macrophage PPARγ, a Lipid Activated Transcription Factor Controls the Growth Factor GDF3 and Skeletal Muscle Regeneration. *Immunity.*

Tang, D. et al., 2012. PAMPs and DAMPs: signal 0s that spur autophagy and immunity. *Immunol Rev,* p. 158–175.

Tang, J. et al., 2021. BAY 60-6583 Enhances the Antitumor Function of Chimeric Antigen Receptor-Modified T Cells Independent of the Adenosine A2b Receptor. *Front Pharmacol.*

Tarban, N. et al., 2022. Regenerating Skeletal Muscle Compensates for the Impaired Macrophage Functions Leading to Normal Muscle Repair in Retinol Saturase Null Mice. *Cells.*

Tecchio, C., Micheletti, A. & Cassatella , M. A., 2014. Neutrophil-derived cytokines: facts beyond expression. *Front Immunol.*

Teixeira, C. F. P. et al., 2003. Neutrophils do not contribute to local tissue damage, but play a key role in skeletal muscle regeneration, in mice injected with Bothrops asper snake venom. *Muscle Nerve,* pp. 449-59.

Theret, M., Rossi, F. M. V. & Contreras, O., 2021. Evolving Roles of Muscle-Resident Fibro-Adipogenic Progenitors in Health, Regeneration, Neuromuscular Disorders, and Aging. *Front Physiol.*

Thorsell, A. & Mathé, A. A., 2017. Neuropeptide Y in Alcohol Addiction and Affective Disorders. *Front Endocrinol (Lausanne).*

Tidball, J. G., Dorshkind, K. & Wehling-Henricks, M., 2014. Shared signaling systems in myeloid cell-mediated muscle regeneration. *Development,* pp. 1184-96.

Tidball, J. G. & Welc, S. S., 2015. Macrophage-Derived IGF-1 Is a Potent Coordinator of Myogenesis and Inflammation in Regenerating Muscle. *Mol Ther,* pp. 1134-1135.

Tu, H. & Li, . Y.-L., 2023. Inflammation balance in skeletal muscle damage and repair. *Front. Immunol.*

Tu, Q. et al., 2022. RETSAT associates with DDX39B to promote fork restarting and resistance to gemcitabine based chemotherapy in pancreatic ductal adenocarcinoma. *J Exp Clin Cancer Res.*

Tyurina, Y. Y. et al., 2007. Nitrosative stress inhibits the aminophospholipid translocase resulting in phosphatidylserine externalization and macrophage engulfment: implications for the resolution of inflammation. *J Biol Chem,* pp. 8498-509.

Uezumi, A. et al., 2010. Mesenchymal progenitors distinct from satellite cells contribute to ectopic fat cell formation in skeletal muscle. *Nature Cell Biology,* pp. 143-152.

Uribe-Querol, E. & Rosales, C., 2020. Phagocytosis: Our Current Understanding of a Universal Biological Process. *Front Immunol.*

Urso, M. L., Wang, R., J. Zambraski, E. & T. Liang, B., 2012. Adenosine A3 receptor stimulation reduces muscle injury following physical trauma and is associated with alterations in the MMP/TIMP response. *Journal of Applied Physiology*, Volume 112.

Varga, T. et al., 2016. Macrophage PPARγ, a Lipid Activated Transcription Factor Controls the Growth Factor GDF3 and Skeletal Muscle Regeneration. *Immunity*, pp. 1038-1051.

Villalta, S. A. et al., 2009. Shifts in macrophage phenotypes and macrophage competition for arginine metabolism affect the severity of muscle pathology in muscular dystrophy. *Hum Mol Genet*, pp. 482-96.

Wakelam, M. J., 1985. The fusion of myoblasts. *Biochem J*, pp. 1-12.

Wang, X. et al., 2023. Diverse effector and regulatory functions of fibro/adipogenic progenitors during skeletal muscle. *cell press.*

Wang, X. & Zhou, L., 2022. The Many Roles of Macrophages in Skeletal Muscle Injury and Repair. *Front Cell Dev Biol.*

Wang, X. & Zhou, L., 2023. The multifaceted role of macrophages in homeostatic and injured skeletal muscle. *Front Immunol.*

Wang, Y., Lu, J. & Liu, Y., 2022. Skeletal Muscle Regeneration in Cardiotoxin-Induced Muscle Injury Models. *Int J Mol Sci.*

Wan, T. C. et al., 2008. The A3 adenosine receptor agonist CP-532,903 protects against myocardial ischemia/reperfusion injury via the sarcolemmal ATP sensitive potassium channel. *J Pharmacol Exp Ther*, p. 234–243.

Weber, P., Flores, R. E., Kiefer, M. F. & Schupp, M., 2020. Retinol Saturase: More than the Name Suggests. *Trends Pharmacol Sci.*

Wei, C. J., Li, W. & Chen, J.-F., 2011. Normal and abnormal functions of adenosine receptors in the central nervous system revealed by genetic knockout studies. *Biochim Biophys Acta*, pp. 1358-79.

Westman, J., Grinstein, S. & Marques, P. E., 2020. Phagocytosis of Necrotic Debris at Sites of Injury and Inflammation. *Front. Immunol*, Volume 10 - 2019.

Witte, N. et al., 2015. The Glucose Sensor ChREBP Links De Novo Lipogenesis to PPARγ Activity and Adipocyte Differentiation. *Endocrinology*, pp. 4008-19.

Yablonka-Reuveni, Z., Day, K., Vine, A. & Shefer, G., 2008. Defining the transcriptional signature of skeletal muscle stem cells. *Journal of Animal Science*, p. E207–E216.

Yan, G., Elbadawi, M. & Efferth, T., 2020. Multiple cell death modalities and their key features (Review). *WORLD ACADEMY OF SCIENCES JOURNAL*, pp. 39-48.

Yang, W. & Hu, P., 2018. Skeletal muscle regeneration is modulated by inflammation. *J Orthop Translat*, pp. 25-32.

Yan, L., Singh, L. S., Zhang, L. & Xu, Y., 2014. Role of OGR1 in myeloid-derived cells in prostate cancer. *Oncogene*, p. 157–164 .

Yao, Y., Xu, X.-H. & Jin, L., 2019. Macrophage Polarization in Physiological and Pathological Pregnancy. *Front Immunol.*

Yoshida, T. & Delafontaine, P., 2020. Mechanisms of IGF-1-Mediated Regulation of Skeletal Muscle Hypertrophy and Atrophy. *Cells.*

Yuan, S. et al., 2021. Sympathetic activity is correlated with satellite cell aging and myogenesis via β2-adrenoceptor. *Stem Cell Res Ther*.

Yunna, C., Mengru, H., Lei, W. & Weidong, C., 2020. Macrophage M1/M2 polarization. *European Journal of Pharmacology*, Volume Volume 877.

Yutin, N., Wolf, M. Y., Wolf, Y. I. & Eugene , V. K., 2009. The origins of phagocytosis and eukaryogenesis. *Biol Direct.*

Yu, Y. et al., 2022. Macrophages play a key role in tissue repair and regeneration. *PeerJ.*

Zammit, P. S. et al., 2006. Pax7 and myogenic progression in skeletal muscle satellite cells. *J Cell Sci,* pp. 1824-32.

Zamora, R., Vodovotz, Y. & R. Billiar , T., 2000. Inducible Nitric Oxide Synthase and Inflammatory Diseases. *Molecular Medicine,* p. 347–373.

Zargarian, S. et al., 2017. Phosphatidylserine externalization, "necroptotic bodies" release, and phagocytosis during necroptosis. *PLoS Biol.*

Zhang, Q. et al., 2010. Circulating Mitochondrial DAMPs Cause Inflammatory Responses to Injury. *Nature,* p. 104–107.

Zhang, T. et al., 2021. LJ529 attenuates mast cell-related inflammation via A3R-PKCε-ALDH2 pathway after subarachnoid hemorrhage in rats. *Exp Neurol.*

Zhang, W., Liu, Y. & Zhang , H., 2021. Extracellular matrix: an important regulator of cell functions and skeletal muscle development. *Cell & Bioscience.*

Zhang, Y. et al., 2021. Regulation of neuropeptide Y in body microenvironments and its potential application in therapies: a review. *Cell Biosci.*

Zhao, Z. et al., 2002. Overexpression of A3 adenosine receptors in smooth, cardiac, and skeletal muscle is lethal to embryos. *Microvasc Res,* pp. 61-9.

Zheng, J. et al., 2007. Protective roles of adenosine A1, A2A, and A3 receptors in skeletal muscle ischemia and reperfusion injury. *Am J Physiol Heart Circ Physiol.*

Zhong, L., Peng, Q. & Zeng, X., 2022. The role of adenosine A1 receptor on immune cells. *Inflamm Res,* pp. 1203-1212.

11. List of publication

UNIVERSITY of DEBRECEN

UNIVERSITY AND NATIONAL LIBRARY
UNIVERSITY OF DEBRECEN
H-4002 Egyetem tér 1, Debrecen
Phone: +3652/410-443, email: publikaciok@lib.unideb.hu

Registry number: DEENK/45/2024.PL
Subject: PhD Publication List

Candidate: Nastaran Tarban
Doctoral School: Doctoral School of Molecular Cellular and Immune Biology
MTMT ID: 10076381

List of publications related to the dissertation

1. **Tarban, N.**, Papp, A. B., Deák, D., Szentesi, P., Halász, H. E., Patsalos, A., Csernoch, L., Sarang, Z., Szondy, Z.: Loss of adenosine A3 receptors accelerates skeletal muscle regeneration in mice following cardiotoxin-induced injury.
   Cell Death Dis. 14 (10), 706, 2023.
   DOI: http://dx.doi.org/10.1038/s41419-023-06228-7
   IF: 9 (2022)
2. **Tarban, N.**, Halász, H. E., Gogolák, P., Garabuczi, É., Moise, A. R., Palczewski, K., Sarang, Z., Szondy, Z.: Regenerating Skeletal Muscle Compensates for the Impaired Macrophage Functions Leading to Normal Muscle Repair in Retinol Saturase Null Mice.
   Cells. 11 (8), 1-16, 2022.
   DOI: http://dx.doi.org/10.3390/cells11081333
   IF: 6

List of other publications

3. Adil Ali, M., Garabuczi, É., **Tarban, N.**, Sarang, Z.: All-trans retinoic acid and dexamethasone regulate phagocytosis-related gene expression and enhance dead cell uptake in C2C12 myoblast cells.
   Sci. Rep. 13 (1), 1-8, 2023.
   DOI: http://dx.doi.org/10.1038/s41598-023-48492-9
   IF: 4.6 (2022)
4. Garabuczi, É., **Tarban, N.**, Vincze-Fige, É., Patsalos, A., Halász, L., Szendi-Szatmári, T., Sarang, Z., Király, R., Szondy, Z.: Nur77 and PPARγ regulate transcription and polarization in distinct subsets of M2-like reparative macrophages during regenerative inflammation.
   Front. Immunol. 14, 1-14, 2023.
   DOI: http://dx.doi.org/10.3389/fimmu.2023.1139204
   IF: 7.3 (2022)

UNIVERSITY AND NATIONAL LIBRARY
UNIVERSITY OF DEBRECEN
H-4002 Egyetem tér 1, Debrecen
Phone: +3652/410-443, email: publikaciok@lib.unideb.hu

5. Szondy, Z., Al Zaeed, N., **Tarban, N.**, Vincze-Fige, É., Garabuczi, É., Sarang, Z.: Involvement of phosphatidylserine receptors in the skeletal muscle regeneration: therapeutic implications. *J. Cachexia Sarcopenia Muscle. 13* (4), 1961-1973, 2022.
DOI: http://dx.doi.org/10.1002/jcsm.13024
IF: 8.9

6. Ajorloo, M., Mirzaei, H., Sadeghi, Y., **Tarban, N.**, Soltani, S., Mohammadi, F. S., Davarinejad, P., Roudy, M. A., Jahantigh, H. R., Abouhamzeh, K., Mohammadhosayni, M., Nikoo, H. R., Alamdary, A., Norouzi, M.: Evaluation and Phylogenetic Analysis of Regular Rabies Virus Vaccine Strains.
21 (3), 101-110, 2018.
IF: 1.141

7. Tofigh, R., Akhavan, S., **Tarban, N.**, Sadrabadi, A. E., Jalili, A., Moridi, K., Tutunchi, S.: Doxorubicin Induces Apoptosis through down Regulation of miR-21 Expression and Increases miR-21 Target Gene Expression in MCF-7 Breast Cancer Cells.
IJCM. 8 (6), 386-394, 2017.
DOI: http://dx.doi.org/10.4236/ijcm.2017.86036

8. Mohammadhosayni, M., Hajighasemi, F., Rezaee, A., Mozayani, F., Mohammadi, F. S., **Tarban, N.**, Momenifar, N., Norouzi, M.: Investigation of the Relationship between HTLV-1 Infection and MMP-3 Gene Expression in HTLV-1 Positive Cardiac Patients.
Iran. J. Virol. 11 (3), 13-18, 2017.

9. **Tarban, N.**, Habibi, R. M., Shafifar, M., Mohammad, h. M., Rezaee, S. A., Jazayeri, S. M., Norouzi, M.: Comparative Analysis and Molecular Structure of the Protease Molecule from Human Lymphotropic Virus Type-1 (HTLV-1).
Iran. J. Virol. 10 (2-3), 31-39, 2016.

Total IF of journals (all publications): 36,941
Total IF of journals (publications related to the dissertation): 15

The Candidate's publication data submitted to the iDEa Tudóstér have been validated by DEENK on the basis of the Journal Citation Report (Impact Factor) database.

09 February, 2024

DEBRECENI EGYETEM Egyetemi és Nemzeti Könyvtár